

Electronic Thesis and Dissertation Repository

8-16-2021 2:00 PM

Establishing Intratumoral Modulation Therapy as a New Treatment Modality for High Grade Gliomas

Andrew M.A. Deweyert, *The University of Western Ontario*

Supervisor: Hebb, Matthew O., *The University of Western Ontario*

Co-Supervisor: Schmid, Susanne, *The University of Western Ontario*

A thesis submitted in partial fulfillment of the requirements for the Doctor of Philosophy degree in Anatomy and Cell Biology

© Andrew M.A. Deweyert 2021

Follow this and additional works at: <https://ir.lib.uwo.ca/etd>



Part of the [Diseases Commons](#), and the [Nervous System Commons](#)

Recommended Citation

Deweyert, Andrew M.A., "Establishing Intratumoral Modulation Therapy as a New Treatment Modality for High Grade Gliomas" (2021). *Electronic Thesis and Dissertation Repository*. 7985.

<https://ir.lib.uwo.ca/etd/7985>

This Dissertation/Thesis is brought to you for free and open access by Scholarship@Western. It has been accepted for inclusion in Electronic Thesis and Dissertation Repository by an authorized administrator of Scholarship@Western. For more information, please contact wlsadmin@uwo.ca.

Abstract

Glioblastoma (GBM) is the most common and lethal primary brain cancer in adults despite aggressive treatments with surgery and chemo-radiation. Advances in electrotherapeutics offer a foundation for developing new treatment modalities that exploit an innate vulnerability of glioblastoma (GBM). Low intensity, non-ablative electric fields are innocuous to normal neural structure, but incite GBM cell apoptosis by putatively disrupting cytokinesis and transmembrane ion homeostasis. Our collaborative research group is pioneering a new electrotherapeutic technology for GBM called Intratumoral Modulation Therapy (IMT) which uses customized, implanted bioelectrodes to deliver sustained, titratable and focused therapeutic electric fields into tumor-affected brain regions. My work has confirmed and expanded the group's previous *in vitro* evidence of IMT efficacy against GBM and diffuse intrinsic pontine glioma (DIPG) and has demonstrated potent anti-neoplastic, pro-apoptotic effects of IMT *in vitro* without significant impact on non-cancerous post-mitotic neurons. The co-application of IMT also potentiates the benefits of chemotherapy and gene therapy. We have created a robust *in vivo* IMT model using allograft GBM cells in Fischer rats to test the efficacy of IMT *in vivo*. The GBM animal studies to date have demonstrated proof-of-concept efficacy of IMT against GBM using rudimentary, single-contact bioelectrodes. However, single-contact electrodes cannot adequately accommodate the entire tumor or GBM resection bed where recurrence is otherwise inevitable. To translate this technology to clinical use, new special purpose bioelectrodes must be designed and tested to optimize and contour IMT coverage. This thesis yielded key insight into the bioelectrode configuration and treatment settings for effective and safe IMT delivery in GBM and DIPG. Advances in this technology will facilitate clinical translation of IMT as a critically needed therapy for these devastating brain cancers.

Keywords

Key Words: Glioblastoma, Diffuse Intrinsic Pontine Glioma, Electrotherapy, Intratumoural Modulation Therapy, Neuro-oncology, High Grade Glioma, Tumour Treating Fields, Bioelectrodes

Summary for Lay Audience

High-Grade Gliomas (HGG) are deadly brain tumors with very poor treatment outcomes. Glioblastoma (GBM) and diffuse intrinsic pontine glioma (DIPG) are categorized as high-grade gliomas (HGGs) and remain among the most deadly brain cancers in adults and children, respectively. Treatment only extends life approximately 12 months, therefore research into new therapies is crucial. Our team has developed a new biotechnology called Intratumoral Modulation Therapy (IMT). This technology uses an implanted electrical system to treat and kill tumors within the brain. IMT has shown to be an effective first line treatment and enhances the effects of chemoradiotherapy. We hypothesized that IMT delivered via specially designed, implantable bioelectrodes within HGG tissue or resection cavity (where these tumors always recur in a short time after surgery) will slow HGG growth, kill tumor cells, and increase the sensitivity of HGG to standard chemotherapy and radiation. Advanced brain imaging techniques were used to assess tumor growth and survival alone and in combination with standard doses of chemotherapy and radiation. The clinical vision of IMT is to provide a concealed, anatomically focused, patient-specific therapy that can effectively fight these cancers and enhance the benefits of existing treatment options. The results of this project have provided key information used to advance IMT towards clinical application. The successful development of IMT technology has the potential to markedly improve the survival and quality of life for patients facing these deadly cancers.

Co-Authorship Statement

Chapter 1 of this thesis was partially adapted from a review article (unpublished) coauthored by Andrea R. Di Sebastiano, Mike D. Staudt, N. Farhani, Hu Xu, Eugene Wong, Susanne Schmid, Matthew O. Hebb. I was responsible for the literature review, manuscript writing and editing.

Chapter 2 of this thesis was published in Scientific Reports and was coauthored by Andrea R. Di Sebastiano, Simon Benoit, Erin Iredale, Hu Xu, Cleusa De Oliveira, Eugene Wong, Susanne Schmid & Matthew O. Hebb. For this paper Andrea and I worked together as a team. We designed, oversaw, and conducted all experimental procedures, performed all data collection and analyses, and wrote/edited the manuscript.

Chapter 3 of this thesis was published in the Journal of Neuro-oncology and was coauthored by Erin Iredale, Hu Xu, Eugene Wong, Susanne Schmid, Matthew O. Hebb. For this manuscript I produced the data with validation being performed by our lab technician Hu Xu. I was responsible for data analysis and manuscript writing. Editing and submission was performed by my supervisors Matthew Hebb and Susanne Schmid.

Chapter 4 of this thesis is being prepared for submission and was coauthored by Mila Uzelac, Erin Iredale, Hu Xu, Eugene Wong, Susanne Schmid, Matthew O. Hebb. For this manuscript I produced the data using in-lab custom models with validation being performed by our lab technician Hu Xu and master student Mila Uzelac. Additionally, I was responsible for the data analysis and a large part of the manuscript writing. Editing and submission were performed by my supervisors Matthew Hebb and Susanne Schmid.

Acknowledgments

I would first like to thank my supervisors, Dr. Matthew Hebb and Dr. Susanne Schmid, they have provided an enormous amount of guidance and mentorship over the past 5 years. Dr. Matthew Hebb has challenged me to become a better scientist and taught me to be a critical thinker, detail orientated and to hold myself and our scientific work to a high standard. His commitment to research on top of his clinical duties has inspired me to work hard and pursue excellence in my academic career. Dr. Susanne Schmid has always encouraged me to look at the big picture to see how the research extends to the community. She is an inspiring PI demonstrating passion and resilience which she has instilled in each of her trainees. I want to thank Matt and Susanne for all the opportunities and experience they have afforded me throughout my PhD, I have felt incredibly supported. I know I will use the skills I obtained under their tutelage for the rest of my academic career.

I would like to extend a special thank you to Dr. De Oliveira and Dr. Hu Xu our lab managers without them the research in this thesis would not have been possible. Thank you for helping to run the lab so smoothly and your unwavering technical support. I would also like to extend my gratitude to the members of my advisory committee: Drs. Silvia Penuela, and Shawn Whitehead for their guidance and support.

A special thank you to everyone in the Department of Anatomy and Cell Biology, and all the present and past members of the Hebb and Schmid labs. It has been an amazing experience working with such a cohesive team and supportive department. Grad school experiences are often dependent of those you work with, thank you for creating an excellent, supportive work environment, I could not have succeeded without all of you.

Lastly, I would like to thank my family, their support, love, and encouragement allowed me to continue down this road of graduate school to follow my passion for science.

Table of Contents

| | |
|--|-----|
| Abstract..... | ii |
| Summary for Lay Audience..... | iv |
| Co-Authorship Statement..... | v |
| Acknowledgments..... | vi |
| List of Tables | x |
| List of Figures | xii |
| Chapter 1..... | 1 |
| 1 General Introduction | 1 |
| 1.1 Glial Tumors | 1 |
| 1.1.1 Glioblastoma..... | 2 |
| 1.1.2 Diffuse Intrinsic Pontine Glioma..... | 5 |
| 1.2 Electrotherapies for HGG..... | 6 |
| 1.2.1 Putative Applications of Electrotherapy in Cancer..... | 6 |
| 1.3 Intratumoral Modulation Therapy..... | 10 |
| 1.4 Hypotheses and Objectives..... | 12 |
| 1.5 References..... | 14 |
| Chapter 2..... | 25 |
| 2 Preclinical Outcomes of Intratumoral Modulation Therapy for Glioblastoma ¹ | 25 |
| 2.1 Introduction..... | 25 |
| 2.2 Results..... | 34 |
| 2.2.1 Intermediate frequency IMT selectively kills GBM cells and provides cumulative anti-neoplastic effects when administered with TMZ chemotherapy | 34 |
| 2.2.2 IMT significantly attenuates GBM growth <i>in vivo</i> | 38 |
| 2.2.3 Computer simulation predicts IMT electric field properties in GBM tumor and brain | 43 |
| 2.3 Discussion..... | 45 |

| | | |
|----------------|---|----|
| 2.4 | Materials and Methods..... | 28 |
| 2.4.1 | GBM cell cultures..... | 28 |
| 2.4.2 | Primary neuronal cultures..... | 29 |
| 2.4.3 | <i>In vitro</i> IMT model..... | 29 |
| 2.4.4 | Cell viability assays..... | 30 |
| 2.4.5 | <i>In vivo</i> GBM model and IMT..... | 31 |
| 2.4.6 | GBM tumor analysis..... | 32 |
| 2.4.7 | IMT electric field simulation..... | 33 |
| 2.4.8 | Magnetic resonance imaging..... | 33 |
| 2.4.9 | Statistical analysis..... | 34 |
| 2.5 | References..... | 49 |
| Chapter 3..... | | 53 |
| 3 | Diffuse Intrinsic Pontine Glioma Cells are Vulnerable to Low Intensity Electric Fields Delivered by Intratumoral Modulation Therapy ² | 53 |
| 3.1 | Introduction..... | 54 |
| 3.2 | Materials and Methods..... | 55 |
| 3.2.1 | Patient-derived DIPG cells..... | 55 |
| 3.2.2 | <i>In vitro</i> IMT model..... | 56 |
| 3.2.3 | IMT field simulation..... | 56 |
| 3.2.4 | Multi-modality treatment of DIPG cells..... | 56 |
| 3.2.5 | Cell viability assay..... | 57 |
| 3.2.6 | Flow cytometry..... | 57 |
| 3.2.7 | Statistical analysis..... | 58 |
| 3.3 | Results..... | 58 |
| 3.3.1 | IMT field mapping for <i>in vitro</i> DIPG cell treatment..... | 58 |
| 3.3.2 | Patient DIPG cells are vulnerable to low intensity IMT fields..... | 60 |
| 3.3.3 | IMT significantly enhances multi-modality treatment platforms for DIPG..... | 62 |
| 3.4 | Discussion..... | 64 |
| 3.5 | References..... | 67 |

| | |
|--|-----|
| Chapter 4..... | 71 |
| 4 Simulation and treatment of high-grade glioma with dynamically-oriented electric fields ³ | 71 |
| 4.1 Introduction..... | 72 |
| 4.2 Materials and Methods..... | 73 |
| 4.2.1 Glioma spheroid and organoid preparations | 73 |
| 4.2.2 Computer simulation of IMT electric fields | 75 |
| 4.2.3 Tumor viability assays | 76 |
| 4.2.4 <i>In vivo</i> IMT control studies..... | 77 |
| 4.2.5 Statistical Analysis..... | 77 |
| 4.3 Results..... | 78 |
| 4.3.1 Phase-shifting markedly enhances IMT electric field distribution | 78 |
| 4.3.2 Patient demographics and HGG specimens | 80 |
| 4.3.3 Evidence of HGG spheroid response to IMT | 80 |
| 4.3.4 Solid GBM organoids are highly sensitive to phase-shift IMT that does not injure normal brain parenchyma | 82 |
| 4.4 Discussion..... | 84 |
| 4.5 References..... | 88 |
| Chapter 5..... | 92 |
| 5 Discussion..... | 92 |
| 5.1 Summary of Major Results | 92 |
| 5.2 Experimental Limitations..... | 95 |
| 5.3 Future Directions | 96 |
| 5.4 Significance and Overall Conclusions | 98 |
| 5.5 References..... | 99 |
| Curriculum Vitae | 102 |

List of Tables

| | |
|--|----|
| Table 2-1. Spectrophotometric viability (MTT) analysis in patient GBM cells..... | 35 |
| Table 2-2. Individual flow cytometry measures of IMT response in patient GBM cells. | 38 |
| Table 2-3 Cumulative <i>in vivo</i> tumor burden in sham and IMT-treated GBM within the 15- animal cohort. | 43 |
| Table 3-1. Summary of flow cytometry data in patient DIPG cell samples | 62 |
| Table 4-1. Patient and tumor characteristics..... | 80 |

List of Abbreviations

| | |
|-----------|--|
| 1. GBM | Glioblastoma Multiforme |
| 2. IMT | Intratumoral Modulation Therapy |
| 3. DIPG | Diffuse Intrinsic Pontine Glioma |
| 4. HGG | High Grade Glioma |
| 5. CNS | Central Nervous System |
| 6. WHO | World Health Organization |
| 7. IDH1 | Isocitrate Dehydrogenase 1 |
| 8. EGFR | Epidermal Growth Factor Receptor |
| 9. PTEN | Phosphatase and Tensin Homolog |
| 10. PDGF | Platelet Derived Growth Factor |
| 11. TMZ | Temozolomide |
| 12. PFS | Progression Free Survival |
| 13. OS | Overall Survival |
| 14. RT | Radiation Therapy |
| 15. NCAM1 | Neural Cell Adhesion Molecule 1 |
| 16. GFAP | Glial Fibrillary Acidic Protein |
| 17. Olig2 | Oligodendrocyte Transcription Factor 2 |
| 18. MAP2 | Microtubule-Associated Protein 2 |
| 19. BBB | Blood Brain Barrier |
| 20. IRE | Irreversible Electroporation |
| 21. AEFs | Alternating Electric Fields |
| 22. TTFs | Tumor Treating Fields |
| 23. MTT | 3-(4,5-dimethylthiazol-2-yl)-2,5-diphenyltetrazolium bromide |
| 24. PI | Propidium Iodide |
| 25. DBS | Deep Brain Stimulation |
| 26. ZR | Zombie Red |
| 27. CED | Convection Enhanced Delivery |
| 28. PD | Parkinson's Disease |
| 29. EVH | Electric Field Volume Histogram |
| 30. BLI | Bioluminescence Imaging |
| 31. ICH | Intracranial Hemorrhage |
| 32. LITT | Laser Interstitial Thermal Therapy |
| 33. sEEG | Stereoelectroencephalography |

List of Figures

| | |
|---|----|
| Figure 2-1. Impact of intermediate frequency IMT on GBM cells <i>in vitro</i> | 36 |
| Figure 2-2. Flow cytometry measures of IMT response in patient GBM cells. | 37 |
| Figure 2-3. <i>In vivo</i> model to evaluate IMT in GBM..... | 39 |
| Figure 2-4. IMT attenuates locoregional GBM growth <i>in vivo</i> | 41 |
| Figure 2-5. Paired <i>in vivo</i> GBM responses to sham and IMT conditions..... | 42 |
| Figure 2-6. Image-based simulation of IMT electric fields. | 44 |
| Figure 2-7. Predicted relations between IMT electric field amplitude, radial field dimensions and extent of GBM region coverage in the present <i>in vivo</i> treatment model. | 45 |
| Figure 3-1. Computer simulation of the IMT model. | 59 |
| Figure 3-2. DIPG cells are highly susceptible to low intensity IMT. | 61 |
| Figure 3-3. IMT enhances apoptosis and death fractions in DIPG cell cultures. | 61 |
| Figure 3-4. IMT significantly augments multi-modality treatment platforms for DIPG..... | 63 |
| Figure 4-1. Transition from single to multiple stimulating electrodes with phase-shift output enhances electric field coverage. | 79 |
| Figure 4-2. Phase-shift IMT reduces patient HGG spheroid viability..... | 81 |
| Figure 4-3. BLI reveals the robust impact of IMT in patient-derived HGG spheroids. | 82 |
| Figure 4-4. Patient GBM organoids are highly sensitive to dynamically-oriented electric fields..... | 83 |
| Figure 4-5. Multi-electrode phase-shift IMT does not produce overt injury non-neoplastic brain organoids..... | 83 |

Figure 4-6. Multi-electrode phase-shift IMT does not produce overt injury in the normal living brain..... 84

Chapter 1

1 General Introduction

1.1 Glial Tumors

Glial tumors are primary malignant tumors of the central nervous system (CNS). The World Health Organization (WHO) categorizes these tumors as diffuse astrocytic tumors, other astrocytic tumors, oligodendroglia tumors, and other gliomas. Glial tumors arise from the glial cells within the brain such as astrocytes, oligodendrocytes, and ependyma cells [Louis, 2016; Rushing, 2021]. An emerging hypothesis suggest that progression of glial tumors is driven by a small subpopulation of tumor stem cells, termed cancer stem cells [Das, 2008]. These cells likely arise from mutations in neural progenitor cells and demonstrate the capability to self-renew, proliferate, and give rise to multiple neuroepithelial lineages [Cahill, 2018]. In Europe and North America, glial tumors have an incidence of approximately 21.5/10,000 people per year [Louis, 2016; Ostrom QT 2016], with men having a higher risk of developing glioma than women [McKinley, 2000]. The WHO describes a systematic method for grading CNS tumors from Grade I-IV to predict the biological behavior, choice of therapy, and prognosis [Louis, 2016; Rushing, 2021]. Low-grade gliomas encompass grades I and II which generally have low proliferative potential and are associated with favorable patient outcomes. Grade I gliomas may be cured with surgical resection and are associated with long-term survival [Louis, 2016]. Grade II gliomas are also usually relatively slow growing; however, some can infiltrate into the surrounding brain parenchyma and transform into high grade tumors. High-grade gliomas (HGG) include grade III anaplastic astrocytoma and grade IV glioblastoma (GBM). HGGs display histological evidence of diffuse malignancy, nuclear atypia, brisk mitotic activity, and necrosis. Molecular diagnostics in CNS tumor classification has identified tumor families grouped according to genetic mutations, such as in genes for isocitrate dehydrogenase (IDH) and Histone H3. These molecular signatures have provided predictive prognostics, molecular biomarkers, and led to the refinement of glioma classification [Masui, 2016; Fan, 2021]. GBM accounts for 60-70% of HGGs in adults, the other 30-40% is made up of anaplastic astrocytoma (15%) and

oligodendroglial tumors (e.g., oligodendrogliomas, oligoastrocytoma;10%). Another ~10% includes anaplastic variants of ependymoma and ganglioglioma [Rushing, 2021]. The median age of onset of HGGs in adults is 45 years and 60 years for Grade III and Grade IV tumors, respectively. Approximately 90% of HGG cases are *de novo* in nature [Ostrom, 2014] with the remaining 10% of tumors corresponding to a previous history of lower grade glioma transforming into HGG [Louis, 2016]. In pediatric neuro-oncology, HGG are the most common CNS neoplasms in children between the ages 10-15 years old [Bondy, 2008], and represent approximately 8–12% of all pediatric CNS tumors [Fangusaro, 2012]. Brainstem gliomas such as diffuse intrinsic pontine glioma (DIPG) affect approximately 300 children in the United States per year and are the leading cause of death in children with brain tumors [Williams, 2020; Kaatsch 2001].

1.1.1 Glioblastoma

Glioblastoma (GBM) represents the most common primary brain tumor in adults, accounting for approximately 15% of intracranial neoplasms and 45-50% of all primary malignant brain tumors. In Europe and North America, the incidence of GBM is approximately 4/100,000 of the population [Holland, 2000]. GBM is characterized by a diffuse and infiltrative growth pattern and will often cross the corpus callosum into the contralateral hemisphere, rendering the tumor inoperable. GBM rarely invades into the subarachnoid space and metastases beyond the CNS are seldom reported [Wen, 2008]. Histologically, GBM displays brisk mitotic activity, increased cellularity, nuclear atypia, and a wide range of intra and intertumoral heterogeneity [Berens, 1999] The presence of tissue necrosis is also commonly found in GBM.

GBM can occur *de novo* (95%) or, less commonly, progress from a lower grade glioma [Ohgaki, 2004]. It may be further subdivided into (1) isocitrate dehydrogenase (IDH) wildtype (about 90% of cases), which is more often associated with primary or *de novo* GBM [Louis, 2016]; (2) IDH1 R132H mutant (about 10% of cases) is more often associated with a previous history of lower grade diffuse glioma with transformation to GBM in younger patients [Rushing, 2021]. IDH-wildtype GBM may be characterized by

gene amplification of epidermal growth factor receptor (EGFR), loss of heterozygosity (LOH) of chromosome 10q containing phosphatase and tensin homolog (PTEN) genes, and deletion of p16 [Yan, 2009; Davis, 2016]. IDH-mutant GBM tumors may harbor mutations in TP53 and retinoblastoma (Rb) genes, overexpression of genes for platelet-derived growth factor A and platelet-derived growth factor receptor alpha (PDGF α /PDGFR α), and LOH of 19q, however there may be overlap in the genetic signatures with IDH-wildtype [Yan, 2009; Davis, 2016]. The molecular characterization of GBM is a complex emerging science, and the role of genes in classifying GBM subtypes remains poorly understood. Studies have reported that the IDH1 mutation is associated with both increased overall and progression-free survival in patients with GBM [Yan, 2009].

The presentation of newly diagnosed GBM can vary widely depending on the size, location, and the anatomical structures affected within the brain [Alexander, 2017; Young, 2015]. Patients with GBM often present with subacute neurological symptoms and may have signs of increased intracranial pressure, including headache and focal or progressive neurologic deficits [Hanif, 2017]. Initial diagnosis is made utilizing medical imaging, including computed tomography (CT) and magnetic resonance imaging (MRI).

Treatment of GBM requires a multidisciplinary approach. The current standard of care involves maximal safe surgical resection with adjuvant radiotherapy and temozolomide (TMZ) chemotherapy. The main factors influencing the feasibility and extent of GBM resection include involvement of eloquent CNS regions, patient age and comorbidities. Extensive surgical resection of GBM may be limited when these tumors present in eloquent brain regions, such as in areas implicated in motor function, sensation, vision, and speech production. Even when radical surgical resection is possible, it is not curative due to tumor cell invasion into the surrounding brain structures. The GBM cells that are not captured by resection inevitably initiate tumor recurrence; therefore, local tumor control with surgery remains poor (Wilson, 2014). Though surgical resection is not curative, multiple studies have demonstrated that aggressive surgical resection when possible is associated with a significant increase in both progression-free survival (PFS) and overall survival [Kuhnt, 2011; Roder, 2014; Keles, 1999; Lacroix 2001; Mukherjee,

2011; Stummer, 2006]. Surgery is also an option for some patients following disease recurrence. Additional surgery can help alleviate mass effect and symptoms of recurrent GBM; however, is generally a palliative procedure and may not enhance OS [Lukas, 2019; Bloch, 2012; McGirt, 2009; Brandes, 2013; Franceschi, 2015].

For many patients, major surgical resection is not feasible, and these patients may be offered partial resection or stereotactic biopsy, which may be followed by chemotherapy and radiotherapy. Depending on the degree of resection, the procedure can reduce intracranial pressure and provide symptom palliation. The degree to which partial resection increases overall survival is still debated and likely case dependent [Young, 2015]. Stereotactic biopsy may be offered when tumors are not safe to resect (e.g., infiltrating eloquent brain regions), or in patients with high-risk medical comorbidities or who choose not to undergo a major resective operation. Stereotactic biopsy is indicated to confirm diagnosis but is not an effective tumor treatment in and of itself. Optimal standard of care including major resection and chemoradiation offers a median survival of 14-16 months, whereas untreated GBM typically claims the lives of patient within several weeks to months of diagnosis [Hanif, 2017]. Following maximal safe surgical resection or biopsy, the patient commonly receives adjuvant radiation therapy (RT) with a dose of 60 Gy in 30 fractions. RT beyond 60 Gy showed no additional survival benefits and was associated with increased toxicity [Barani, 2015].

Concurrent TMZ is now a first line chemotherapy for GBM in many regions and developed in part from a pivotal phase III clinical trial demonstrated that RT with concomitant TMZ chemotherapy was more effective than RT alone [Stupp, 2005]. The clinical trial showed that patients who received RT with concurrent TMZ had a median survival of 14.6 months compared to 12.1 months seen with RT alone. TMZ is typically given at a dose of 75 mg/m² every day during radiation therapy, followed by a 6-week rest period. TMZ maintenance dosing may then be continued for six 1-week cycles dosed at 150-200 mg/m² daily for five days, followed by two days of rest [Barani, 2015]. Despite maximal multimodality therapy, approximately 70% of patients will experience disease recurrence and progression within one year of diagnosis [Stupp, 2005]. The

prognosis for GBM patients remains dismal, with median survival of only 14 months [Louis, 2007] and a 5-year survival of less than 5% [Ostrom, 2014; Batash, 2017].

1.1.2 Diffuse Intrinsic Pontine Glioma

Diffuse intrinsic pontine glioma (DIPG) represents ~15% of all pediatric brain tumors and ~80% of pediatric brainstem gliomas, with an incidence of 0.14 per 100,000 [Lu, 2019]. These patients generally present between the ages of 5 and 11 years old with long tract signs, ataxia, and cerebrospinal fluid obstruction developing over a period of several months. In most centres, radiographic diagnosis without biopsy is made when a *de novo* tumor is delineated in the midline of the neuraxis, most commonly in the pons [Williams, 2020]. The histopathology of pediatric HGGs overlaps with those of their adult counterparts; however, DIPGs have distinct genetic alterations. Most tumor cells within a DIPG harbour NCAM1, S100, and Olig2 mutations. Other mutations such as in GFAP, MAP2, NeuN, and p53 are variable [Wu, 2012; Johung, 2017]. Subgroups of DIPG express mutations in histone H3.3 (gene name *H3F3A*), K27M, or G34V/R. These mutations have also been shown to be molecular drivers of pediatric GBM corresponding to WHO grade IV and suggest a worse prognosis [Johung, 2017; Karremann 2018].

Due to diffuse infiltration of DIPG within eloquent brain regions, surgical resection is often not safely feasible. The mainstay treatment includes steroid therapy at the time of diagnosis, which aims to improve neurological symptoms by reducing tumor-associated edema. Patients then undergo fractionated radiation therapy (RT) typically to achieve a total dose of 54 Gy in 30 fractions [Gallitto, 2019]. RT is a palliative treatment that improves neurological symptoms in ~80% of patients and prolongs survival by 2-3 months. Unfortunately, no chemotherapy drugs to date are known to have an impact on survival. These limited therapies offer patients a median survival of 9 months and fewer than 10% of children survive beyond 2 years [Karremann, 2018; Vanan, 2015; Fonseca, 2021].

1.2 Electrotherapies for HGG

The rationale to develop electrotherapeutic strategies for GBM is based on a critical need for new treatment approaches and the demonstrated vulnerability of rapidly proliferating neoplastic cells due to disruptions in the electrochemical environment [Pless, 2011; Davies, 2013]. Various types of tumor cells exposed to appropriate electrical stimuli may also be sensitized to chemotherapy and radiation paradigms [Cadossi, 2014; Kim, 2016]. The therapeutic action of electrotherapy in cancer is likely mediated through various cellular mechanisms that are contingent upon the frequency and amplitude of the applied electric fields. For example, electrical stimulation applied to cells in culture may interfere with the naturally occurring weak electric field present within cells. The cells use these fields to arrange charged molecules, such as microtubules that form the spindle apparatus during cytokinesis. The disruption of this process can impede spindle formation and proliferation of tumor cells [Kirson et al., 2004]. Other potential mechanisms of the anti-cancer effect include disruption of ion homeostasis, lipid bilayer integrity, and gene regulation. It is likely that each of these hypothesized mechanisms trigger unique signaling cascades resulting in cell death through apoptosis or necrosis [Cemazar, 2012; Weaver, 2012]. In the brain, highly proliferative HGG possess a greater susceptibility to electrochemical perturbations compared to slowly dividing or post-mitotic neural cells [Xu, 2016; Krison, 2004; Krison, 2014; Stuup, 2017]. The relative selectivity likely reflects the brisk mitotic rate and metabolic instability of neoplastic cells and presents a promising niche for electrotherapeutic development.

1.2.1 Putative Applications of Electrotherapy in Cancer

1.2.1.1 Electrochemotherapy

It is well established that administration of electric pulses can reversibly permeabilize cells to allow molecules that are normally membrane impermeant, such as hydrophilic or large molecules, to enter the cytosol [Neumann, 1988; Belehradec, 1993; Orłowski, 1988]. The earliest studies demonstrating that electrical stimulation could potentiate the effects of chemotherapeutics were done *in vivo* in rats implanted with hepatocellular

carcinoma. The combination of high-voltage electrical impulses (5 kV/cm, 2 msec) administered following bleomycin (a poorly membrane-permeant cytotoxic agent) significantly decreased tumor cell viability [Glass, 1996]. In 1988, Orłowski et al. demonstrated that *in vitro* electroporation of DC-3F sarcoma cells enhanced the uptake and cytotoxicity of bleomycin. Combining bleomycin with reversible electroporation increases the cytotoxicity of bleomycin by up to 10,000-fold [Okino, 1987].

Numerous clinical studies have been conducted using electrochemotherapy as a potential treatment for different types of cancer. An early Phase 1/2 clinical trial demonstrated that four or eight 100-microsecond pulses of 1300 V/cm administered via external electrodes in combination with 10 mg/m² bleomycin was safe and well-tolerated, with anti-tumor effects demonstrated in nodules of head and neck squamous cell carcinomas [Mir, 1991]. Bleomycin-mediated electrochemotherapy has been shown to be clinically effective in the treatment of basal cell carcinoma [Quaglino, 2008] subcutaneous metastatic breast adenocarcinomas [Campana, 2008], metastases of malignant melanoma [Glass, 1996; Quaglino, 2008; Campana, 2014], soft tissue sarcomas, [Belehradek, 1993] and pancreatic adenocarcinoma [Granataa, 2015]. Thus, electrochemotherapy is effective in the treatment of cutaneous, subcutaneous, and visceral tumors. Electrochemotherapy is continuing to be developed to treat deeper tumors, such as those of the bone and internal organs, using a pulse generator and long needle electrodes [Edhemovic, 2011].

Electrochemotherapy can be individualized based on the shape and the size of the tumor [Pavlihaa, 2012], and mathematical models can assist in calculating specific electrical pulse parameters to induce maximal necrosis inside the tumor mass, without affecting the normal peripheral tissue [Edhemovic, 2011; Pavlihaa, 2012]. Mathematical modeling can also predict the degree of blood brain barrier (BBB) disruption for adequate transfer of chemotherapeutic agents to the tumor mass [Hjouj, 2012], suggesting electrochemotherapy may be a promising treatment for difficult to reach tumors in the brain, such as GBM.

1.2.1.2 Irreversible electroporation

Electroporation utilizes high voltage electrical pulses (hundreds to thousands of V/cm), to enhance membrane permeability via the creation of nanoscale pores. [Weaver, 2000; Ivorra, 2010]. Reversible electroporation has been used for years to enhance uptake of chemotherapeutic drugs; however, higher intensity electroporation can in fact produce irreversible pore formation as a monotherapy to destroy cells [Weaver, 1995]. This technique is termed irreversible electroporation (IRE). IRE can destroy unwanted tissues, similar to selective ablation therapies, such as radiofrequency, cryosurgery, or focused ultrasound [Rubinsky, 2007]. IRE leads to cell death via creation of nanoscale aqueous pores, resulting in membrane lysis, loss of homeostasis, loss of organelles, or influx of cytotoxic molecules [Weaver, 1995; Cemazar, 2012]. IRE can selectively ablate cancerous cells both *in vitro* and *in vivo* and has been tested clinically in tumors of the liver, pancreas, kidney, lung, lesser pelvis, and lymph nodes [Scheffer, 2014].

1.2.1.3 Electrogene Therapy

The clinical use of gene therapies in cancer has been limited primarily due to the lack of efficient and effective delivery methods for the genetic material. Similar to use of electrical stimulation to enhance uptake of chemotherapeutics, electroporation or electro-permeabilization techniques have been successfully utilized to deliver genetic material to solid tumors by transiently permeabilizing the plasma membrane [Heller, 1996; Nishi, 1996]. These transiently formed pores act as non-specific aqueous channels and allow for the passive diffusion of molecules less than 4 kDa across the plasma membrane, including chemotherapeutics and siRNA [Bureau, 2000]. Larger (greater than 4 kDa) or charged molecules, such as plasmid DNA (pDNA), can also enter the cell when the U_m reaches 0.2-1 V through alternate mechanisms. pDNA is then actively transported to the nucleus by cytoskeletal transport and can be expressed or incorporated into the host genome [Vaughan, 2006]. There are notable challenges to the utilization of gene electrotherapy in treatment of GBM. A principle of gene electrotherapy is the injection and incorporation of DNA at the expected site of gene transfer. As GBM is a diffuse neoplasm, this may limit the efficacy to an area of local administration. Furthermore, much work needs to be done regarding the optimal electroporation parameters needed to

permeabilize glial cells and facilitate gene transfer prior to developing brain-specific protocols for human patients with GBM.

1.2.1.4 Alternating Electric Fields

In living cells, natural electric fields contribute to a host of physiological processes. For example, polar molecules, such as microtubules, will orient along the line of a uniform electric field, and when the field is not uniform, molecules move towards higher field intensity in a process known as dielectrophoresis [Clague, 2005; Gonzalez; 2005]. The application of low-voltage, alternating electric fields (AEFs) induces ionic flow oscillations and dipole rotations that disrupt the organization and function of these molecules [Giladi, 2015].

In vitro, AEFs have a strong inhibitory effect on growth and proliferation of many cancers cell lines, including human GBM cells [Kirson, 2004; Kirson, 2007]. GBM cells exposed to AEFs in culture can also potentiate the effects of chemotherapeutics [Kirson, 2009] and ionizing radiation [Kim et al., 2016]. Preclinical *in vivo* studies have also demonstrated that AEFs can significantly inhibit tumor growth in a Fischer rat F98 glioma model [Kirson et al., 2007]. The prevailing theory for the mechanism of AEFs is that in cells, polar molecules orient themselves along the lines of a uniform electric field. When this field is not uniform, polar molecules move towards the higher field intensity. It is hypothesized that low-intensity (1-3 V/cm), intermediate-frequency (100-300 KHz) AEFs applied to cancer cells act on polarized microtubules and disrupt spindle formation during metaphase. The resulting dielectrophoretic movement of polar molecules organized along the weak electromagnetic field of the cell during cytokinesis leads to mitotic arrest, membrane blebbing, and cell death via apoptosis [Kirson, 2007]. In support of this hypothesis, microphotographic images of cells exposed to AEFs demonstrate prolonged mitosis, nuclear rotation, and apoptotic cell death [Kirson, 2004; Tuszynski, 2016; Wenger, 2016]. However, emerging evidence of differential expression of voltage gated membrane channels, such as big potassium channels and pannexins, may be implicated in apoptotic pathway initiation [Wei, 2015; Penuela, 2012].

AEFs have now been translated into clinical use under the term Tumor Treating Fields (TTFs). TTFs are low-intensity, intermediate-frequency, alternating electric fields delivered across the entire cranium via external, scalp-mounted electrode arrays. A phase III randomized clinical trial demonstrated the safety and efficacy of TTFs used during maintenance treatment with TMZ following chemoradiation therapy for GBM. This clinical trial treated patients with a maintenance therapy of TMZ (150-200 mg/m²/day) or TMZ + TTFs delivered for 18 hours/day for 28 days via 4 transducer arrays placed onto the shaved scalp connected to a portable pulse generator. Progression-free survival was 6.7 months in the TMZ + TTF versus 4 months in the TMZ alone group, and overall survival was 20.9 months in the TMZ + TTF group versus 16 months for TMZ alone [Stupp, 2017]. The results of this trial indicate the promise of TTFs in concert with standardized GBM therapy. Patients who received TTFs demonstrated improved cognitive and emotional function compared to those treated with chemotherapy and did not display nausea, vomiting, fatigue, pain, and constipation [Lacouture, 2014]. This novel treatment has been approved by the FDA for clinical use in the treatment of GBM [Stupp, 2017; Rominiyi, 2021; Rehman, 2015; Sampson, 2015]. At the time of this writing, TTFs are not approved by Health Canada and have not been widely implemented into GBM treatment in North America. There remain many questions about the true efficacy and utility in the clinical setting and several well-described shortcomings of TTFs have been published are likely responsible for limited efficacy and both patient and clinician acceptance of this technology to date [Wenger, 2018; Lacouture, 2014; Mittal, 2017].

1.3 Intratumoral Modulation Therapy

It is clear that cancer cells are often highly sensitive to low intensity perturbations in the electrical environment. However, the translation of this knowledge and approach to the clinical care of brain cancer patients has presented a major challenge. In efforts to maximize impact, safety and acceptance, our group has been pioneering the first brain-implantable, low intensity electric field cancer therapy, called Intratumoral Modulation

Therapy (IMT). IMT is being developed with the premise that internalized electric fields will exploit HGG electrosensitivity with fewer limitations than externally applied delivery systems [Wenger, 2018; Lacouturea, 2014; Mittal, 2017]. Still in the proof-of-concept stage, the vision of IMT encompasses the delivery of therapeutic electric fields via MRI-compatible bioelectrodes strategically positioned within tumor-affected brain regions. Compared to the externally delivered electric fields, IMT is delivered by indwelling hardware that provides focused and titratable therapeutic electric fields directly to CNS tumors and is not diminished by delivery through extra-cerebral tissues such as the scalp, skull, meninges and uninvolved brain. A significant strength of IMT is the ability to place the electrodes anywhere in the CNS, allowing for the effective capture of infratentorial and brainstem disease which is inaccessible to scalp-mounted delivery systems [Ghiaseddin, 2020]. In addition, the IMT system would be totally concealed to provide continuous, perpetual therapy to treat unresectable tumors, residual tumors or tumor resection beds to prevent recurrence. The hope is that IMT will attenuate tumor growth, bolster multi-modality treatment platforms, and thereby improve patient outcomes and quality of life.

Prior to my joining this project, the research team had already produced substantial proof of concept data that demonstrated efficacy of IMT *in vitro*, with preferential impact on GBM compared to non-neoplastic neural cells, and a significant improvement in therapeutic impact when IMT was combined with chemotherapy or gene-targeting approaches [Xu, 2016]. Our lab established an *in vitro* IMT model which delivered continuous, low-frequency, low-intensity stimulation (130Hz, 4V) to GBM cell lines and patient-derived GBM cells [Xu, 2016]. The model consisted of culture dishes fashioned with clinical grade, platinum-based, reference strip electrodes (AD-Tech, Racine, WI,USA) around the periphery and a central stimulating electrode (Medtronic Ltd., Brampton, ON, Canada). Cell monolayers were then seeded to the bottom of the well and the electric fields were delivered by connecting the electrodes to a waveform generator with the option to produce a myriad of stimulation parameters. IMT caused significant cell death (>40%) in both human glioma LN229 cells and patient derived GBM cells, without affecting the viability of post-mitotic neurons [Xu, 2016]. It was also demonstrated that the mechanism of cell death by IMT was largely apoptotic. When IMT

was applied with concomitant TMZ, GBM cell death increased to 70% compared to 30% with TMZ alone. Finally, when IMT was administered in combination with siRNA targeted to the pro-tumor chaperone, HSP27, uptake was increased and cell death enhanced by 65% compared to 30% with HSP27 knockdown alone [Xu, 2016]. However, the low-frequency stimulation settings used in these early studies mirrored those used in clinical neuromodulation methods and were known to entrain neural systems [McCairn, 2015]. The research team raised concern that such settings would have a high chance of creating off-target neural side effects when treating brain cancer and so sought alternative parameters that would be out of the range of neural entrainment. It was at this point that I joined the team and sought to contribute to the early development of exploratory studies investigating the efficacy and delivery strategies for new IMT strategies.

1.4 Hypotheses and Objectives

My project took multiple facets that aimed at advancing our knowledge of IMT efficacy and improved delivery strategies for HGG. At the outset of this thesis, the team had confirmed GBM sensitivity to directly-applied, non-ablative electrical pulses, using low-frequency (i.e., Hertz, Hz) stimulation that posed risk of neuronal entrainment and off-target neurological side effects if applied within eloquent CNS areas. ***We hypothesized that intermediate frequency (i.e., kHz) stimulation above the known neural entraining range would provide a safe, effective niche for therapeutic development against GBM while remaining inert to non-neoplastic cells.*** The objective of Chapter 2 was to evaluate a novel profile of *in vitro* IMT parameters using intermediate-frequency (200 kHz) stimulation with a sinusoidal waveform to deliver continuous, low-intensity (± 2 V), alternating electric fields in order to provide maximal tumor cell disruption. Following *in vitro* validation of intermediate-frequency IMT, the next step was to translate the treatment paradigm *in vivo*; however, cancer models with implanted hardware for the delivery of electric fields do not exist. ***We hypothesized that F98 tumors grown in immunocompetent Fischer rats would be vulnerable to IMT delivered electric fields.*** We aimed to develop and implement a completely novel IMT system in a syngeneic F98

Fischer rat model. The results in Chapter 2 demonstrated the robust efficacy of IMT *in vitro* and limited efficacy *in vivo* and prompted the exploration of IMT impact in additional primary brain cancers in Chapter 3. ***We hypothesized that IMT electric fields would provide an effective mean of disease control for DIPG and sensitize the cancer cells to chemoradiotherapy.*** The objective of Chapter 3 was to determine the vulnerability of patient-derived DIPG cells to low-intensity electric fields delivered using our established IMT protocol. The impact of IMT on DIPG resistance to conventional radiation and chemotherapy options was also investigated. To explain the limited efficacy observed *in vivo* observed in Chapter 2, we initiated a collaboration with Dr. Eugene Wong in the Department of Medical Biophysics to computationally investigate IMT electric fields. These investigations revealed the inadequate distribution of IMT electric fields using our single electrode delivery system that had been used so far *in vitro* and *in vivo*. We also know that multiple electrodes are commonly implanted in standard neurosurgical operations performed for movement disorders, epilepsy and pain management. Our IMT data and the existing clinical experience in non-cancer therapies led us to ***the hypothesis that multi-electrode IMT would maximize electric field distribution across targeted tumor areas and provide a more appropriate platform to develop translation models for HGG care.*** The objective in Chapter 4 was to develop and validate a completely novel multiple electrode IMT system and validate the electric field delivery and efficacy in customized 3-dimensional human GBM spheroid and organoid preparations. I also had the privilege of comparing the impact of IMT, for the first time, in primary GBM and normal brain organoids harvested directly for human patients undergoing real-time neurosurgical procedures.

1.5 References

1. Louis, D., Perry, A., Reifenberger, G. (2016). The 2016 World Health Organization Classification of Tumors of the Central Nervous System: a summary. *Acta Neuropathol.* 131:803–820. DOI 10.1007/s00401-016-1545-1
2. Louis, E. (2021) WHO classification of tumors of the nervous system: preview of the upcoming 5th edition. *Acta Neuropathol.* 14:188–191. doi.org/10.1007/s12254-021-00680-x
3. Das, S., Srikanth, M., Kessler, J. (2008) Cancer stem cells and glioma. *Nat Rev Neurol.* 4:427–435. doi.org/10.1038/ncpneuro0862
4. Cahill, D., Turcan, S. (2018) Origin of Gliomas. *Semin Neurol.* 38(1):5-10. doi: 10.1055/s-0037-1620238
5. Ostrom, Q., Gittleman, H., Xu, J., et al. (2016) CBTRUS statistical report: primary brain and other central nervous system tumors diagnosed in the United States in 2009-2013. *Neuro Oncol.* 18(Suppl 5):v1–v75.
6. Matteoni, S., Abbruzzese, C., Villani, V., et al (2020) The influence of patient sex on clinical approaches to malignant glioma. *Cancer Lett.* 1;468:41-47.
7. Masui, K., Mischel, P., Reifenberger, G. (2016) Molecular classification of gliomas. *Handb Clin Neurol.* 134:97-120. doi: 10.1016/B978-0-12-802997-8.00006-2. PMID: 26948350
8. Fan, F., Zhang, H., Dai, Z. et al. (2021) A comprehensive prognostic signature for glioblastoma patients based on transcriptomics and single cell sequencing. *Cell Oncol.* doi.org/10.1007/s13402-021-00612-1
9. Ostrom, Q., Bauchet, L., Davis, F., et al. (2014) The epidemiology of glioma in adults: a "state of the science" review. *Neuro Oncol.* 16(7):896-913. doi: 10.1093/neuonc/nou087

10. Bondy, M., Scheurer, M., Malmer, B. (2008). Brain tumor epidemiology: consensus from the Brain Tumor Epidemiology Consortium. *Cancer*. 113:1953–1968.
11. Fangusaro, J., (2012) Pediatric high grade glioma: a review and update on tumor clinical characteristics and biology. *Front. Oncol.* doi.org/10.3389/fonc.2012.00105
12. Williams, J., Young, C., Vitanza, N., et al (2020) Progress in diffuse intrinsic pontine glioma: advocating for stereotactic biopsy in the standard of care. *Neurosurgical Focus*. 48(1):E4.
13. Kaatsch, P., Rickert, C., Köhl, J., et al. (2001) Population-based epidemiologic data on brain tumors in German children. *Cancer*. 92: 3155-3164. doi.org/10.1002
14. Weller. M., Wick, W., Aldape, K., et al. (2015) Glioma. *Nat Rev Dis Primers*. 16(1):15017. doi: 10.1038/nrdp.2015.17
15. Tucha, O., Smely, C., Preier, M., et al. (2000) Cognitive Deficits before Treatment among Patients with Brain Tumors. *Neurosurgery*. 47(2):324–334. doi.org/10.1097/00006123-200008000-00011
16. Chang, S., Parney, I., Huang, W., et al. (2005) Patterns of Care for Adults With Newly Diagnosed Malignant Glioma. *JAMA*. 2005;293(5):557–564. doi:10.1001/jama.293.5.557
17. Holland, C. (2000). Glioblastoma multiforme: the terminator. *Proceedings of the National Academy of Sciences of the United States of America*. 97(12):6242–6244.
18. Wen, P., Kesari, S. (2008). Malignant Gliomas in Adults. *N Engl J Med*. 359:1850. doi.org/10.1056/NEJMc086380
19. Berens, M., Giese, A. (1999) “...those left behind.” Biology and oncology of invasive glioma cells. *Neoplasia*. 1(3):208–19. doi.org/10.1038/sj.neo.7900034

20. Ohgaki, H., Dessen, P., Jourde, B. (2004). Genetic pathways to glioblastoma: a population-based study. *Cancer Research*, 64(19):6892–6899. doi.org/10.1158/0008-5472.can-04-1337
21. Yan, H., Parsons, D., Jin, G., et al. (2009) IDH1 and IDH2 mutations in gliomas. *N Engl J Med* 19;360(8):765-773. doi: 10.1056/NEJMoa0808710
22. Davis, M (2016). Glioblastoma: Overview of Disease and Treatment. *Clin J Oncol Nurs*. 20(5 Suppl):S2-S8. doi:10.1188/16.CJON.S1.2-8
23. Alexander, B., Cloughesy, T. (2017) Adult Glioblastoma. *Journal of Clinical Oncology*. 35:21:2402-2409
24. Young, R., Jamshidi, A., Davis, G., et al. (2015) Current trends in the surgical management and treatment of adult glioblastoma. *Ann Transl Med*. 3(9):121. doi:10.3978/j.issn.2305-5839.2015.05.10
25. Hanif, F., Muzaffar, K., Perveen, K., et al. (2017) Glioblastoma Multiforme: A Review of its Epidemiology and Pathogenesis through Clinical Presentation and Treatment. *Asian Pac J Cancer Prev*. 18(1):3-9. doi:10.22034/APJCP.2017.18.1.3
26. Wilson, T., Karajannis, M., Harter, D. (2014) Glioblastoma multiforme: State of the art and future therapeutics. *Surg Neurol Int*. 5:64. doi:10.4103/2152-7806.132138
27. Kuhnt, D., Becker, A., Ganslandt, O., et al. (2011) Correlation of the extent of tumor volume resection and patient survival in surgery of glioblastoma multiforme with high-field intraoperative MRI guidance. *Neuro-Oncology*. 13(12):1339–1348. doi.org/10.1093/neuonc/nor133
28. Roderac, C., Bisdasbc, s., Ebnera, F., et al. (2014) Maximizing the extent of resection and survival benefit of patients in glioblastoma surgery: High-field iMRI versus conventional and 5-ALA-assisted surgery. *EJSO*. 40(3):297-304.

29. Keles, G., Anderson, B., Berger, M., et al. (1999) The effect of extent of resection on time to tumor progression and survival in patients with glioblastoma multiforme of the cerebral hemisphere. *Surgical Neurology*. 52(4):371-379.
30. Lacroix, M., Abi-Said, D., Fourney, D., et al. (2001). A multivariate analysis of 416 patients with glioblastoma multiforme: prognosis, extent of resection, and survival. *Journal of Neurosurgery*. 95(2):190-198
31. Grossman, R., Mukherjee, Chang, D., et al. (2011) Preoperative Charlson Comorbidity Score Predicts Postoperative Outcomes Among Older Intracranial Meningioma Patients. *World Neurosurgery*. 75(2):279-285.
32. Stummer, W., Pichlmeier, U., Meinel, T., et al. (2006) Fluorescence-guided surgery with 5-aminolevulinic acid for resection of malignant glioma: a randomised controlled multicentre phase III trial. *The Lancet Oncology*. 7(5):392-401.
33. Lukas, R., Wainwright, D., Ladomersky, E., et al. (2019) Newly Diagnosed Glioblastoma: A Review on Clinical Management. *Oncology*. 13;33(3):91-100
34. Bloch, O., Han, J., Cha, S., et al. (2012). Impact of extent of resection for recurrent glioblastoma on overall survival. *Journal of Neurosurgery*. 117(6):1032-1038.
35. McGirt, J., Chaichana, L., Gathinji, M., et al. (2009). Independent association of extent of resection with survival in patients with malignant brain astrocytoma. *Journal of Neurosurgery*. 110(1):156-162.
36. Brandes, A., Bartolotti, M., & Franceschi, E. (2013) Second surgery for recurrent glioblastoma: advantages and pitfalls. *Expert Review of Anticancer Therapy*. 13:5:583-587. DOI: 10.1586/era.13.32
37. Franceschi, E., Bartolotti, M., Tosoni, A., et al. (2015) The Effect of Re-operation on Survival in Patients with Recurrent Glioblastoma. *Anticancer Research*. 35(3):1743-1748.

38. Barani, I., Larson, D. (2015) Radiation Therapy of Glioblastoma. *Current Understanding and Treatment of Glioma*. 49-73. doi.org/10.1007/978-3-319-12048-5_4
39. Stupp, R., Mason, W., van den Bent, M., et al. (2005). Radiotherapy plus concomitant and adjuvant temozolomide for glioblastoma. *The New England Journal of Medicine*. 352(10):987–996. doi.org/10.1056/NEJMoa043330
40. Louis, D., Ohgaki, H., Wiestler, O., et al. (2007). The 2007 WHO classification of tumours of the central nervous system. *Acta Neuropathologica*. 114(2);97–109. doi.org/10.1007/s00401-007-0243-4
41. Batash, R., Asna, N., Schaffer, P., et al. (2017) Glioblastoma Multiforme, Diagnosis and Treatment; Recent Literature Review. *Current Medicinal Chemistry*. 24(27):3002-3009(8)
42. Lu, V., Welby, J., Mahajan, A., et al. (2019) Reirradiation for diffuse intrinsic pontine glioma: a systematic review and meta-analysis. *Childs Nerv Syst*. 35:739–746 2019. doi.org/10.1007/s00381-019-04118-y
43. Wu, G., Broniscer, A., McEachron, T., et al. (2012) Somatic histone H3 alterations in pediatric diffuse intrinsic pontine gliomas and non-brainstem glioblastomas. *Nat Genet*. 44(3):251-253. doi:10.1038/ng.1102
44. Johung, T., Monje, M. (2017) Diffuse intrinsic pontine glioma: new pathophysiological insights and emerging therapeutic targets. *Curr Neuropharmacol* 15(1):88–97
45. Karremann, M., Gielen, G., Hoffmann, M., et al. (2018) Diffuse high-grade gliomas with H3 K27M mutations carry a dismal prognosis independent of tumor location. *Neuro-Oncology*. 20(1):123–131. doi.org/10.1093/neuonc/nox149
46. Gallitto, M., Lazarev, S., Wasserman, I., et al. (2019) Role of Radiation Therapy in the Management of Diffuse Intrinsic Pontine Glioma: A Systematic Review. *Advances in Radiation Oncology*. 4(3):520-531.

47. Vanan, M., Eisenstat, D. (2015) DIPG in children – what can we learn from the past? *Front. Oncol.* doi.org/10.3389/fonc.2015.00237
48. Fonseca, A., Bouffet, E. (2021) Brainstem gliomas ... the devil is in the details. *Neuro-Oncology.* 23(6):869–871. doi.org/10.1093/neuonc/noab064
49. Pless, M., Weinberg, U. (2011) Tumor Treating Fields: Concept, Evidence And Future. *Expert Opinion on Investigational Drugs.* 20:8:1099-1106. DOI:10.1517/13543784.2011.583236
50. Davis, M. (2016) Glioblastoma: Overview of Disease and Treatment. *Clin J Oncol Nurs.* 20(5 Suppl):S2-S8. doi:10.1188/16.CJON.S1.2-8
51. Cadossi, R., Ronchetti, M., Cadossi, M. (2014) Locally enhanced chemotherapy by electroporation: clinical experiences and perspective of use of electrochemotherapy. *Future Oncology.* 10(5). doi.org/10.2217/fon.13.235
52. Kim, Y., Cho, S., Seo, Y. (2016) The activation of melanogenesis by p-CREB and MITF signaling with extremely low-frequency electromagnetic fields on B16F10 melanoma. *Life Sciences.* 162:25-32.
53. Kirson, E., Gurvich, Z., Schneiderman, R., et al. (2004). Disruption of Cancer Cell Replication by Alternating Electric Fields. *Cancer Res.* 64(9):3288-3295. DOI: 10.1158/0008-5472.CAN-04-0083
54. Čemažar, J., and Kotnik, T. (2012) Dielectrophoretic field-flow fractionation of electroporated cells. *Electrophoresis.* 33:2867-2874. doi.org/10.1002/elps.201200265
55. Weaver, J., Smith, K., Essera, A., et al. (2012) A Brief Overview Of Electroporation Pulse Strength–Duration Space: A Region Where Additional Intracellular Effects Are Expected. *Bioelectrochemistry.* 87:236-243.
56. Xu, H., Bihari, F., Whitehead, S., et al. In Vitro Validation of Intratumoral Modulation Therapy for Glioblastoma. *Anticancer Research.* 36(1):71-80.

57. Kirson, E., Dbalý, V., Tovaryš, F., et al. (2007). Alternating Electric Fields Arrest Cell Proliferation in Animal Tumor Models and Human Brain Tumors. *Proceedings of The National Academy of Sciences*. 104(24):10152-10157.
doi:10.1073/pnas.0702916104
58. Stupp, R., Taillibert, S., Kanner, A. et al. (2017) Effect of Tumor-Treating Fields Plus Maintenance Temozolomide vs Maintenance Temozolomide Alone on Survival in Patients With Glioblastoma: A Randomized Clinical Trial. *JAMA*.318(23):2306–2316. doi:10.1001/jama.2017.18718
59. Neumann, E. (1988) The electroporation hysteresis. *Ferroelectrics*. 86(1):325-333.
doi:10.1080/00150198808227023
60. Belehradek, M., Domenge, C., Luboinski, B., et al. (1993) Electrochemotherapy, a new antitumor treatment. *Cancer*, 72:3694-3700. doi.org/10.1002/1097-0142(19931215)72:12<3694::AID-CNCR2820721222>3.0.CO;2-2
61. Orlowski, S., Belehradek, J., Paoletti, C., et al. (1988) Transient Electroporation of Cells In Culture: Increase Of The Cytotoxicity Of Anticancer Drugs. *Biochemical Pharmacology*. 37(24):4727-4733.
62. Glass, F., Neil, M., Fenske, M., et al. (1996) Bleomycin-mediated electrochemotherapy of basal cell carcinoma. *Journal of the American Academy of Dermatology*. 34(1):82-86.
63. Okino, M., Mohri O. (1987) Effects Of A High-Voltage Electrical Impulse And An Anticancer Drug On In Vivo Growing Tumors. *Japanese Journal of Cancer Research*. 78(12):1319-1321
64. Mir, L., Orlowski, S., Belehradek, J., et al. (1991) Electrochemotherapy potentiation of antitumour effect of bleomycin by local electric pulses. *European Journal of Cancer and Clinical Oncology*. 27(1):68-72.
65. Forde, P., Hall, L., de Kruijf, M. et al. (2015) Non-viral immune electrogene therapy induces potent antitumour responses and has a curative effect in murine colon

- adenocarcinoma and melanoma cancer models. *Gene Ther.* 22:29–39.
doi.org/10.1038/gt.2014.95
66. Glass, L., Pepine, M., Fenske, N., et al. (1996) Bleomycin-Mediated Electrochemotherapy of Metastatic Melanoma. *Arch Dermatol.* 132(11):1353–1357.
doi:10.1001/archderm.1996.03890350095015
67. Quaglino, P., Mortera, C., Osella-Abate, S. et al. (2008) Electrochemotherapy with Intravenous Bleomycin in the Local Treatment of Skin Melanoma Metastases. *Ann Surg Oncol.* 5(8):2215-22. doi.org/10.1245/s10434-008-9976-0
68. Campana. L., Mali, B., Sersa, G. (2014) Electrochemotherapy In Non-Melanoma Head And Neck Cancers: A Retrospective Analysis Of The Treated Cases. *The British Journal Of Oral And Maxillofacial Surgery.* 52(10):957-964.
69. Granataa, V., Fuscoa, R., Piccirillo, M., et al. (2015) Electrochemotherapy In Locally Advanced Pancreatic Cancer: Preliminary Results. *International Journal of Surgery.* 18:230-236.
70. Wei, L., Yang, X., Shi, X., et al. (2015). Pannexin1 Silencing Inhibits the Proliferation of U87MG cells. *Mol Med Rep.* 11:3487-3492.
71. Penuela, S., Gyenis, L., Ablack, A., et al. (2012) Loss of Pannexin 1 Attenuates Melanoma Progression by Reversion to a Melanocytic Phenotype. *J Biol Chem.* 287:29184-29193.
72. Belehradec, M., Domenge, C., Luboinski, B., et al. (1993), Electrochemotherapy, a new antitumor treatment. *Cancer.* 72:3694-3700. doi.org/10.1002/1097-0142(19931215)72:12<3694::AID-CNCR2820721222>3.0.CO;2-2
73. Edhemovic, I., Gadzije, E., Breclj, E., et al. (2011) Electrochemotherapy: A New Technological Approach in Treatment of Metastases in the Liver. *Technology in Cancer Research & Treatment.* 10(5):475-485. doi:10.7785/tcrt.2012.500224

74. Pavlihaa, D., Kosa, B., Županiča, A., et al. (2012) Patient-Specific Treatment Planning Of Electrochemotherapy: Procedure Design And Possible Pitfalls. *Bioelectrochemistry*. 87:265-273.
75. Hjouj, M., Last, D., Guez, D. (2012) MRI Study on Reversible and Irreversible Electroporation Induced Blood Brain Barrier Disruption. *PLOS One*. doi.org/10.1371/journal.pone.0042817
76. Weaver, J. (2000) Electroporation of cells and tissues. *IEEE*. 28(1):24-33. doi: 10.1109/27.842820.
77. Ivorra, A., Rubinsky, B. (2010) Historical Review of Irreversible Electroporation in Medicine. *Irreversible Electroporation*. doi.org/10.1007/978-3-642-05420-4_1
78. 1, J. (1995) Electroporation Therapy. *Methods in Molecular Biology*. 47.
79. Rubinsky, B., Onik, G., Mikus, P. (2007) Irreversible Electroporation: A New Ablation Modality —Clinical Implications. *Technology in Cancer Research & Treatment*. 37-48. doi:10.1177/153303460700600106
80. Scheffer, H., Nielsen, K., de Jong, M. (2014) Irreversible Electroporation for Nonthermal Tumor Ablation in the Clinical Setting: A Systematic Review of Safety and Efficacy *Journal of Vascular and Interventional Radiology* 25(7):997-1011
81. Nishi, T., Yoshizato, K., Yamashiro, S. (1996) High-Efficiency in Vivo Gene Transfer Using Intraarterial Plasmid DNA Injection following in Vivo Electroporation. *Cancer Res*. 56(5):1050-1055
82. Heller, R., Jaroszeski, M., Atkin, A. (1996) In vivo gene electroinjection and expression in rat liver. *FEBS Letters*. 389(3):225-228.
83. Bureaua, M., Gehlb, J., Deleuzea, V., et al. (2000) Importance Of Association Between Permeabilization And Electrophoretic Forces For Intramuscular DNA Electrotransfer. *Biochimica et Biophysica Acta*. 1474(3):353-359.

84. Vaughan, E., DeGiulio, J., Dean, D. (2006) Intracellular Trafficking of Plasmids for Gene Therapy: *Mechanisms of Cytoplasmic Movement and Nuclear Import Current Gene Therapy*. 6(6):671-681.
85. Clague, D., Wheeler, E. (2005) Dielectrophoretic Manipulation of Macromolecules: The Electric Field. *Phys. Rev. E*. 64:026605.
86. Gonzalez, C., Remcho, V. (2005) Harnessing Dielectric Forces for Separations of Cells, Fine Particles And Macromolecules. *Journal of Chromatography*. 1079(1–2):59-68.
87. Giladi, M., Schneiderman, R., Porat, V. (2015) Mitotic Spindle Disruption by Alternating Electric Fields Leads to Improper Chromosome Segregation and Mitotic Catastrophe in Cancer Cells. *Sci Rep*. 11(5):18046. doi: 10.1038/srep18046.
88. Kirson, E., Schneiderman, R., Dbalý, V., et al. (2009) Chemotherapeutic Treatment Efficacy and Sensitivity are Increased by Adjuvant Alternating Electric Fields (Ttfields). *BMC Med Phys*. 8(9):1. doi.org/10.1186/1756-6649-9-1
89. Tuszynski, J., Wenger, C., Friesen, D., et al. (2016) An Overview of Sub-Cellular Mechanisms Involved in the Action of TTFIELDS. *Int. J. Environ. Res*. 13:1128. doi.org/10.3390/ijerph13111128
90. Wenger, C., Pedro, C., Salvador, S., et al. (2018) A Review on Tumor-Treating Fields (TTFIELDS): Clinical Implications Inferred From Computational Modeling. *IEEE Reviews in Biomedical Engineering*. 11:195-207 doi: 10.1109/RBME.2017.2765282.
91. Lacouture M., Elizabeth, M., Elzinga, D. (2014) Characterization and Management of Dermatologic Adverse Events with the NovoTTF-100A System, a Novel Anti-mitotic Electric Field Device for the Treatment of Recurrent Glioblastoma. *Seminars in Oncology*. 41(Sup4):S1-S14.
92. Rominiyi, O., Vanderlinden, A., Clenton, S., et al. (2021) Tumour treating fields therapy for glioblastoma: current advances and future directions. *Br J Cancer*. 124(4):697-709. doi: 10.1038/s41416-020-01136-5.

93. Kissling, C., Di Santo, S. (2020) Tumor Treating Fields – Behind and Beyond Inhibiting the Cancer Cell Cycle. *CNS & Neurological Disorders - Drug Targets*. 19(8):599-610.
94. Rehman, A., Elmore, K., Mattei, A. (2015). The effects of alternating electric fields in glioblastoma: current evidence on therapeutic mechanisms and clinical outcomes. *Neurosurgical Focus*. 38(3):E14. DOI: 10.3171/2015.1.FOCUS14742
95. Sampson, J. (2015) Alternating Electric Fields for the Treatment of Glioblastoma. *JAMA*. 314(23):2511-2513.
96. Mittal, S., Klinger, N., Michelhaugh, S., et al. (2017) Alternating Electric Tumor Treating Fields for The treatment Of Glioblastoma, Rationale, Preclinical, and Clinical Studies. *J Neurosurg*. 24:1-8.
97. Ghiaseddin, A., Shin, D., Melnick, K., et al. (2020) Tumor Treating Fields in the Management of Patients with Malignant Gliomas. *Curr. Treat. Options in Oncol*. 21(76) doi.org/10.1007/s11864-020-00773-5
98. McCairn, K., Iriki, A., Isoda, M. (2015) Common therapeutic mechanisms of pallidal deep brain stimulation for hypo- and hyperkinetic movement disorders. *J Neurophysiol*. 114(4):2090-104.

Chapter 2

2 Preclinical Outcomes of Intratumoral Modulation Therapy for Glioblastoma¹

Glioblastoma (GBM) is the leading cause of high fatality cancer arising within the adult brain. Electrotherapeutic approaches offer new promise for GBM treatment by exploiting innate vulnerabilities of cancer cells to low intensity electric fields. This report describes the preclinical outcomes of a novel electrotherapeutic strategy called Intratumoral Modulation Therapy (IMT) that uses an implanted stimulation system to deliver sustained, titratable, low intensity electric fields directly across GBM-affected brain regions. This pilot technology was applied to *in vitro* and animal models demonstrating significant and marked reduction in tumor cell viability and a cumulative impact of concurrent IMT and chemotherapy in GBM. No off target neurological effects were observed in treated subjects. Computational modeling predicted IMT field optimization as a means to further bolster treatment efficacy. This sentinel study provides new support for defining the potential of IMT strategies as part of a more effective multimodality treatment platform for GBM.

2.1 Introduction

Glioblastoma (GBM) is the most common and aggressive primary brain cancer in adults, affecting ~1 in 33,333 people annually and ending the life of an untreated patient within 3 months after diagnosis [Nam, 2016]. The current standard of care is surgical resection, when possible, along with radiation and temozolomide (TMZ) chemotherapy.

A version of this chapter is published as:

Andrew Deweyert*, Andrea R. DiSebastiano*, Simon Benoit, Erin Iredale, Hu Xu, Cleusa De Oliveira, Eugene Wong, Susanne Schmid, Matthew O. Hebb. (2018). Preclinical outcomes using direct-targeting Intratumoral Modulation Therapy for glioblastoma. *Scientific Reports*. 8(1): 7301.

Despite maximum available treatment, the cancer inevitably recurs and yields a median survival of only 14 months [Nam, 2016]. There is now mounting evidence that electrotherapy may offer new promise as an effective treatment modality much needed for GBM patients [Mun, 2017]. The rationale for this strategy is based on an innate sensitivity of GBM cells to non-ablative electric current or fields that are innocuous to normal neural tissues, thus creating a putative safety margin for therapeutic development [Xu, 2016; Kirson, 2004]. Such low intensity electrotherapy likely works through multiple mechanisms that relate, in part, to disruption of polarized cellular elements necessary for cytokinesis as well as changes in membrane permeability and channel homeostasis [Pawlowski, 1993; Gera, 2015]. There is presently a single electrotherapy approved for GBM in the United States. This system includes a portable electric field generator to deliver low intensity (1–3 V/Cm), intermediate frequency (200 kHz) alternating electric fields, called tumor treating fields (TTFs), to supratentorial brain regions. TTFs are administered through arrays of insulated electrodes adhered to the patient's scalp [Hottinger, 2016]. Continuous, long-term application is recommended, and the transducer arrays are replaced every few days. The clinical impact of TTFs in GBM has been evaluated in two randomized, multi-centre trials [Stupp, 2012; Stupp, 2017]. The studies had methodological constraints but produced results supporting a significant clinical benefit in both recurrent and newly diagnosed disease. Potential drawbacks of TTF therapy include the need for a shaved head, frequent electrode changes, scalp complications from chronic electrode wear, stigmata of an external treatment device, inability to target infratentorial or spinal disease and high treatment-related costs [Sampson, 2015; Mittal, 2017].

The most common (>90%) pattern of GBM progression occurs as aggressive, continuous extension from the site of the original lesion [Gaspar , 1992; Halperin, 1988; Lee , 1999; Loeffler, 1990]. This important recognition has led to decades of research attempting to develop effective locoregional strategies to control growth of inoperable tumors and prevent recurrence following surgical resection [Ashby , 2016; Barbarite, 2017; de Paula, 2017; Hersh, 2016]. Our group has been pioneering a novel locoregional electrotherapy, called Intratumoral Modulation Therapy (IMT), with the premise that an internalized

electric field will exploit GBM electrosensitivity to greater advantage and with fewer limitations than an externally applied (e.g., scalp-mounted) source [Xu, 2016].

Still in the proof-of-concept stage, the clinical vision of IMT uses special purpose, magnetic resonance imaging (MRI)-compatible bioelectrodes strategically positioned within, or adjacent, tumor-affected regions of the central nervous system (CNS). A key feature of IMT is the ability to reach any aspect of the CNS to provide focused, titratable therapy directly within areas of disease. Bioelectrodes could be designed for personalized and comprehensive treatment coverage of GBM resection beds or non-operated lesions within eloquent or deep-seated CNS regions. The proximity of the IMT field source to GBM pathology will permit a broad, versatile spectrum of stimulation parameters custom optimized to tumor location and treatment response. Such a concealed, indwelling system is expected to support patient quality of life while providing sustained, low maintenance therapy that potentially complements radiation and ongoing chemotherapeutic options.

We recently described an *in vitro* IMT approach using monophasic, low amplitude (4 V), low frequency (130 Hz) square wave pulses that induced apoptosis in patient GBM cells without notable impact on primary neurons [Xu, 2016]. Adjuvant IMT significantly increased GBM cell death when combined with TMZ or oncogene-targeting therapies [Xu, 2016]. These early results confirmed GBM sensitivity to directly applied, non-ablative electrical pulses but the low frequency parameters posed risk of neuronal entrainment and off-target neurological effects if applied within eloquent CNS areas [Palti, 1996]. The objective of the present study was to evaluate a novel profile of IMT parameters using intermediate frequency (200 kHz) stimulation with low risk of neuronal entrainment and a sinusoidal waveform to deliver continuous, alternating polarity, low intensity (± 2 V) electric fields. These new parameters were first validated using our established *in vitro* methods then translated to test IMT for the first time in a customized *in vivo* GBM model.

2.2 Materials and Methods

2.2.1 GBM cell cultures

These protocols were approved by the Human Research Ethics Board and the Animal Care Committee at Western University and carried out in accordance with the Tri-Council Policy for research involving human subjects and the Canadian Council on Animal Care. Informed consent was obtained from all patients or their legal guardians prior to using their GBM tissue in this study. Human GBM cells were isolated from operative tumor specimens obtained from 3 patients (39 y male, 44 y female, 65 y female). Specimens were not genetically screened for study purposes. The tumor samples were collected into phosphate-buffered saline (PBS) with 0.5% fetal bovine serum (FBS; Life Technologies) at the time of surgery. The tissue was digested and filtered then suspended in Dulbecco's modified Eagle's medium (DMEM; Wisent Bioproducts) supplemented with 10% FBS, 1% non-essential amino acids and 1% penicillin/streptomycin (Life Technologies). Homogenates were plated on a 35 mm dish for 30 minutes to allow for separation of blood cells. The upper cell suspension was then transferred to two wells of a 24-well plate, freshly pre-coated with 10 µg/ml poly-L-lysine (Trevigen Inc) and incubated at 37 °C with 5% CO². Cultures were passaged at approximately 80% confluence and split 1:2 using 0.25% trypsin with 0.53 mM ethylenediaminetetraacetic acid (EDTA; Wisent). The medium was changed twice per week. All assays were conducted using GBM cells from cultures at passages 4 through 12.

The F98 GBM cell line (CRL2397TM; ATCC) was originally created following a single N-ethyl-N-nitrosourea injection to a pregnant Fischer rat to produce offspring with malignant glioma tumors that were then maintained in culture [Mathieu, 2004; Mathieu, 2007]. The low immunogenicity of F98 cells in syngeneic Fischer rats offers advantages over xenogeneic and allogeneic models that require immunosuppression or may exhibit spontaneous tumor regression. F98 GBM tumors are highly proliferative, invasive, and recalcitrant to conventional therapies, closely mimicking the human disease. F98 cells were cultured in 100 mm dishes in DMEM supplemented with 10% FBS, 1% non-essential amino acids and 1% penicillin/streptomycin (Life Technologies) in a humidified

incubator at 37 °C with 5% CO². The medium was changed twice per week and cultures passaged at ~80% confluence and split 1:2 using 0.25% trypsin with 0.53 mM EDTA (Wisent).

2.2.2 Primary neuronal cultures.

IMT was evaluated in post-mitotic primary neurons isolated from embryonic rat brains (N = 3). Cerebral cortices from E18 Wistar embryo were dissected into a 14 ml conical tube containing 1.8 ml of Hank's balanced salt solution (HBSS; Wisent) and centrifuged at 4000 × g for 1 min at room temperature. HBSS was aspirated and 1.8 ml of solution A containing 5 ml HBSS, 6 µl MgSO₄ (1 M) and 2 ml trypsin (Sigma Aldrich) were added. The tube was mixed well and placed in an automated rotator at 37 °C for 25 minutes. After rotation, 3.6 ml of solution B containing 7 ml HBSS, 8 µl MgSO₄ (1 M), 175 µl DNase1 (10 mg/ml) and 112 µl trypsin inhibitor (100 µg/ml; Roche Life Sciences) were added and mixed for 2 minutes, centrifuged at 4000 × g for 5 min at room temperature, and then the HBSS was aspirated. Finally, 6 ml of solution C containing 20 ml of HBSS, 48 µl MgSO₄ (1 M), 1.3 ml DNase1 (10 mg/ml), and 1 ml trypsin inhibitor (100 µg/ml) were added to the resulting cell pellet (Roche). These cells were transferred to a 50 ml falcon tube and another 6 ml of solution C was added. The cells were titrated, centrifuged at 4000 × g for 5 minutes and the supernatant aspirated. The cell pellet was re-suspended in 36 ml of media containing 96% neural basal media (Wisent), 2% B27 supplement, 0.8% N2 Supplement, 0.5% penicillin/streptomycin, 0.25% Glutamax (Life Technologies), and 0.1% Amphotericin B solution (Sigma Aldrich). Cells were counted with a hemocytometer, plated in 35 mm wells coated with 7% poly-L-Ornithine (Sigma Aldrich) at density of 0.5 × 10⁶ cells/well and kept in a humidified incubator at 37 °C with 5% CO². On the third day of culture, the media was changed, and wells were fitted with the IMT apparatus for delivery of 72 h of sham or IMT conditions.

2.2.3 *In vitro* IMT model

The impact of IMT alone and combined with TMZ was independently evaluated in triplicate using primary human GBM cells, rodent F98 GBM cells and post-mitotic rodent primary neurons. GBM cells and primary neurons (1–5 × 10⁵ cells) were cultured

in 35 mm wells in standard 6-well plates. GBM cells were grown to ~70% confluence before treatment. The IMT model was created by fitting each well with a clinical grade, platinum-based strip bioelectrode (AD-Tech) around the periphery and a single contact platinum-iridium bioelectrode (Medtronic Ltd.) at the center of the well and cell culture [Xu, 2016]. A waveform generator (Rigol DG1022; Electro-Meters Ltd.) was used to deliver biphasic sinusoidal pulses with low amplitude (+ /-2 V; peak-to-peak 4 V) and intermediate frequency (200 kHz) for a period of 72 hours. Control wells (i.e. sham-treated) were fitted with electrodes but no current was delivered. GBM cells treated with chemotherapy were plated with DMEM containing TMZ (50 μ M; Sigma Aldrich) and received 72 hours of concomitant IMT or sham conditions. This TMZ concentration reflects clinically relevant levels corresponding to the *in vivo* plasma concentration of 150 mg/m² in the adjuvant phase of GBM treatment [Ostermann, 2004].

2.2.4 Cell viability assays

Cell viability was evaluated using the 3-(4,5-dimethylthiazol-2-yl)-2,5-diphenyltetrazolium (MTT) spectral analysis (Sigma Aldrich). This spectrophotometric assay measures the reduction of yellow MTT by mitochondrial succinate dehydrogenase to an insoluble, dark purple Formosan product. Immediately following the GBM cell treatments described above, MTT (80 μ l at 5 mg/ml) was added to the 35 mm wells and incubated for 3 hours at 37 °C in a humidified 5% CO² atmosphere. The cells were then lysed to release the purple Formosan product by the addition of 600 μ l dimethyl sulfoxide for 15 minutes at room temperature. Absorbance was measured using an enzyme-linked immunosorbent assay plate reader (Fisher Scientific). Cell viability was estimated using optical density values at 570 nm with references at 655 nm detected in each well.

Trypan blue exclusion was used as a confirmatory, qualitative measure of cell viability. Briefly, 0.1 ml of a 0.4% trypan blue solution (Lonza) was added for every 1 ml culture media and the cells incubated for 2 minutes at room temperature. Brightfield images of cells stained with MTT and trypan blue were obtained using a Motic AE31 inverted microscope fitted with an Infinity 1–3 scientific complementary metal-oxide semiconductor camera (Lumenera Corp).

An Annexin V Apoptosis Detection Kit with propidium iodide (PI; BioLegend) was used to quantify live, apoptotic, and dead GBM cell fractions, as per the manufacturer's instructions. Cell fractions were analyzed using a Becton Dickinson LSR II SORP flow cytometer running FACSDiva software (BD Biosciences). Cells were first gated on forward scatter (FSC-) versus side scatter (SSC-) characteristics before excluding doublets using consecutive gating FSC-Area versus FSC-Width and SSC-Area versus SSC-Width plots. The populations of annexin V+/PI-, annexin V+/PI+, annexin V-/PI+ and annexin V-/PI- were then calculated with quadrant gates. Approximately 15,000–30,000 single GBM cells were acquired per each of three patient samples at a maximum event rate of 5,000 events per second. Data were analyzed using FlowJo v 9.6.3 (TreeStar, Inc).

2.2.5 *In vivo* GBM model and IMT

Bilateral orthotopic GBM tumors were established by implanting F98 cells into the brain of syngeneic adult female Fischer rats (Charles River) [Mathieu, 2004; Mathieu, 2007]. A cohort size of 25 was chosen to adequately temper inter-animal variability and account for unexpected problems or deaths. Subjects were maintained under isoflurane anesthesia for stereotactic implantation of chronic cannula-bioelectrode constructs (Plastics One) into bilateral striata (coordinates from bregma: anteroposterior 1 mm, lateral +/-3 mm, dorsoventral -6 mm). The constructs consisted of a 5 mm long steel cannula with 1 mm luminal diameter, running parallel to a 6-mm-long, rigid lead with a 1 mm long, 0.25 mm diameter bioelectrode contact at the distal tip. The reference bioelectrode was connected by a flexible 1 cm long insulated wire and positioned extracranially in the temporal or nuchal soft tissues. These three components were secured at a common, accessible pedestal cemented to the skull. A key advantage of this cannula-bioelectrode construct was the ability to implant GBM cells that form a large tumor mass centered around the IMT bioelectrode within the brain. In two animals (#10, 11), the bioelectrode contact was insulated with a thin layer of Entellan (Sigma Aldrich) prior to implantation. This pilot modification was intended to assess the anti-GBM effect of an intratumoral electric field without current flowing between the bioelectrodes and tissue.

F98 GBM cells (4×10^4 in 2 μ l DMEM) were delivered bilaterally through the implanted cannulae, after which the pedestal was covered with a protective cap. Two operators were present for quality assurance in all surgeries. On postoperative day 4, IMT was randomized to the right or left tumor and the respective bioelectrode was connected to a waveform generator (Rigol DG1022; Electro-Meters Ltd) via an extension cable and a commutator that permitted the animal to move freely throughout the home cage. The contralateral tumor served as an internal sham control (i.e., identical tumor and hardware implants but without stimulation). Continuous IMT monotherapy was delivered between postoperative days 4–11 using the *in vitro* parameters (i.e., sinusoidal waveform, ± 2 V, 200 kHz). Three control subjects received bilateral hardware without GBM cell delivery to assess potential adverse effects of IMT on normal brain structure. Five subjects had unilateral implantation of GBM cells, as described above, using a Hamilton syringe and without IMT hardware. Four of these subjects were used to assess GBM size after 4 days of growth (i.e., the size at the onset of IMT). One animal underwent MRI on postoperative day 7 as part of the simulation studies, described below. All animals were given free access to food and water, perioperative antibiotics, and analgesics, and monitored daily for medical or neurological complications. On post-operative day 11, animals were deeply anesthetized with sodium pentobarbital and transcardially perfused with 4% paraformaldehyde. The brains were extracted, cryoprotected and frozen. Brains were cut into 16–35 μ m thick sections through the rostrocaudal extent of the tumors, mounted onto microscope slides and stained with thionine. Processed sections were digitally imaged with a Nikon Eclipse Ni-E microscope.

2.2.6 GBM tumor analysis

Digitized brain images were imported into ImageJ v.2.0.0 software for tumor measurement by a blinded observer. The wand tracing tool was used to select the GBM tissue from surrounding brain with identical tolerance detection settings for the IMT- and sham-treated tumors. Tolerance detection ranged from 10–40 pixels in 8-connected mode and was adjusted accordingly between serial sections for variations in staining intensity. Cross-sectional areas in serial sections were quantified in pixels and summed to provide relative estimates of tumor volume. The whole tumor was measured using serial sections

through the rostrocaudal extent of the GBM. A more focused measure of the tumor ‘core’ was calculated to assess the impact of IMT in the region of highest GBM burden (i.e., at the implantation site) and anticipated center of the IMT electric field. This core region was objectively defined within 4 brain sections containing the largest cross-sectional area of both sham- and IMT-treated tumors in addition to the two immediately flanking sections.

2.2.7 IMT electric field simulation

The IMT electric field created by the treatment parameters used in this study was simulated based on 9.4 T MRI data from a representative control animal with a unilateral 7-day GBM, as described above. Imaging at this time point depicts the tumor size midway through the treatment period (i.e., day 4–11). MRI data was imported to Brainsuite v.16a1 for segmentation of the GBM tumor mass, associate cerebral edema, whole brain and skull. Segmented volumes were then imported to Multiphysics v.5.2a (COMSOL Inc.) where the intratumoral bioelectrode, reference bioelectrode and cannula geometry was simulated according to the *in vivo* IMT paradigm. The bioelectrode was modeled with stainless steel insulated with a 0.025 mm thick layer of polyimide except for the distal tip where a 1 mm contact was exposed. The conductance and dielectric properties of the segmented brain tissues, skull and bioelectrode apparatus were then specified within the COMSOL Electric Currents user interface which was employed to compute the electric field [Wenger, 2015; Wenger, 2016]. A constant voltage of 2.0 V at 200 kHz was applied across the intratumoral and reference bioelectrodes within this computer model. The resulting map of the electric field amplitude was exported and merged with the MR images for visualization in 3D Slicer v.4.4.0. The dimensions and amplitude of the electric field within the tumor and brain were analyzed using MATLAB R2015b (MathWorks Inc).

2.2.8 Magnetic resonance imaging

MRI studies were performed at The Centre for Functional and Metabolic Mapping, Robarts Research Institute, Western University. An Agilent small animal 9.4 T MRI unit was used to obtain true fast imaging with steady state precession (TrueFISP; TR = 7 ms,

TE = 3.5 ms, flip angle = 30 degrees, number of frequencies = 4, number of averages = 4, total acquisition time = 42 minutes, field of view=28mm×28mm×28mm, acquisition matrix=140×140×140).

2.2.9 Statistical analysis

A t-test or Wilcoxon signed-rank test was used to compare single and paired *in vitro* data sets that followed or deviated from a normal distribution, respectively. Multiple pairwise comparisons were performed using one-way analysis of variance (ANOVA) followed by Tukey post-hoc analysis. *In vivo* tumor measures were evaluated using the Dixon's and Grubb's tests for outliers. The *in vivo* IMT response was assessed by calculating the percent change in tumor volume for each subject and using a single sample t-test to compare the cohort values to a hypothetical mean change of zero percent. A complementary analysis did not assume uniform untreated rates of growth amongst tumors and compared the cumulative GBM burden following sham and IMT treatment within the entire cohort using a paired sample t-test. One-tailed analyses were used for statistical comparisons based on the known *in vitro* efficacy of IMT against GBM [Xu, 2016]. Statistical software used included Sigma Stat (Systat Software Inc) and SPSS v 14.0 (IBM). Data are presented as mean \pm standard deviation with significance assumed at $p < 0.05$. Data availability. All data analyzed during this study are included in this published article.

2.3 Results

2.3.1 Intermediate frequency IMT selectively kills GBM cells and provides cumulative anti-neoplastic effects when administered with TMZ chemotherapy

The MTT assay generated spectrophotometric values that reflected cell viability. Results of each treatment condition were normalized to those of the sham group. GBM cells from 3 patient tumors were independently treated and the data pooled for analysis. The individual MTT values are provided in Table 2.1. TMZ produced a modest but significant

reduction in patient GBM cell viability to $82.6 \pm 3.0\%$ ($P = 0.001$), whereas IMT resulted in a greater drop to $65.1 \pm 4.0\%$ ($P < 0.001$) of sham values. Co-administration of TMZ with IMT resulted in a dramatic cumulative loss of GBM cell viability to $45.8 \pm 4.0\%$ ($P < 0.001$) of sham values (Fig. 2.1). The difference in GBM cell viability between TMZ and IMT ($P < 0.001$), and between TMZ ($P < 0.001$) or IMT ($P < 0.001$) and the combined TMZ + IMT treatments were all highly significant. The F98 GBM cells were similarly vulnerable to IMT, with a reduction to $54.9 \pm 6.3\%$ ($N = 3$; $P = 0.008$) of sham values. In contrast, primary neuronal cultures did not exhibit obvious changes in morphology nor were the MTT measures notably affected by IMT, with a mean group viability of $105.5 \pm 5.3\%$ ($N=4$; $P = 0.091$) of sham values (Fig. 2.1).

Table 2-1. Spectrophotometric viability (MTT) analysis in patient GBM cells

| GBM # | Temozolomide | IMT | Temozolomide + IMT |
|--------------|---------------------|------------|---------------------------|
| 1 | 0.79 | 0.68 | 0.49 |
| 2 | 0.85 | 0.67 | 0.47 |
| 3 | 0.84 | 0.59 | 0.41 |

Shown are the MTT values, normalized to the respective sham control, for GBM cells obtained from 3 patients. Cells were exposed to the indicated conditions for 3 days preceding analysis. IMT was statistically superior to temozolomide in reducing GBM cell viability and the combination of temozolomide and IMT produced dramatic, highly significant anti-neoplastic effects. These data are summarized in Fig. 2.1.

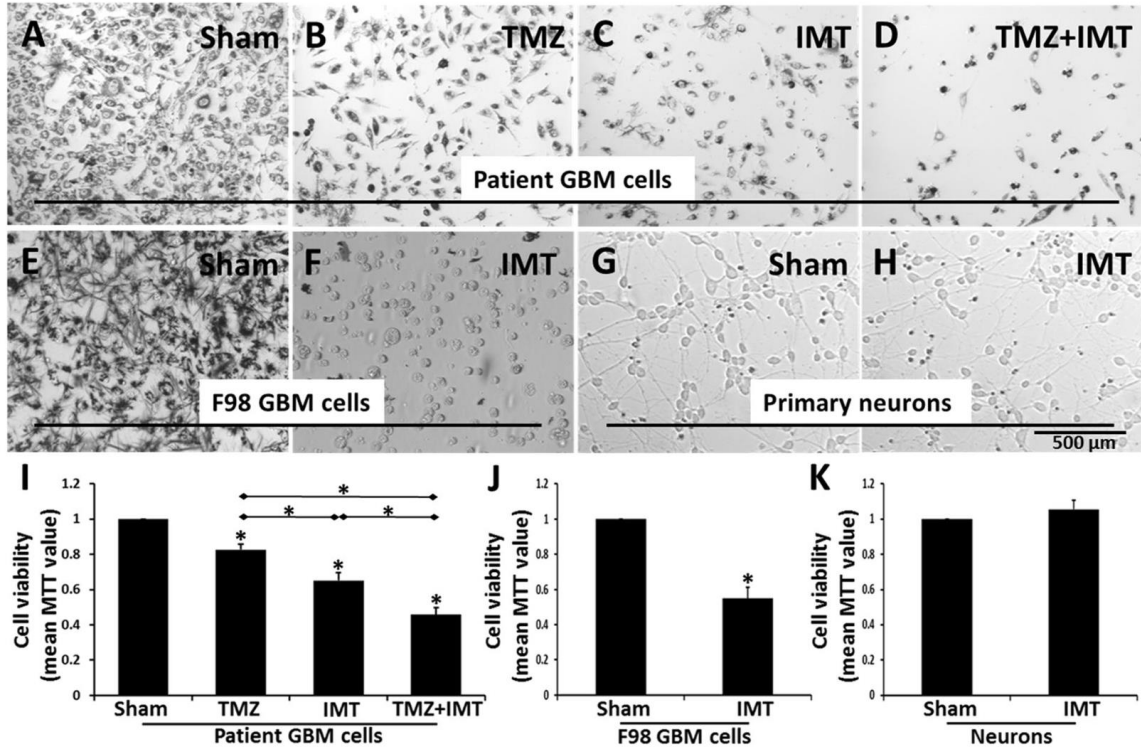


Figure 2-1. Impact of intermediate frequency IMT on GBM cells *in vitro*.

Brightfield photomicrographs of patient and rodent F98 GBM cells and primary neurons are shown following a 3-day exposure to the indicated treatments. The images captured cell fields adjacent to the bioelectrode implanted within the cultures (not shown). (A) Patient GBM cells stained with the dark MTT chromogen demonstrate robust viability under sham conditions. A moderate reduction in staining, accompanied by pyknosis and decreased cell density was observed with (B) TMZ or (C) IMT monotherapy. (D) Concomitant TMZ+IMT resulted in a dramatic loss of cell viability compared to that achieved with either treatment alone. (E, F) Susceptibility to the same stimulation parameters was also evident in rodent F98 GBM cells as shown by MTT staining. (G, H) In contrast, the morphology and density of post-mitotic primary neuronal cultures, as shown here following trypan blue exposure, was not notably affected by IMT. (I) The viability of GBM cells from 3 different patient tumors was significantly reduced by TMZ or IMT alone. A cumulative GBM cell loss was produced by the combination of both treatments, likely reflective of distinct mechanisms of action. Asterisks directly above the data bars indicate a significant ($P < 0.001$) difference from the sham control. The significance ($P < 0.001$) between indicated data pairs is depicted by an asterisk above the horizontal lines. (J) F98 GBM ($N = 3$; $P = 0.008$) but not (K) primary post-mitotic neuronal ($N = 4$; $P = 0.091$) cultures were susceptible to IMT. Asterisks directly above the data bars indicate a significant difference from the sham control. All data are presented as mean \pm standard deviation

Flow cytometry with Annexin V and PI labeling permitted quantification of live, apoptotic, and dead GBM cell fractions. Primary neurons were not able to withstand the flow cytometry methods. The assay was conducted on 15–30,000 GBM cells for each treatment condition using biological replicates from 3 patients. The values for apoptotic and dead cells were combined into a single category. The flow cytometry revealed $15.1 \pm 12.2\%$ apoptotic/dead GBM cells in the sham group compared with a progressive increase in this fraction following treatment with TMZ ($28.2 \pm 7.1\%$; $P = 0.488$), IMT ($38.8 \pm 6.0\%$; $P = 0.032$) and the combination TMZ + IMT ($73.7 \pm 2.1\%$; $P < 0.001$; Fig. 2.2; Table 2.2).

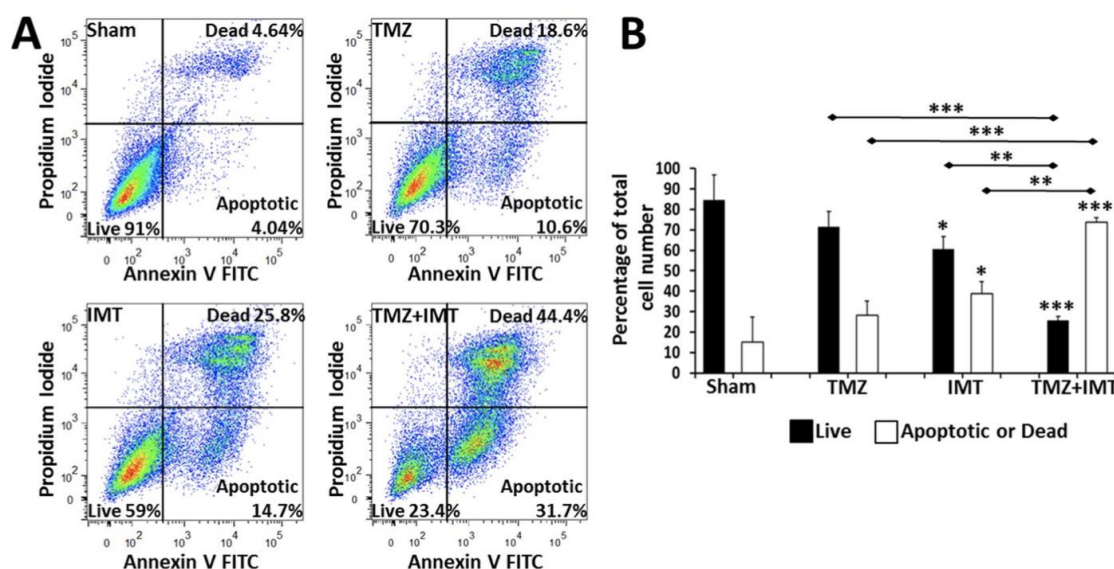


Figure 2-2. Flow cytometry measures of IMT response in patient GBM cells.

(A) Representative scatterplots of annexin and propidium iodide (PI) labeling of apoptotic and dead patient GBM cells, respectively, after a 3-day exposure to the indicated treatment. IMT produced a greater cytotoxic effect than TMZ but the number of apoptotic and dead GBM cells rose dramatically with combined therapy. (B) Quantitative flow cytometry revealed a significant difference ($P < 0.001$) between live and apoptotic/dead fractions within each of the sham, TMZ and TMZ+IMT groups, but not in the IMT group ($P = 0.053$). This corresponded to a significant loss of GBM cell viability with IMT, but not TMZ, and a cumulative increase in cytotoxicity with the combination of the two treatments. These studies were performed in triplicate using primary GBM cells from 3 different patients. Asterisks directly above the data bars indicate a significant difference from the respective sham value (e.g., live compared to live). Significance between indicated data pairs is depicted by the asterisk(s) above the horizontal lines. Data

are presented as mean \pm standard deviation with significance indicated at $P^* < 0.05$, $** < 0.01$ and $*** < 0.001$.

Table 2-2. Individual flow cytometry measures of IMT response in patient GBM cells.

| GBM # | Sham | | Temozolomide | | IMT | | Temozolomide + IMT | |
|-------|------|-------------------|--------------|-------------------|------|-------------------|--------------------|-------------------|
| | Live | Apoptotic or Dead | Live | Apoptotic or Dead | Live | Apoptotic or Dead | Live | Apoptotic or Dead |
| 1 | 91.0 | 8.68 | 70.3 | 29.2 | 59 | 40.5 | 23.4 | 76.1 |
| 2 | 92.5 | 7.49 | 79.4 | 20.6 | 67.5 | 32.1 | 27.04 | 72.8 |
| 3 | 70.4 | 29.26 | 64.8 | 34.7 | 55.6 | 43.7 | 26.7 | 72.2 |

Shown are the percentages (%) of live (Annexin⁻/PI⁻) versus apoptotic (Annexin⁺/PI⁻) or dead (Annexin⁺/PI⁺) patient GBM cells quantified with flow cytometry. Each condition was evaluated in 3 biological replicates with 15,000–30,000 patient GBM cells exposed to the indicated treatment for 3 days. The differences in therapeutic impact between groups were highly significant and are summarized in Fig. 2.2.

2.3.2 IMT significantly attenuates GBM growth *in vivo*

The syngeneic rodent F98 GBM model was customized to evaluate IMT efficacy against GBM in the living brain (Fig. 2.3A–C). The treatment period spanned post-operative days 4–11 during which no neurological, behavioral or pain symptoms related to the stimulation were observed. Of the original 25-animal cohort, 15 animals were included in the final analysis. The excluded animals were: 4 with evidence of overt infection extending into the brain, 1 with insufficient tumor take, 3 with incomplete histological preparations and 2 that expired from undetermined causes. The first death occurred on postoperative day 3, prior to initiating IMT. The second death occurred 3 days after IMT initiation. The brain of this animal was examined histologically and no evidence of treatment-related complication (e.g., electrolysis, hematoma) was identified. In addition to the 25-animal cohort, control animals with unilateral tumor-only implants (N = 4) evaluated on postoperative day 4 (i.e., the time point of IMT initiation) revealed the expected GBM growth consistent across the group (Fig. 2.3D). Animals that received

IMT and sham treatments without previous GBM implants (N = 3) revealed no obvious stimulation-related injury to normal brain parenchyma (Fig. 2.3E).

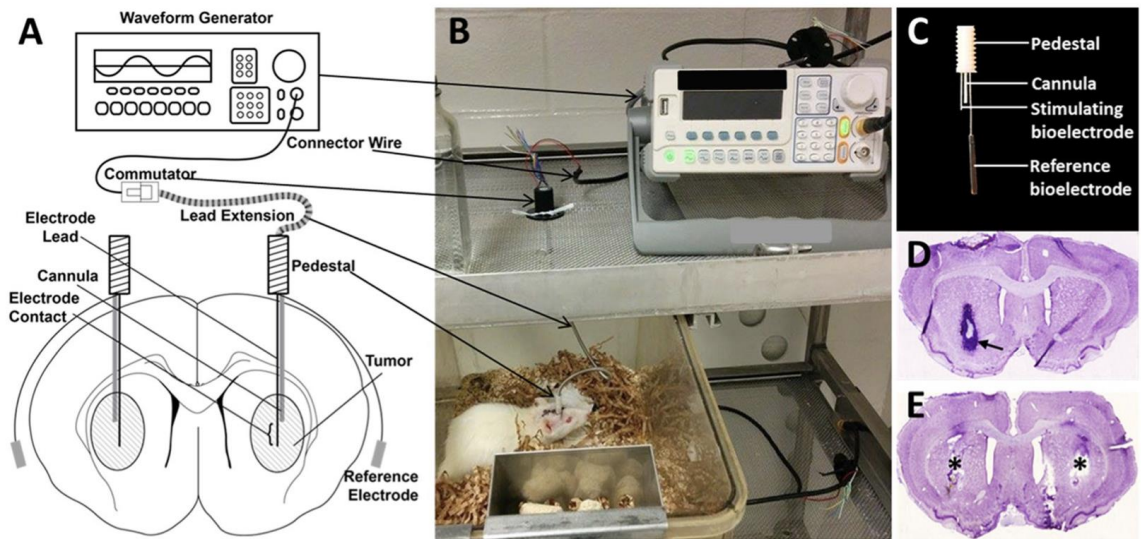


Figure 2-3. *In vivo* model to evaluate IMT in GBM.

In vivo model to evaluate IMT in GBM. (A) Schematic and (B) photographic depiction of the *in vivo* IMT model. The animals could roam freely throughout the home cage. Bilateral GBM tumors were randomized so that one would receive sham treatment (i.e., hardware but no stimulation) and the other IMT between postoperative days 4–11. This provided an internal control tumor for every subject. (C) The IMT construct consisted of a lead with a single 1-mm stimulating bioelectrode, a cannula to deliver the GBM cells and a reference bioelectrode. The stimulating bioelectrode was located at the core of the GBM tumors and the reference bioelectrode positioned extracranially under the scalp. (D) Representative thionine-stained section of a control brain demonstrating a 4-day GBM, reflecting the tumor size when IMT was initiated (arrow). (E) Representative thionine-stained section through another control brain to show the effects of IMT on normal parenchyma. There was no tumor in this subject however bilateral IMT constructs were placed for delivery of 1 week of sham (left) or IMT (right). Symmetric hardware defects were evident (asterisks) without overt parenchymal injury from the stimulation.

The bilateral GBM tumors were randomized to sham treatment or IMT, with 8 right- and 7 left-sided tumors receiving IMT by the end of the study. GBM tumors that received IMT were typically more rounded and compact compared to the oblong, irregular

configuration of sham-treated lesions. GBM volumes were estimated through the rostrocaudal extent of the tumor ('whole tumor') and within a core region at the presumed centre of the IMT electric field ('core tumor'). The whole tumor measures revealed smaller IMT-treated, compared to sham-treated, tumors in 11/15 (73%) animals. There was a single, statistically-proven outlier (subject #7) in which the discrepancy between IMT- and sham-treated tumors was drastically reversed. The reason for this finding was not identified, however hypothesized to be technical in origin, such as a problem with the GBM implant or the laterality marker. The change in tumor volume for this animal fell well past 2 standard deviations from the mean (i.e., >95th %-tile of the normal data distribution) and was identified by both the Dixon's ($P = 0.028$) and Grubb's ($P = 0.016$) tests as a significant outlier. The statistical evidence supported its exclusion; however, the cumulative GBM measures for the entire cohort were calculated both in the presence and absence of the outlier subject (Figs. 2.4 and 2.5). With the outlier included, there was a non-significant 14.5% reduction in IMT-treated whole tumor volume ($P = 0.107$) that rose to a significant 19.5% reduction ($P = 0.047$) with the outlier excluded (Table 2.3). The percent change in the IMT tumor volume relative to that of the sham tumor was also calculated in each subject and averaged over the cohort. These data aligned with the cumulative tumor measure analysis and showed that with inclusion of the outlier, IMT produced a whole tumor reduction of $12.7 \pm 35.8\%$ ($P = 0.096$). With subject #7 excluded, the volume reduction of the IMT-treated GBM increased to a highly significant $19.7 \pm 24.3\%$ ($P = 0.005$).

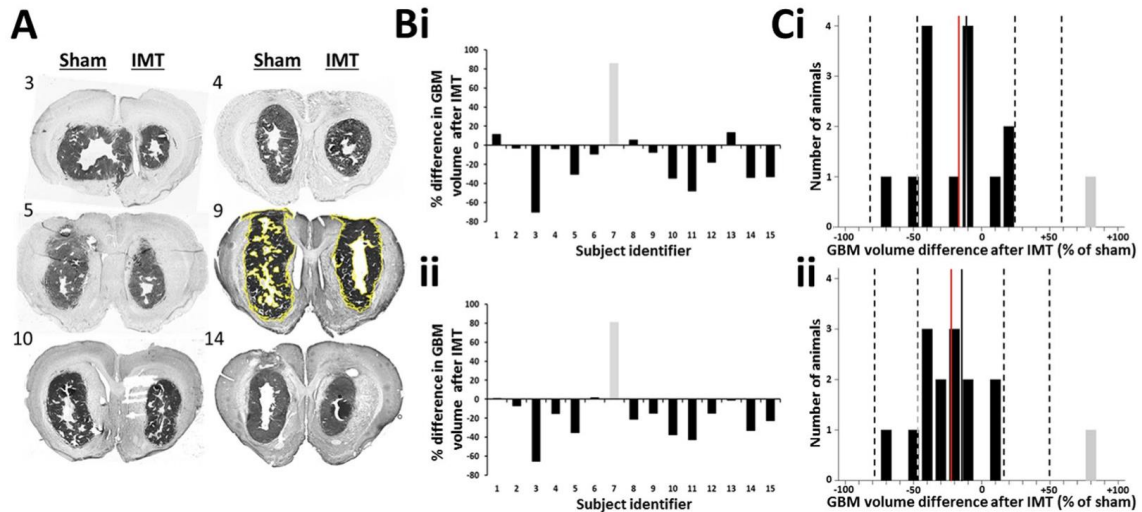


Figure 2-4. IMT attenuates locoregional GBM growth *in vivo*.

(A) Representative, thionine-stained brain sections from 6 animals with GBM treated throughout this study. The 7-day course of IMT was randomized to the right or left GBM (treatment sides have been aligned in this figure for comparative purposes), with the contralateral tumor used as a sham control. The subject identifier is shown to the upper left of each section. GBM volumes were estimated by cumulative cross-sectional tumor areas quantified using ImageJ software, as demonstrated by the yellow tracing in subject 9. (B) The difference in estimated whole (i) and core (ii) GBM volume following IMT, relative to the internal sham control, is provided for every animal. Negative values are consistent with treatment response. The whole tumor measures incorporate serial sections through the rostrocaudal extent of the GBM whereas the core tumor measures were limited to the region surrounding the bioelectrode. There was one outlier (#7, shown in gray) with a reversal of expected effects, presumed technical in origin. (C) Distribution plots showing volume differences in the IMT-treated i) whole and ii) core tumor over 10% intervals. For example, a data bar on the -50% tick mark depicts the number of animals that had a 50–60% tumor reduction. The solid black-to-white lines indicate the cohort means when the data included the outlier shown in gray. The dashed lines indicate the standard deviation of this mean. Note that the outlier is well beyond 2 standard deviations of the mean. The red lines depict the cohort means with the outlier excluded.

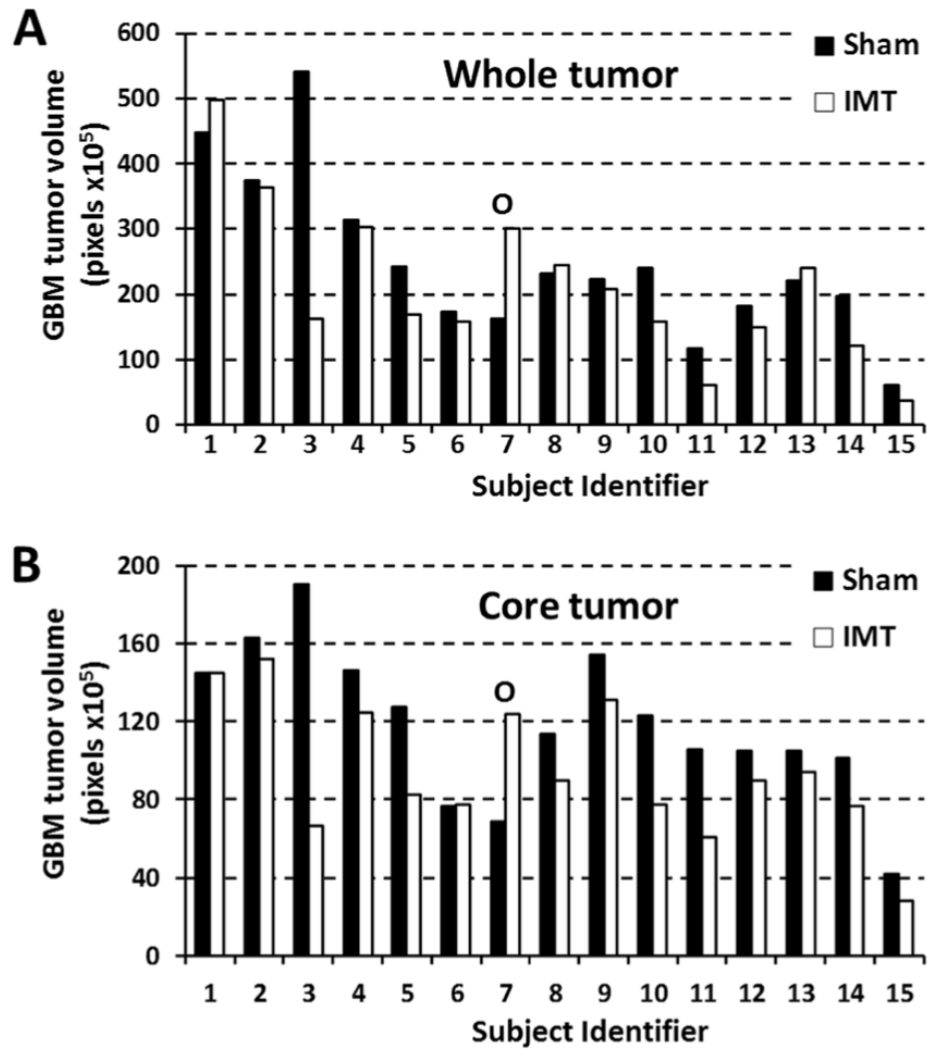


Figure 2-5. Paired *in vivo* GBM responses to sham and IMT conditions.

Raw tumor measures calculated from the (A) whole tumor and (B) core tumor are shown after sham treatment (black) or IMT (white). The statistical outlier shown in Fig. 4 has been left in this dataset for completion (subject #7; labeled O). The IMT-treated GBM was smaller than the sham-treated tumor in 11 of 15 (73%) and 12 of 15 (80%) subjects using whole and core tumor measures, respectively.

Table 2-3 Cumulative *in vivo* tumor burden in sham and IMT-treated GBM within the 15-animal cohort.

| | Cumulative whole tumor volume (pixels $\times 10^6$) | | Whole tumor reduction with IMT (%) | P-value | Cumulative core tumor volume (pixels $\times 10^6$) | | Core tumor reduction with IMT (%) | P-value |
|------------------|---|-------|------------------------------------|---------|--|-------|-----------------------------------|---------|
| | Sham | IMT | | | Sham | IMT | | |
| Outlier included | 366.3 | 313.4 | 14.5 | 0.107 | 176.6 | 141.9 | 19.7 | 0.015 |
| Outlier excluded | 356.2 | 286.9 | 19.5 | 0.047 | 169.7 | 129.5 | 23.7 | 0.002 |

Core tumor analysis focused on the GBM region nearest the bioelectrode and identified 12/15 (80%) animals with smaller IMT-treated, compared to sham-treated, core tumors. Subject #7 was again identified as a statistical outlier using the Dixon's ($P = 0.004$) and Grubb's ($P = 0.002$) tests. Cumulative core GBM burden for the whole group was 19.7–23.7% smaller in IMT tumors compared to sham controls, a highly significant response regardless of the outlier measure (Table 2.3). There was also a significant mean individual reduction of $15.8 \pm 32.0\%$ ($P = 0.038$) when assessed with the outlier included. This measure rose to $22.7 \pm 18.3\%$ ($P = 0.0002$) with the outlier excluded.

2.3.3 Computer simulation predicts IMT electric field properties in GBM tumor and brain

These studies sought to define the extent of *in vivo* treatment coverage produced within the GBM environment using the present IMT hardware and stimulation parameters. IMT electric field modeling was performed in a representative 7-day rodent GBM to best estimate the tumor size and brain conditions at the mid-way point of the current IMT protocol which extended between days 4–11 following GBM cell implantation. The simulation analysis demonstrated a tightly constrained electric field centered near the core of the GBM mass with radial extension to a modest fraction of the tumor and surrounding edematous brain (Fig. 2.6). The amplitude of the IMT electric field decreased logarithmically with the radial distance from the bioelectrode. Field strengths of 4 V/cm, 3 V/cm, 2 V/cm and 1 V/cm extended to 0.32 mm, 0.43 mm, 0.63 mm, 1.24 mm, respectively, from the source. It was estimated that the fractions of GBM tumor that received an IMT electric field amplitude above these thresholds were 3.0%, 4.8%, 9.5% and 24.2% respectively. When combining the regions of GBM tumor and associated

edematous brain, the fractions predicted to receive these field thresholds were 0.5%, 1.0%, 2.4% and 12.1%, respectively (Fig. 2.7).

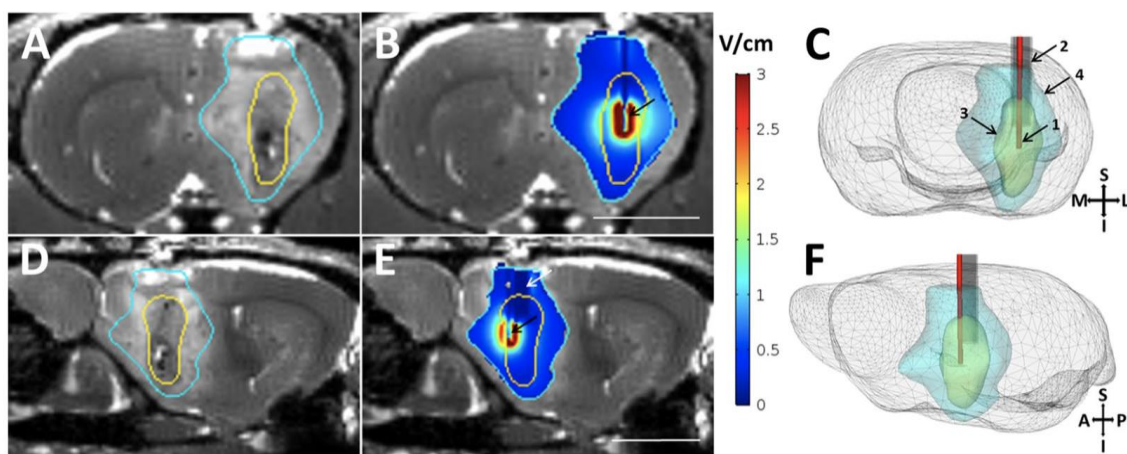


Figure 2-6. Image-based simulation of IMT electric fields.

A 9.4T MRI system was used to generate true fast imaging with steady state precession (TrueFISP) images of a 7-day GBM tumor in the rodent brain. Coronal (A,B) and sagittal (D,E) images are shown. (A,D) Brainsuite software (v.16a1) was used to segment the tumor (yellow trace) and edema (turquoise trace). The segmented volumes were imported to COMSOL Multiphysics (v.5.2a), where the intratumoral bioelectrode and cannula geometries were simulated. (B,E) The conductance and dielectric values of the hardware (bioelectrode, black arrow; cannula, white arrow) and neural elements were used with the boundary condition of constant voltage amplitude of 2.0 V at 200 kHz for the bioelectrode and the reference electrode applied outside the skull. The resulting map of the electric field magnitude was exported and combined with the TrueFISP MR images for visualization in 3D Slicer (v.4.4.0). The electric field data within the tumor was analyzed using MATLAB R2015b to estimate the fraction of tumor receiving specific field amplitudes (see Fig. 7). Three-dimensional rendering of the rodent brain shown in (C) coronal and (F) oblique sagittal views depict the relationship between the 1) intratumoral bioelectrode, 2) cannula, 3) GBM mass and 4) region of tumor-associated cerebral edema. S, superior; I, inferior; M, medial; L, lateral; A, anterior; P, posterior. The scale bar in B corresponds to panels A and B; that in E to panels D and E; both depict 5 mm.

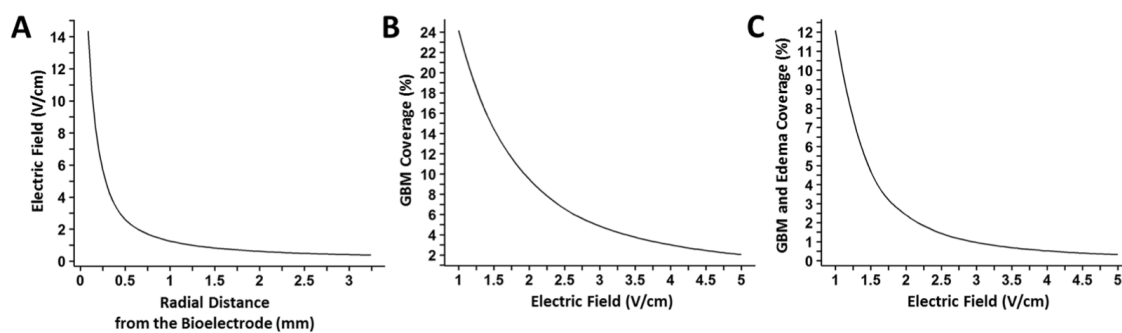


Figure 2-7. Predicted relations between IMT electric field amplitude, radial field dimensions and extent of GBM region coverage in the present *in vivo* treatment model.

2.4 Discussion

This preclinical study is, to our knowledge, the first to demonstrate the efficacy of an implantable electrotherapy using non-ablative, intermediate frequency stimulation in patient-derived GBM cells and in a cohort of living animals with intracerebral GBM. Primary GBM cells, but not neurons, were exquisitely sensitive to low amplitude, sinusoidal pulses at a frequency out of range for neuronal entrainment or thermal injury [Palti, 1996; Storm, 1982]. IMT-mediated cytotoxicity was largely apoptotic and enhanced GBM cell death when co-administered with TMZ chemotherapy. This *in vitro* proof-of-concept was translated to an animal model in which a 1-week course of continuous IMT monotherapy produced a significant reduction of mean GBM volume in the living brain. These highly promising data likely do not reflect the full potential of IMT. There are technical and biological aspects of the present *in vivo* model which may have led to an underestimation of therapeutic efficacy. For example, the rudimentary, single-contact bioelectrode and applied stimulation parameters were predicted to generate an IMT electric field ≥ 1 V/cm (i.e., the lower threshold recommended for the external TTF device) throughout only $\sim 24\%$ of the estimated volume of a 7-day tumor [Mittal, 2017]. The compact IMT field dimensions (i.e., ~ 1.24 mm radius for a ≥ 1 V/cm field) would poorly accommodate a suboptimally positioned bioelectrode, particularly if located near or beyond the GBM boundary, which may explain the inter-animal

variability in treatment response. The measured therapeutic impact, while significant, was likely less than what may be achieved using hardware and stimulation parameters that provide comprehensive coverage of the tumor-affected region. The large GBM burden in the F98 model also created a greater treatment challenge than would be expected with small volume or recurrent/residual tumors. In our hands, a deposit of 40,000 F98 cells produced robust growth, expanding into moderate-sized lesions as early as day 4 and massive GBM tumors with cerebral edema and central necrosis by day 11 post-implantation. Others have reported a mean survival between 18–25 days in rats harboring these GBM tumors [Mathieu, 2005; Mathieu, 2007]. Anecdotally, the rate of growth may be proportionally greater than typical for GBM in humans, creating a highly formidable model in which to evaluate a putative new therapeutic device.

The development of an indwelling electrotherapy for GBM is predicated on a global experience using deep brain stimulation (DBS) devices engineered to treat non-oncological conditions, such as movement, pain, psychiatric and seizure disorders [Udupa, 2015; Wichmann, 2016]. DBS entails stereotactic placement of in-line, multi-contact leads into target brain regions, controlled by a remote-accessed, implantable pulse generator. This technology typically delivers continuous, monophasic, square wave pulses at low amplitude (e.g., 1–5 V) and frequency (e.g., 90–185 Hz) to disrupt and entrain pathological firing patterns in a reversible, non-injurious manner [Herrington, 2016]. DBS and IMT are starkly different in indication, operational parameters, and hardware design. The electrical output of prospective IMT systems will be defined by non-ablative pulses coupled to customized and distinct profiles of waveform, polarity, and frequency parameters titrated to individual tumor response and location. This study utilized a low amplitude (± 2 V), intermediate frequency (200 kHz), sinusoidal waveform with reversing polarity intended to maximally disrupt electrical homeostasis in GBM cells. The pulse frequency was 1000-fold higher than typical for DBS and well beyond the range of neuronal entrainment so not to incite adverse neurological effects when stimulating tumor-infiltrated CNS regions. This amplitude and frequency are also below the threshold for producing thermal injury and have been shown to selectively target GBM cells with relative safety in preclinical studies and human TTF therapy [Xu, 2016; Kirson, 2004; Hottinger, 2016; Storm, 1982]. The irregular and variable anatomy

of GBM disease also mandates unique IMT hardware design. Rather than a single, in-line row of contacts typical of DBS systems, comprehensive tumor coverage requires bioelectrodes with versatile, multi-dimensional configurations driven by a field generator capable of producing a unique spectrum of IMT parameters. DBS has traditionally used a voltage-driven treatment platform, however newer devices are available that utilize constant current parameters with or without directional control [Contarino, 2014; Tagliati, 2015]. Tight regulation of current flow within disease-affected brain regions may provide greater therapeutic impact when the goal is to re-program pathological firing patterns in non-oncological disease; however, it remains unknown whether the same logic applies to electrotherapies designed for CNS cancer. Conductive (uninsulated) bioelectrodes may be powered by a voltage-driven system with the resultant current flow gated by local tissue resistivity. The heterogeneous architecture of the brain and GBM tumors would result in constant voltage with variable and dynamic current flow. In contrast, the same bioelectrodes powered by a constant current platform could provide a defined rate of flow maintained by feedback modulation that adjusts the voltage to accommodate varying resistivity. A third option for IMT delivery is to establish an intratumoral electric field without current flowing between the bioelectrodes and the tissues using non-conductive (insulated) bioelectrodes within the GBM-affected region. In the present work, IMT was voltage-driven with a peak-to-peak pulse amplitude of 4 volts (± 2 V) which did not elicit overt behavioral changes, seizures, or focal neurological deficits, nor histological evidence of electrolysis in the brain or tumor. As a pilot investigation, a small fraction (2/15) of the cohort received insulated bioelectrodes with other IMT parameters remaining constant. There was a positive treatment response in these animals measured by both whole and core tumor analysis, indicating that an applied intratumoral electric field may be sufficient to attenuate tumor growth. Further studies are needed to define the properties of conductive versus non-conductive implanted bioelectrodes in GBM disease.

This study demonstrated the *in vitro* efficacy of intermediate frequency IMT in patient GBM cells and showed that a rudimentary, pilot IMT device could significantly reduce GBM volume across a 15-animal cohort. This is the first demonstration that GBM tumors may be therapeutically impacted using an implantable system to chronically deliver low

intensity, non-ablative electric fields. The current data provide strong justification to develop IMT hardware and application settings that provide more comprehensive tumor coverage and, hopefully, enhanced therapeutic benefit. Successful advances in IMT technology could lead to a novel treatment modality desperately needed for GBM and other high fatality CNS cancers.

2.5 References

1. Nam, J. Y. & Groot, J. F. D. Treatment of Glioblastoma. *J. Oncol. Pract.* 13, 629–638 (2017).
2. Mun, E. J., Babiker, H. M., Weinberg, U., Kirson, E. D. & Von Hoff, D. D. Tumor-Treating Fields: A Fourth Modality in Cancer Treatment. *Clin. Cancer Res.* (2017).
3. Hu, X. et al. In Vitro Validation of Intratumoral Modulation Therapy for Glioblastoma. *Anticancer Res.* 36, 71–80 (2016).
4. Kirson, E. D. et al. Disruption of Cancer Cell Replication by Alternating Electric Fields. *Cancer Res.* 64, 3288–3295 (2004).
5. Pawlowski, P., Szutowicz, I., Marszalek, P. & Fikus, M. Bioelectrorheological model of the cell. 5. Electrodestruction of cellular membrane in alternating electric field. *Biophys. J.* 65, 541–549 (1993).
6. Gera, N. et al. Tumor treating fields perturb the localization of septins and cause aberrant mitotic exit. *PLoS One* 10, e0125269 (2015).
7. Hottinger, A. F., Pacheco, P. & Stupp, R. Tumor treating fields: a novel treatment modality and its use in brain tumors. *Neuro Oncol.* 18, 1338–1349 (2016).
8. Stupp, R. et al. NovoTTF-100A versus physician's choice chemotherapy in recurrent glioblastoma: A randomised phase III trial of a novel treatment modality. *Eur. J. Cancer* 48, 2192–2202 (2012).
9. Stupp, R. et al. Effect of Tumor-Treating Fields Plus Maintenance Temozolomide vs Maintenance Temozolomide Alone on Survival in Patients with Glioblastoma: A Randomized Clinical Trial. *JAMA* 318, 2306–2316 (2017).
10. Sampson, J. Alternating electric fields for the treatment of glioblastoma. *JAMA* 314, 2511–2513 (2015).

11. Mittal, S. et al. Alternating electric tumor treating fields for the treatment of glioblastoma, rationale, preclinical, and clinical studies. *J. Neurosurg.* 24, 1–8 (2017).
12. Gaspar, L. E. et al. Supratentorial malignant glioma: Patterns of recurrence and implications for external beam local treatment. *Int. J. Radiat. Oncol. Biol. Phys.* 24, 55–57 (1992).
13. Halperin, E. C., Burger, P. C. & Bullard, D. E. The fallacy of the localized supratentorial malignant glioma. *Int. J. Radiat. Oncol. Biol. Phys.* 15, 505–509 (1988).
14. Lee, S. W. et al. Patterns of failure following high-dose 3-D conformal radiotherapy for high-grade astrocytomas: a quantitative dosimetric study. *Int. J. Radiat. Oncol. Biol. Phys.* 43, 79–88 (1999).
15. Loeffler, J. et al. Clinical patterns of failure following stereotactic interstitial irradiation for malignant gliomas. *Int. J. Radiat. Oncol. Biol. Phys.* 19, 1455–1462 (1990).
16. Ashby, L. S., Smith, K. A. & Stea, B. Gliadel wafer implantation combined with standard radiotherapy and concurrent followed by adjuvant temozolomide for treatment of newly diagnosed high-grade glioma: a systematic literature review. *World J. Surg. Oncol.* 14, 225 (2016).
17. Barbarite, E. et al. The role of brachytherapy in the treatment of glioblastoma multiforme. *Neurosurg. Rev.* 40, 195–211 (2017).
18. de Paula, L. B., Primo, F. L. & Tedesco, A. C. Nanomedicine associated with photodynamic therapy for glioblastoma treatment. *Biophys. Rev.* 9, 761–773 (2017).
19. Hersh, D. S. et al. Emerging Applications of Therapeutic Ultrasound in Neuro-oncology Moving Beyond Tumor Ablation. *Neurosurgery* 79, 643–654 (2016).
20. Palti, Y. Stimulation of internal organs by means of external applied electrodes. *J. Appl. Physiol.* 21, 1619–1623 (1966).

21. Storm, F. et al. Clinical radiofrequency hyperthermia: a review. *J. Natl. Cancer Inst. Monogr.* 61, 343–350 (1982).
22. Mathieu, D., Lamarche, J. & Fortin, D. The Importance of a Syngeneic Glioma Implantation Model: Comparison of the F98 Cell Line in Fischer and Long-Evans Rats. *J Appl Res* 5, 17–25 (2005).
23. Mathieu, D., Lecomte, R., Tsanaclis, A. M. & Larouche, A. Standardization and Detailed Characterization of the Syngeneic Fischer/F98 Glioma Model. *Can. J. Neurol. Sci.* 34, 296–306 (2007).
24. Udupa, K. & Chen, R. The mechanisms of action of deep brain stimulation and ideas for the future development. *Prog. Neurobiol.* 133, 27–49 (2015).
25. Wichmann, T. & DeLong, M. Deep brain stimulation for movement disorders of basal ganglia origin: restoring function or functionality? *Neurotherapeutics* 12, 264–283 (2016).
26. Herrington, T., Cheng, J. & Eskandar, E. Mechanisms of deep brain stimulation. *J. Neurophysiol* 115, 19–38 (2016).
27. Contarino, M. et al. Directional steering: A novel approach to deep brain stimulation. *Neurology* 83, 1163–1169 (2014).
28. Tagliati, M. Multiple-source current steering: a new arrow in the DBS quiver. *Lancet Neurol.* 14, 670–671 (2015).
29. Ostermann, S. et al. Plasma and cerebrospinal fluid population pharmacokinetics of temozolomide in malignant glioma patients. *Clin. Cancer Res.* 10, 3728–3736 (2004).
30. Wenger, C., Salvador, R., Basser, P. & Miranda, P. The electric field distribution in the brain during TTFIELDS therapy and its dependence on tissue dielectric properties and anatomy: a computational study. *Phys. Med. Biol.* 60, 7339–7357 (2015).

31. Wenger, C., Salvador, R., Basser, P. & Miranda, P. Improving tumor treating fields treatment efficacy in patients with glioblastoma using personalized array layouts. *Int. J. Radiat. Oncol. Biol. Phys.* 95, 1137–1143 (2016).

Chapter 3

3 Diffuse Intrinsic Pontine Glioma Cells are Vulnerable to Low Intensity Electric Fields Delivered by Intratumoral Modulation Therapy²

Introduction Diffuse intrinsic pontine glioma (DIPG) is a high fatality pediatric brain cancer without effective treatment. The field of electrotherapeutics offers new potential for other forms of glioma but the efficacy of this strategy has not been reported for DIPG. This pilot study evaluated the susceptibility of patient-derived DIPG cells to low intensity electric fields delivered using a developing technology called intratumoral modulation therapy (IMT). **Methods** DIPG cells from autopsy specimens were treated with a custom-designed, *in vitro* IMT system. Computer-generated electric field simulation was performed to quantify IMT amplitude and distribution using continuous, low intensity, intermediate frequency stimulation parameters. Treatment groups included sham, IMT, temozolomide (TMZ) chemotherapy and radiation therapy (RT). The impact of single and multi-modality therapy was compared using spectrophotometric and flow cytometry viability analyses. **Results** DIPG cells exhibited robust, consistent susceptibility to IMT fields that significantly reduced cell viability compared to untreated control levels. The ratio of viable:non-viable DIPG cells transformed from ~ 6:1 in sham-treated to ~ 1.5:1 in IMT-treated conditions. The impact of IMT was similar to that of dual modality TMZ–RT therapy and the addition of IMT to this treatment combination dramatically reduced DIPG cell viability to ~ 20% of control values.

² A version of this chapter is published as:

Andrew Deweyert, Erin Iredale, Hu Xu, Eugene Wong, Susanne Schmid, Matthew. O. Hebb. (2019). Diffuse intrinsic pontine glioma cells are vulnerable to low intensity electric fields delivered by Intratumoral Modulation Therapy. *Journal of Neuro-Oncology*. 43(1):49-56.

Conclusions This proof-of-concept study provides a novel demonstration of marked DIPG cell susceptibility to low intensity electric fields delivered using IMT. The potent impact as a monotherapy and when integrated into multi-modality treatment platforms justifies further investigations into the potential of IMT as a critically needed biomedical innovation for DIPG.

3.1 Introduction

Diffuse intrinsic pontine glioma (DIPG), also called H3 K27M-mutant diffuse midline glioma, is the most common brainstem cancer in children, representing 80% of tumors in this region of the central nervous system (CNS) [Wu , 2012; Johung , 2017]. The average age at diagnosis is 6–9 years old and affected children typically present with a progressive spectrum of neurological deficits. Magnetic resonance imaging most often reveals an expansile, T2-hyperintense, poorly-enhancing mass centered in the pons [Harward, 2018]. The infiltration of DIPG within the brainstem parenchyma precludes safe surgical resection. The mainstay of treatment is fractionated radiation therapy (RT) which can provide transient symptom and tumor control resulting in median patient survival of 9 months and a 2-year survival rate < 10% [Cohen, 2017]. Multiple chemotherapy protocols and agents have been trialed but have not demonstrated further survival benefit [Long, 2017; Gwak, 2017]. Despite international efforts in defining the molecular underpinnings of DIPG, there have been no recent therapeutic advances that substantially improve patient outcomes [Johung, 2017; Cohen, 2017].

There is emerging evidence that electrotherapy may offer a novel means to control malignant glioma and considerable progress has been made treating the high fatality CNS cancer, glioblastoma (GBM). A single clinical electrotherapy system with demonstrated survival benefit has been approved for new and recurrent GBM. Unfortunately this device is not engineered for the treatment of infratentorial tumors such as DIPG [Stupp , 2012; Fonkem , 2012; Stupp , 2017]. Current PubMed searches using the terms diffuse intrinsic pontine glioma and electrotherapy or electric fields produced no reports. Thus, the potential impact of electrotherapy on DIPG remains unknown. Intratumoral modulation therapy (IMT) is a developing technology which may offer an electrotherapeutic option for tumors located anywhere within the CNS, including the

brainstem [Xu, 2016; DiSebastiano, 2018]. IMT exploits the electrosensitivity of cancer cells using implanted field-generating sources (e.g., bioelectrodes) to deliver non-ablative, low intensity electric fields that attenuate tumor growth and bolster multi-modality treatment platforms. Preclinical studies demonstrated potent efficacy of IMT as a monotherapy and when combined with chemotherapeutic or oncogene-silencing agents in primary human GBM cells and *in vivo* allogeneic GBM models [Xu, 2016; DiSebastiano, 2018]. To date, however, there have been no reports of the application of IMT to other CNS cancers. The goal of this pilot study was to determine the vulnerability of patient-derived DIPG cells to low intensity electric fields delivered using an established IMT protocol. The impact of IMT on DIPG resistance to conventional radiation and chemotherapy options was also investigated.

3.2 Materials and Methods

3.2.1 Patient-derived DIPG cells

Patient-derived DIPG cells, labeled SU-DIPG-IV, SU-DIPG-XIX and SU-DIPG-XXIV, were kindly received from Dr. Michelle Monje at Stanford University. The tumor collection protocol, culture methods at derivation, patient demographics and tumor genetics have been previously described [Lin, 2017; Venkatesh, 2017; Qin, 2017; Ostermann, 2004]. The cells were derived from early post-mortem DIPG specimens in three pediatric patients, aged 2, 2, and 6 years old respectively, who had received radiation and chemotherapy during their care. Upon arrival to the Hebb lab, frozen DIPG cells were thawed and cultured in 6-well plates (Corning, NY, United States) at 37 °C with humidified air containing 5% CO² using NeuroCult™ NS-A medium supplemented with 10% proliferation supplement, bFGF (10 ng/mL), EGF (20 ng/mL), heparin sulfate (2µg/ml) and 1% penicillin/streptomycin (Complete NSA; Stemcell Technologies, Vancouver, B.C., Canada). The medium was changed every 72 h and cultures passaged 1:2 at 70–90% confluence.

3.2.2 *In vitro* IMT model

The impact of IMT alone and combined with temozolomide (TMZ) chemotherapy and/or RT was evaluated using primary human DIPG cells cultured in 35 mm wells. The IMT model was created by fitting each well with a clinical grade, platinum-based strip bioelectrode (Ad-Tech Medical Instrument Corporation, Oak Creek, WI, USA) around the periphery and platinum-iridium bioelectrode (Medtronic Ltd., Hertfordshire, United Kingdom) at the center of the well and cell culture [Xu, 2016; DiSebastiano, 2018]. A waveform generator (Rigol DG1022; Electro-Meters Ltd., Pickering, ON, Canada) was used to deliver biphasic sinusoidal pulses with low amplitude (± 2 V; peak-to-peak 4 V) and intermediate frequency (200 kHz) continuously over 3 days. Control wells (i.e. sham-treated) were fitted with bioelectrodes but did not receive stimulation.

3.2.3 IMT field simulation

The IMT electric field was simulated with COMSOL Multiphysics v 5.2a (Comsol Inc., Burlington, MA, USA) AC/DC module, electric currents user interface in the frequency domain. The geometries of the *in vitro* model were manually created utilizing COMSOL Geometry to generate an identical *in silico* model. The dish and electrode apparatus were mimicked in geometry and the appropriate materials simulated utilizing known material conductance and dielectric properties. The boundary conditions were applied as the edge of the 35 mm dish. The centre stimulating electrode was set to emit a 2 V amplitude waveform, and the outer electrodes were grounds. Electrical insulation on outer boundaries was assumed. A mesh of the geometry was created, and a frequency of 200 kHz chosen for evaluation. The dimensions and amplitude of the electric field within the culture dish were analyzed using MATLAB R2015b (MathWorks Inc., Natick, MA, United States).

3.2.4 Multi-modality treatment of DIPG cells

DIPG cells (1×10^5) treated with 50 μ m TMZ were cultured in 35 mm wells fitted with IMT bioelectrodes without stimulation (i.e., sham IMT) for TMZ monotherapy or while receiving concurrent IMT during dual therapy. This TMZ concentration corresponds to plasma levels obtained with 150 mg/m² in the adjuvant treatment phase of other forms of

glioma [15]. Additional DIPG samples received 4 Gy of ionizing radiation in a single fraction using a Cobalt-60 irradiator with average dose rate of 74 cGy/min. This dose was chosen after a RT dose–response study to permit evaluation of cooperative benefits between different therapeutic modalities *in vitro* [Buch, 2012; Smyth, 2018]. The cells were allowed to recover for 1 h after RT and were then plated into 35 mm wells fitted with the IMT system. At this point, DIPG cells were cultured with no further treatment (i.e., RT monotherapy group), or in the presence of TMZ (50 μ M) or IMT (i.e., TMZ-RT or IMT-RT dual therapy groups), or both TMZ and IMT (i.e., TMZ-RT- IMT multi-modality therapy group) for 3 days.

3.2.5 Cell viability assay

Cell viability was evaluated using the 3-(4,5-dimethylthiazol-2-yl)-2,5-diphenyltetrazolium (MTT) spectral analysis (Sigma Aldrich, St. Louis, MO, United States). This colorimetric assay measures the reduction of yellow MTT by mitochondrial succinate dehydrogenase to an insoluble, dark purple formazan product. Immediately following the DIPG cell treatments described above, MTT (80 μ l at 5 mg/ml) was added to the 35 mm wells and incubated for 3 h at 37 °C in a humidified 5% CO² atmosphere. The cells were then lysed to release the purple formazan product by the addition of 300 μ l dimethyl sulfoxide for 15 min at room temperature. Absorbance was measured using an Epoch microplate spectrophotometer (BioTek, Winooski, VT, United States). Cell viability was estimated using optical density values at 570 nm with references at 655 nm detected in each well. Brightfield images of cells stained with MTT were obtained using a Motic AE31 inverted microscope fitted with an Infinity 1–3 scientific complementary metal-oxide semiconductor camera (Lumenera Corp, Nepean, ON, Canada).

3.2.6 Flow cytometry

Annexin V apoptosis detection with zombie red (ZR) was used to quantify fractions of live, apoptotic and dead DIPG cells, as per the manufacturer’s instructions (BioLegend, San Diego, CA, USA). Cell fractions were analyzed using a Becton Dickinson LSR II SORP flow cytometer running FACSDiva software (BD Biosciences, Mississauga, ON, Canada). Cells were first gated on forward scatter (FSC-) versus side scatter (SSC-)

characteristics before excluding doublets using consecutive gating FSC-Area versus FSC-Width and SSC-Area versus SSC-Width plots. The populations of annexin V⁺/ZR⁻, annexin V⁺/ZR⁺, annexin V⁻/ZR⁺ and annexin V⁻/ZR⁻ were then calculated with quadrant gates. Approximately 25,000 single cells were acquired per sample at a maximum event rate of 5000 events per second. Data were analyzed using FlowJo v 9.6.3 software (TreeStar Inc., Ashland, OR, USA).

3.2.7 Statistical analysis

A t test was used to compare paired data sets. Multiple pairwise comparisons were performed using one-way analysis of variance (ANOVA) followed by Tukey post hoc analysis (SPSS Inc., Chicago, IL, USA). Data are presented as mean \pm standard deviation with significance assumed at $p < 0.05$.

3.3 Results

3.3.1 IMT field mapping for *in vitro* DIPG cell treatment

The *in vitro* IMT model utilized clinical grade, biocompatible, platinum (peripheral ground) and platinum-iridium (central stimulating) bioelectrodes fitted within 35 mm culture preparations of patient DIPG cells (Fig. 3.1a). A sinusoidal, biphasic waveform with peak-to-peak amplitude of 4 V was chosen to create reversing polarity and maximally disrupt the electrical environment using low intensity parameters known to be innocuous within the living brain (Fig. 3.1b) [DiSebastiano, 2018]. The 200 kHz stimulation frequency is below that needed to produce thermal injury and surpassed the neuronal entrainment threshold to reduce the potential of off-target IMT effects when translated to eloquent brain regions [Kirson, 2004; Palti, 1996; Storm, 1982]. The bioelectrode configuration and stimulation parameters created a symmetric, low intensity IMT field pattern across the DIPG cultures. The electric field was calculated by simulating the *in vitro* experiments in COMSOL Multiphysics (v 5.3a) using the electrode geometry presented and a constant voltage amplitude waveform generation. Based on this simulation, the largest electric field coverage extended concentrically from

the central stimulating bioelectrode with smaller fields generated at regular intervals around the encircling peripheral bioelectrodes (Fig. 3.1c). The percent area coverage across the culture dish was calculated and plotted over one cycle of the waveform for electric field magnitude with thresholds in the range previously shown to be effective in other glioma cancers (Fig. 3.1d) [Xu, 2016; DiSebastiano, 2018; Wenger, 2015; Wenger, 2016]. The coverage at the peak of the IMT waveform for each of the electric field magnitude thresholds of 1, 0.75, 0.5 and 0.25 V/cm was 6.2%, 8.9%, 16.4% and 54.7% respectively. Although other forms of glioma have been shown to require electric field amplitude > 1 V/cm for optimal electrotherapy benefits, the threshold for DIPG response is not known [Wenger, 2015; Wenger, 2016]. The therapeutic effects described below were therefore generated with this pilot IMT model providing electric field coverage > 0.25 V/cm to roughly half, and 1 V/cm to only a small fraction of the DIPG culture area.

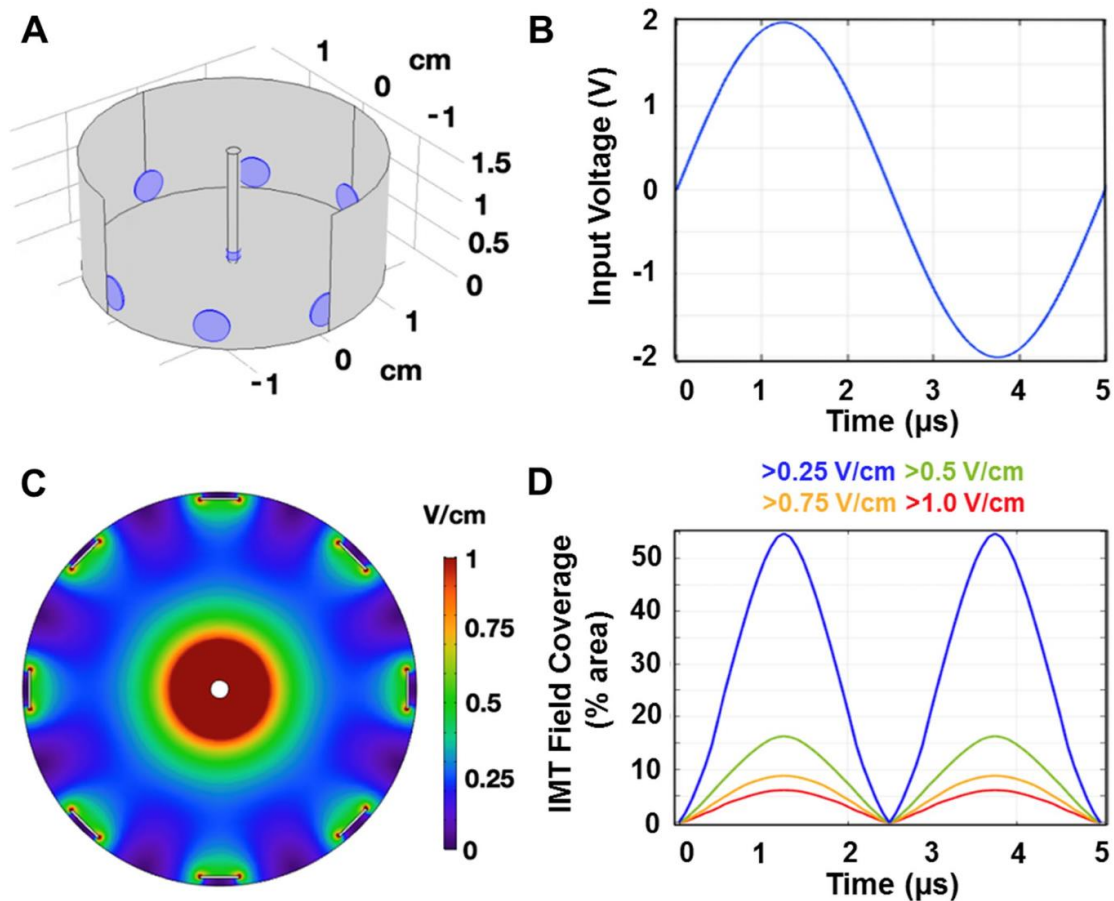


Figure 3-1. Computer simulation of the IMT model.

a The IMT model was created using a central stimulating bioelectrode placed in a 3.5 cm well along with eight peripheral grounded bioelectrodes. b A waveform generator supplied a 200 kHz sinusoidal voltage with constant amplitude of 2 V to the central electrode. c Applying such parameters to this configuration of bioelectrodes resulted in an alternating electric field with the predicted magnitude and distribution plotted as shown. d The percent area coverage across the culture dish reaching the electric field thresholds in the range anticipated to exert biological impact are plotted as a function of time over one cycle of the waveform. This pilot IMT system provided only fractional field coverage to the DIPG cultures.

3.3.2 Patient DIPG cells are vulnerable to low intensity IMT fields

Paired sham and IMT conditions were used to independently assess the impact of IMT monotherapy on primary DIPG cells (SU-DIPG-IV, SU-DIPG-XIX, SU-DIPG-XXIV) obtained from three pediatric patients. The 3-day exposure to low intensity IMT produced a dramatic and consistent reduction in tumor cell viability. IMT-treated cultures were sparse, pyknotic and exhibited faint MTT (formazan) labeling compared to sham-treated DIPG cultures (Fig. 3.2a, b). Statistical assessment performed on MTT measures normalized to those obtained in DIPG cells not exposed to IMT hardware (i.e., untreated controls) revealed a significant reduction in viability following IMT ($51.6 \pm 16.0\%$) compared to sham ($84.0 \pm 33.0\%$) treatment ($p = 0.046$; Fig. 3.2c). Flow cytometry was performed to confirm the MTT findings and evaluate the potential of apoptosis as a mechanism of IMT effect on DIPG cells. The ratio of viable:non-viable DIPG cells decreased from $\sim 6:1$ in sham-treated to $\sim 1.5:1$ in IMT-treated conditions (Fig. 3.3). The significant reduction in DIPG cell viability was accompanied by a concordant rise in apoptotic and dead cell fractions across all patient samples (Table 1).

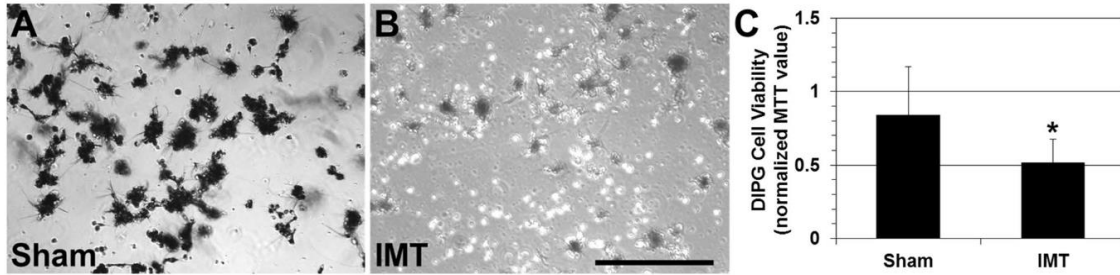


Figure 3-2. DIPG cells are highly susceptible to low intensity IMT.

Representative brightfield microscopy showing patient DIPG cultures following a 3-day exposure to a sham or b IMT conditions. The cultures were stained with the viability dye, MTT which produces a dark chromogen in viable cells. IMT-treated DIPG cells exhibited marked pyknosis with reduced MTT labeling and density. c MTT measures in sham and IMT treated cultures were normalized to those obtained in parallel cultures of untreated DIPG cells. The IMT exposure produced a marked and significant reduction in DIPG cells (asterisk; $p = 0.046$; $n = 3$; mean \pm standard deviation). Scale bar represents $500 \mu\text{m}$ for a and b.

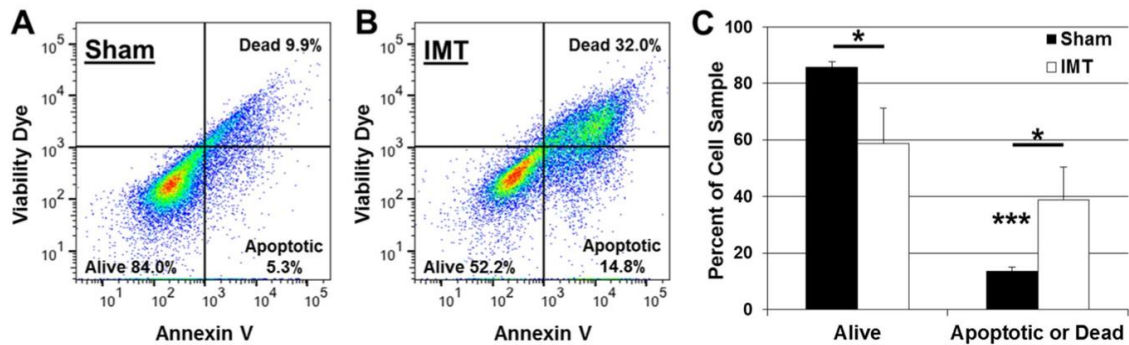


Figure 3-3. IMT enhances apoptosis and death fractions in DIPG cell cultures.

a Representative flow cytometry scatterplots of annexin and the viability dye zombie red (ZR) labeling of apoptotic and dead DIPG cells, respectively, after a 3-day exposure to a sham or b IMT conditions. c Quantification of live and combined apoptotic/dead DIPG cell fractions. In the sham-treated cultures, there was a marked, significant discrepancy between these fractions that was attenuated in IMT treated cultures owing to the significant rise in cell death. Asterisks immediately above the histogram bars indicate significance between the live and apoptotic/dead fractions within the same treatment group. Significance between indicated data pairs is depicted by the asterisk above the horizontal bars. Data are presented as mean \pm standard deviation with significance indicated at $P: * < 0.05$ and $*** < 0.001$.

Table 3-1. Summary of flow cytometry data in patient DIPG cell samples

Table 1 Summary of flow cytometry data in patient DIPG cell samples

| DIPG # and cell fraction | | SU-DIPG-IV | | | SU-DIPG-XIX | | | SU-DIPG-XXIV | | |
|--------------------------|------|------------|---------------|----------|-------------|---------------|----------|--------------|---------------|----------|
| | | Live (%) | Apoptotic (%) | Dead (%) | Live (%) | Apoptotic (%) | Dead (%) | Live (%) | Apoptotic (%) | Dead (%) |
| Treatment group | Sham | 84 | 5.3 | 9.9 | 87.6 | 10 | 2.34 | 85.7 | 12.6 | 0.6 |
| | IMT | 52.2 | 14.8 | 32 | 73 | 18.7 | 6.9 | 51.2 | 32.2 | 11.7 |

3.3.3 IMT significantly enhances multi-modality treatment platforms for DIPG

The impact of IMT monotherapy was compared to single agent TMZ chemotherapy and RT, as well as combined approaches using dual or triple modality platforms (Fig. 3.4). DIPG cells were treated with TMZ at a concentration equivalent to that achieved in plasma during standard care for GBM, another form of high-grade glioma, with known modest, yet significant therapeutic efficacy and an acceptable toxicity profile [Ostermann, 2004]. The applied RT dose (4 Gy) in this study is known to have minimal impact in DIPG cells when used as a monotherapy, based on in-house experience (unpublished) and previous reports by other groups [Buch, 2012; Smyth, 2018]. This dose was chosen to determine if the negligible efficacy could be bolstered by the addition of TMZ and/or IMT to lessen the potential for adverse radiation effects when delivered *in vivo*. MTT analysis was used to assess the viability of DIPG cells following parallel 3-day exposures to sham IMT (i.e., hardware placement without stimulation) or IMT with or without TMZ, RT or combined TMZ-RT. All MTT measures were normalized to those of untreated DIPG controls. The sham IMT conditions had little effect on DIPG cells and yielded $96.0 \pm 6.6\%$ viability. Monotherapy TMZ and RT was assessed in culture wells fitted with a sham IMT system. TMZ ($81.1 \pm 17\%$ viability; $p = 0.564$) and RT ($72.2 \pm 11.9\%$ viability; $p = 0.105$) produced slight reduction in MTT values that were not statistically different from the sham-only controls. In contrast, the combined TMZ-RT exposure (which also included the sham IMT hardware) produced a mean DIPG cell viability of $58.9 \pm 11.3\%$ which was significantly reduced relative to the sham-only treated cells ($p = 0.004$).

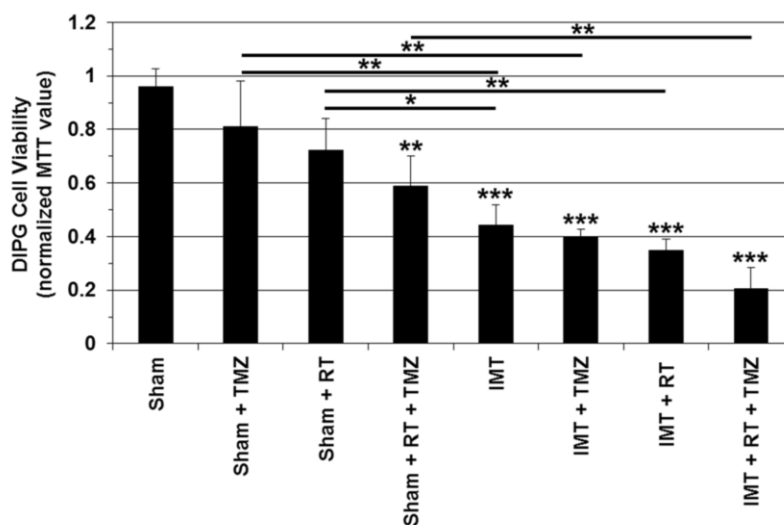


Figure 3-4. IMT significantly augments multi-modality treatment platforms for DIPG.

TMZ, low dose RT and IMT were applied to patient DIPG cultures in 3-day mono- and multi-modality therapies. The MTT viability assay was used to evaluate the impact of each treatment and the resultant data normalized to the mean MTT value obtained in untreated control DIPG cells. Monotherapy TMZ and RT were delivered in culture wells fitted with sham IMT hardware and neither had a significant impact on DIPG cells. In contrast, dual TMZ-RT exposure dramatically reduced DIPG cell viability. The IMT effect did not differ significantly from that of dual TMZ-RT therapy. However, the addition of IMT to the TMZ-RT combination produced marked and highly significant added therapeutic impact and a resultant DIPG viability of approximately 20% of untreated controls. Asterisks immediately above the histogram bars indicate significance between that specific treatment group and sham control. Significance between indicated data pairs is depicted by the asterisk(s) above the horizontal bars. Data are presented as mean \pm standard deviation with significance indicated at P: * <0.05, ** <0.01 and *** < 0.001

IMT monotherapy resulted in DIPG cell viability of $44.2 \pm 7.7\%$ which was also significantly reduced compared to sham values ($p < 0.001$) and significantly more effective than either TMZ ($p = 0.005$) or RT ($p = 0.045$) conditions. Dual therapy created by the addition of IMT significantly reduced DIPG cell viability compared to monotherapy TMZ ($81.1 \pm 17\%$ vs. $40.1 \pm 2.50\%$; $p = 0.002$) or RT ($72.2 \pm 11.9\%$ vs. 34.7 ± 4.4 ; $p = 0.004$). In contrast to TMZ and RT monotherapies, the MTT-measured impact of IMT alone was not significantly different than the combined TMZ-RT

treatment ($p = 0.614$). Likewise, the therapeutic effect of combined TMZ-RT exposure was not significantly different from dual modality exposure to IMT-TMZ ($p = 0.315$) or IMT-RT ($p = 0.113$). Most notably, however, the impact of dual therapy TMZ-RT was potently enhanced by the addition of IMT in the multi-modality treatment platform TMZ-RT-IMT ($58.9 \pm 11.3\%$ vs. $20.50 \pm 7.8\%$ viability, respectively; $p = 0.004$).

3.4 Discussion

This study provided novel evidence of DIPG cell vulnerability to low intensity electric fields delivered using an established preclinical IMT protocol. IMT produced apoptotic tumor cell death using stimulation parameters previously demonstrated to be non-injurious to normal neural cells *in vitro* and *in vivo* [Xu, 2016, DiSebastiano, 2018]. The applied stimulation frequency of 200 kHz is above the range for neural entrainment and below that for thermal injury [Palti, 1996; Storm, 1982]. IMT monotherapy reduced DIPG cell viability by $\sim 50\%$ and was more efficacious than either low dose RT or a clinically utilized concentration of TMZ. The addition of IMT to the combined TMZ-RT paradigm dramatically reduced DIPG cell viability from $\sim 60\%$ to 20% . It remains unclear how IMT incites glioma cell death. There is evidence that non-ablative, non-thermal, low intensity electric fields work through multiple anti-neoplastic mechanisms that disrupt polarized molecules necessary for cell division, membrane permeability and channel homeostasis [Pawłowski, 1993; Gera, 2015]. In GBM studies, IMT has been shown to enhance the impact of TMZ and oncogene-targeted therapy as well as the uptake of hydrophilic genetic inhibitors [Xu, 2016]. The apparent lack of effect on post-mitotic neurons or in normal brain parenchyma suggests that IMT exploits electrochemical vulnerabilities related to the neoplastic phenotype. Further studies are required to better understand these issues.

One possible method of providing IMT to DIPG entails custom configured, implanted bioelectrodes to perpetually deliver therapeutic electric fields across tumor-affected CNS regions using a concealed, titratable system that works cooperatively within a multi-modality treatment platform. Radiation is currently first line care for DIPG and, in this

study, produced cooperative anti-neoplastic impact when delivered concurrently with IMT [Cohen, 2017]. While chemotherapy has not shown significant benefit in DIPG for a potential host of reasons, TMZ is commonly used and beneficial in other forms of malignant glioma [Gwak, 2017; Ostermann, 2004]. In this study, the insignificant impact of RT or TMZ monotherapies was in contradistinction to the potent effect of the triple IMT/RT/TMZ combination, suggestive of sensitizing interactions that dramatically improve overall treatment efficacy. It remains to be determined if this efficacy will persist *in vivo*, and whether the multi-modality platform brings any unexpected toxicities. With respect to safety, a key putative advantage of the envisioned clinical IMT system is the ability to titrate, re-configure and discontinue stimulation. Reversibility of effect with therapy cessation, as typical with conventional forms of neuromodulation such as deep brain stimulation (DBS), is likely given the low amplitude and apparently benign nature of applied IMT fields in normal brain [DiSebastiano, 2018; Udupa, 2015; Wichmann, 2016; Herrington, 2016].

The most readily available IMT prototype will likely include multi-contact leads stereotactically positioned within the brainstem and powered by an indwelling pulse generator. Surgical access to the brainstem is routinely achieved for various neoplastic and non-neoplastic indications and does not present an obvious barrier to development and safe application of IMT for DIPG patients. For example, there has been recent progress directly targeting DIPG tumors with catheters used for convection-enhanced delivery (CED) of pharmacotherapies [Morgenstern, 2018; van Vuurden, 2018]. While the outcome of the neoplastic disease was not altered using CED, there were no significant adversities that resulted from implanting catheters within the DIPG tumors. A longstanding, global experience with DBS provides another important example of the feasibility to implant hardware in the brainstem for treating neurological disease. DBS is the standard of surgical care for Parkinson's Disease (PD) where electrodes are chronically implanted into the subthalamic nucleus and often extending into the mesencephalic substantia nigra [Habets, 2018; Ramirez-Zamora, 2018]. The pedunculopontine nucleus is another brainstem target being evaluated for implanted neuromodulation systems to improve postural and gait instability in PD [Nowacki, 2018]. It is important to note that DBS and IMT are starkly different in neurological indication,

operational parameters and hardware design. The electrical output of putative IMT systems will be defined by customized waveform, polarity, and stimulation parameters titrated to individual tumor response and regional anatomy. DBS technology typically delivers continuous, monophasic, square wave pulses at low frequency (e.g., 90–185 Hz) to disrupt and entrain pathological firing patterns [Udupa , 2015; Wichmann , 2016; Herrington, 2016]. In contrast, the present IMT system used an intermediate frequency (200 kHz), sinusoidal waveform with reversing polarity intended to maximally disrupt electrical homeostasis in DIPG cells. The pulse frequency was 1000-fold higher than typical DBS settings and well out of range for neuronal entrainment in order to selectively target neoplastic cells while averting adverse neurological effects when stimulating tumor-infiltrated CNS regions [DiSebastiano, 2018; Palti, 1996; Hottinger, 2016]. Additionally, the hardware configuration required to deliver personalized, comprehensive IMT field coverage will likely be sharply divergent from that of contemporary DBS electrodes designed to provide highly discrete zones of stimulation.

This proof-of-concept study provided novel evidence of DIPG cell susceptibility to low intensity electric fields delivered using an IMT strategy. The significant treatment response was produced in a pilot IMT model with incomplete field coverage, suggesting even greater efficacy may be realized using a comprehensive delivery system. Additionally, these DIPG cells were derived from fresh autopsy tissue that had been previously exposed to chemotherapy and RT, possibly selecting for tumor cells with heightened treatment resistance. The impact of IMT-based platforms measured in this study may therefore underestimate that attainable in treatment-naïve DIPG cells. While the present observations have yet to be replicated in larger, genetically-diverse cohorts and translational models, these exciting early data provide a new glimpse at the potential of electrotherapeutics to improve the otherwise devastating outcome for DIPG patients.

3.5 References

1. Wu G, Broniscer A, McEachron TA, Lu C, Paugh BS, Becksfort J, Qu C, Ding L, Huether R, Parker M, Zhang J, Gajjar A, Dyer MA, Mullighan CG, Gilbertson RJ, Mardis ER, Wilson RK, Downing JR, Ellison DW, Zhang J, Baker SJ, St. Jude Children's Research Hospital–Washington University Pediatric Cancer Genome Project (2012) Somatic histone H3 alterations in pediatric diffuse intrinsic pontine gliomas and non-brainstem glioblastomas. *Nat Genet* 44:251–253.
2. Johung TB, Monje M (2017) Diffuse intrinsic pontine glioma: new pathophysiological insights and emerging therapeutic targets. *Curr Neuropharmacol* 15(1):88–97
3. Harward S, Harrison Farber S, Malinzak M, Becher O, Thompson EM (2018) T2-weighted images are superior to other MR image types for the determination of diffuse intrinsic pontine glioma intratumoral heterogeneity. *Childs Nerv Syst* 34(3):449–455
4. Cohen KJ, Jabado N, Grill J (2017) Diffuse intrinsic pontine gliomas current management and new biologic insights. Is there a glimmer of hope? *Neuro oncology* 19(8):1025–1034
5. Long W, Yi Y, Chen S, Cao Q, Zhao W, Liu Q (2017) Potential new therapies for pediatric diffuse intrinsic pontine glioma. *Front Pharmacol* 8:1–13
6. Gwak HS, Park HJ (2017) Developing chemotherapy for diffuse pontine intrinsic gliomas (DIPG). *Crit Rev Oncol Hematol* 120:111–119
7. Stupp R, Wong ET, Kanner AA, Steinberg D, Engelhard H, Heidecke V, Kirson ED, Taillibert S, Liebermann F, Dbalý V, Ram Z, Villano JL, Rainov N, Weinberg U, Schiff D, Kunschner L, Raizer J, Honnorat J, Sloan A, Malkin M, Landolfi JC, Payer F, Mehdorn M, Weil RJ, Pannullo SC, Westphal M, Smrcka M, Chin L, Kostron H, Hofer S, Bruce J, Cosgrove R, Paleologous N, Palti Y, Gutin PH (2012) NovoTTF-

- 100A versus physician's choice chemotherapy in recurrent glioblastoma: a randomised phase III trial of a novel treatment modality. *Eur J Cancer* 48:2192–2202
8. Fonkem E, Wong ET (2012) NovoTTF-100A: a new treatment modality for recurrent glioblastoma. *Expert Rev Neurother* 12:895–899
 9. Stupp R, Taillibert S, Kanner A, Read W, Steinberg D, Lhermitte B, Toms S, Idbaih A, Ahluwalia MS, Fink K, Di Meo F, Lieberman F, Zhu JJ, Stragliotto G, Tran D, Brem S, Hottinger A, Kirson ED, Lavy-Shahaf G, Weinberg U, Kim CY, Paek SH, Nicholas G, Bruna J, Hirte H, Weller M, Palti Y, Hegi ME, Ram Z (2017) Effect of tumor-treating fields plus maintenance temozolomide vs maintenance temozolomide alone on survival in patients with glioblastoma: a randomized clinical trial. *JAMA* 318:2306–2316
 10. Xu H, Bihari F, Whitehead S, Wong E, Schmid S, Hebb MO (2016) In vitro validation of intratumoral modulation therapy for glioblastoma. *Anticancer Res* 36:71–80
 11. Di Sebastiano AR, Deweyert A, Benoit S, Iredale E, Xu H, De Oliveira C, Wong E, Schmid S, Hebb MO (2018) Preclinical outcomes of intratumoral modulation therapy for glioblastoma. *Sci Rep* 8:7301
 12. Lin GL, Monje M (2017) A protocol for rapid post-mortem cell culture of diffuse intrinsic pontine glioma (DIPG). *J Vis Exp* 121:e55360
 13. Venkatesh HS, Tam LT, Woo PJ, Lennon J, Nagaraja S, Gillespie SM, Ni J, Duveau DY, Morris PJ, Zhao JJ, Thomas CJ, Monje M (2017) Targeting neuronal activity-regulated neuroligin-3 dependency in high-grade glioma. *Nature* 549(7673):533–537
 14. Qin EY, Cooper DD, Abbott KL, Lennon J, Nagaraja S, Mackay A, Jones C, Vogel H, Jackson PK, Monje M (2017) Neural precursor-derived pleiotrophin mediates subventricular zone invasion by glioma. *Cell* 170(5):845–859

15. Ostermann S, Csajka C, Buclin T, Leyvraz S, Lejeune F, Decosterd LA, Stupp R (2004) Plasma and cerebrospinal fluid population pharmacokinetics of temozolomide in malignant glioma patients. *Clin Cancer Res* 10:3728–3736
16. Buch K, Peters T, Nawroth T, Sanger M, Schmidberger H, Langguth P (2012) Determination of cell survival after irradiation via clonogenic assay versus multiple MTT assay—a comparative study. *Radiat Oncol* 7:1
17. Smyth LM, Rogers PAW, Crosbie JC, Donoghue JF (2018) Characterization of diffuse intrinsic pontine glioma radiosensitivity using synchrotron microbeam radiotherapy and conventional radiation therapy in vitro. *Radiat Res* 189:146–155
18. Kirson ED, Gurvich Z, Schneiderman R, Dekel E, Itzhaki A, Wasserman Y, Schatzberger R, Palti Y (2004) Disruption of cancer cell replication by alternating electric fields. *Cancer Res* 64:3288–3295
19. Palti Y (1996) Stimulation of internal organs by means of external applied electrodes. *J Appl Physiol* 21:1619–1623
20. Storm FK, Morton DL, Kaiser LR, Harrison WH, Elliott RS, Weisenburger TH, Parker RG, Haskell CM (1982) Clinical radiofrequency hyperthermia: a review. *Natl Cancer Inst Monogr* 61:343–350
21. Wenger C, Salvador R, Basser PJ, Miranda PC (2015) The electric field distribution in the brain during TTFIELDS therapy and its dependence on tissue dielectric properties and anatomy: a computational study. *Phys Med Biol* 60:7339–7357
22. Wenger C, Salvador R, Basser PJ, Miranda PC (2016) Improving tumor treating fields treatment efficacy in patients with glioblastoma using personalized array layouts. *Int J Radiat Oncol Biol Phys* 95:1137–1143
23. Pawłowski P, Szutowicz I, Marszałek P, Fikus M (1993) Bioelectrorheological model of the cell 5. Electrodestruction of cellular membrane in alternating electric field. *Biophys J* 65:541–549

24. Gera N, Yang A, Holtzman TS, Lee SX, Wong ET, Swanson KD (2015) Tumor treating fields perturb the localization of septins and cause aberrant mitotic exit. *PLoS ONE* 10:e0125269
25. Morgenstern PF, Zhou Z, Wembacher-Schröder E, Cina V, Tsiouris AJ, Souweidane MM (2018) Clinical tolerance of corticospinal tracts in convection-enhanced delivery to the brainstem. *J Neurosurg* 21:1–7
26. van Vuurden DG (2018) Convection-enhanced delivery: chemosurgery in diffuse intrinsic pontine glioma. *Lancet Oncol* 19(8):1001–1003
27. Habets JGV, Heijmans M, Kuijf ML, Janssen MLF, Temel Y, Kubben PL (2018) An update on adaptive deep brain stimulation in Parkinson's disease. *Mov Disord* 33(12):1834–1843
28. Ramirez-Zamora A, Ostrem JL (2018) Globus pallidus interna or subthalamic nucleus deep brain stimulation for Parkinson disease: a review. *JAMA Neurol* 75(3):367–372
29. Nowacki A, Galati S, Ai-Schlaeppli J, Bassetti C, Kaelin A, Pollo C (2018) Pedunculopontine nucleus: an integrative view with implications on deep brain stimulation. *Neurobiol Dis*. [https:// doi.org/10.1016/j.nbd.2018.08.015](https://doi.org/10.1016/j.nbd.2018.08.015)
30. Udupa K, Chen R (2015) The mechanisms of action of deep brain stimulation and ideas for the future development. *Prog Neurobiol* 133:27–49
31. Wichmann T, DeLong M (2016) Deep brain stimulation for movement disorders of basal ganglia origin: restoring function or functionality? *Neurotherapeutics* 12:264–283
32. Herrington T, Cheng J, Eskandar E (2016) Mechanisms of deep brain stimulation. *J Neurophysiol* 115:19–38
33. Hottinger AF, Pacheco P, Stupp R (2016) Tumor treating fields: a novel treatment modality and its use in brain tumors. *Neuro oncology* 18:1338–1349.

Chapter 4

4 Simulation and treatment of high-grade glioma with dynamically-oriented electric fields³

Introduction: Intratumoral modulation therapy (IMT) is an emerging strategy to control high grade glioma (HGG) with low intensity electric fields delivered by implantable electrodes. The treatment parameters that provide maximal tumor coverage are unknown and direct evidence of IMT efficacy in solid human HGG tumors is lacking. This study quantified the impact of electrode and waveform variations on electric field properties and IMT response in novel human spheroid and organoid HGG models.

Methods: Computer simulations were used to determine the IMT field generated from a multi-electrode configuration based on the applied waveforms and the relative phase-shifts from each electrode. Optimized IMT parameters were then evaluated for therapeutic efficacy in patient-derived, engineered spheroid and naive organoid HGG models, and for adverse neurological and histological impact in living rodent brains.

Results: Simulation analysis demonstrated robust advantage in achieving planned electric field amplitudes and distributions using multiple compared to single electrode IMT systems. The transition to a phase-shifted output waveform to create dynamically-oriented electric fields further dramatically improved tumor coverage. Optimized, phase-shifted IMT parameters produced significant reduction of tumor cell viability in patient-derived HGG spheroids and solid organoids without overt neurological effects or tissue electrolysis in normal living rodent brain.

³ A version of this chapter is going to be published as:

Andrew Deweyert, Erin Iredale, Hu Xu, Eugene Wong, Susanne Schmid, Matthew. O. Hebb. (2021). Malignant glioma sensitivity to dynamically-orientated electric fields delivered by intratumoral modulation therapy. In preparation for submission.

Conclusions: Phase-shift IMT strategies using multiple electrodes produce dynamic, impactful electric fields for comprehensive tumor coverage in human glioma models. This work presents the first direct evidence of IMT response in solid patient HGG specimens.

4.1 Introduction

Glioblastoma (GBM) is the most common high-grade glioma (HGG) and brain cancer arising from the adult central nervous system (CNS) [Nam, 2017]. Maximal safe resection followed by chemo- and radio-therapy is standard treatment yet fails to achieve long-term disease control in most patients. The field of electrotherapeutics holds promise in cancer care, including for GBM and other HGGs, but remains largely under-developed [Mun, 2018]. Tumor cells from a host of somatic and nervous system cancers are sensitive to exogenous, low intensity electric fields [Xu, 2016; Krison, 2004]. Glioma cells, including those derived from GBM, are among those vulnerable to non-ablative stimulation that exerts negligible physical impact on normal brain tissues [DiSebastiano, 2018]. Multiple biological effects in neoplastic cells have been reported including mitotic spindle disruption, direct DNA damage, autophagic responses and increased membrane permeability [Ghiaseddin, 2009; Chang, 2018; Karanam, 2020; Robins, 2018]. The key anti-tumor benefits of low intensity electric fields appear to be the induction of targeted apoptosis and enhanced efficacy of combination treatment platforms [Xu, 20016; DiSebastiano, 2018; Deweyert, 2019].

The emerging concept of intratumoral modulation therapy (IMT) employs an implanted array of electrodes to deliver personalized, low intensity electric fields across tumor-affected CNS regions. The intent of this strategy is to create a means of chronic tumor suppression administered alongside, and beyond, standard treatment options. IMT fields could span contrast-enhancing and non-enhancing diffuse or focal tumors, and target unresected glioma or tumor resection beds anywhere in the CNS. Early studies demonstrated robust *in vitro* efficacy of IMT monotherapy in glioma cells, but not primary neurons, and markedly enhanced impact of chemotherapy and radiation with

adjuvant IMT [Xu, 2016; Deweyert, 2019]. The *in vitro* treatment parameters were translated to an *in vivo* rodent GBM model using a rudimentary IMT system that produced significant reduction in tumor volume but no neurological deficits or tissue injury when delivered to normal brain [DiSebastiano, 2018]. These pilot data raised enthusiasm for further evaluation of IMT in glioma tumors but also highlighted important shortcomings of the early system design. For example, the *in vivo* studies used a single stimulating electrode positioned within the tumor, coupled to an extracerebral ground electrode. GBM viability was reduced even though post-hoc simulation analysis revealed tightly confined electric fields that spanned only a fraction of the tumor region [DiSebastiano, 2018; Deweyert, 2019]. The elicited responses were significant but undoubtedly did not reflect the full capacity of IMT in these models. The field coverage may be improved by modifying individual programming specifications, such as output waveform, amplitude, frequency, electrode number and position, amongst others. In particular, IMT configurations using multiple electrodes will accommodate a wide spectrum of stimulation parameters, including phase-shifted output waveforms to produce rotatory, migrational, or multi-directional (*i.e.*, dynamically-oriented) fields with better tumor coverage than those generated by comparable in-phase waveforms [Iredale, 2020]. The present study seeks to validate these principles of enhanced IMT in preclinical human HGG applications. Specifically, this work compares simulated electric field distribution and target amplitudes achieved using single versus multiple stimulating electrodes and bi-directional versus dynamically-oriented electric fields. The optimized parameters defined by the simulation analysis are then applied in a sentinel evaluation of IMT in novel 3-dimensional (3D) human tumor models using patient-derived HGG spheroids and naïve solid organoids.

4.2 Materials and Methods

4.2.1 Glioma spheroid and organoid preparations

This study was approved by the Human Research Ethics Board at Western University and carried out in accordance with the Tri-Council Policy for research involving human

subjects. Informed consent for tumor and control tissue was obtained from all patients or their legal guardians and tumor diagnosis was confirmed by a neuropathologist. Clinically relevant genetic profiling was performed at the neuropathologist's discretion but not used as study inclusion/exclusion criteria. Tumor specimens were initially collected into DMEM in the operating room and transferred promptly to the lab for cell culture or organoid preparation [Xu, 2016; DiSebastiano, 2018]. Glioma cells from 5 patient tumors were transduced with a lentiviral vector encoding firefly luciferase (FLuc) driven by the constitutive elongation factor 1 alpha promoter to create primary 3D spheroids amenable to real time monitoring with bioluminescence imaging (BLI) [Parkins, 2020; Hamilton, 2018]. HGG spheroids were created in 7 mm diameter culture wells by implanting tumor cells (4×10^4 cells in 2 μ L phosphate-buffered saline (PBS)) into 200 μ L Matrigel matrix (Corning) over a 2-minute period. The matrix with embedded tumor cells was allowed to polymerize at 37 °C with 5% CO² for 20 minutes before the addition of 100 μ L of complete Dulbecco's modified Eagle's medium (DMEM; Wisent Bioproducts) containing 10% fetal bovine serum (FBS; Life Technologies), 1% non-essential amino acids and 1% penicillin/streptomycin (Life Technologies).

Solid glioma organoids and non-neoplastic brain organoids were prepared from an additional 5 patient tumors and 6 non-neoplastic neurosurgery patients respectively. The tissue was washed with PBS and 5 mm punch samples (Integra Milex) suspended in a 7 mm diameter culture well containing 100 μ L Matrigel (Corning). The matrix with embedded tumor fragment was allowed to polymerize at 37 °C with 5% CO² for 20 minutes before the addition of 100 μ L of NeuroCult™ NS-A medium supplemented with 10% proliferation supplement, bFGF (10 ng/mL), EGF (20 ng/mL), heparin sulfate (2 μ g/ml) and 1% penicillin/streptomycin (Stemcell Technologies).

Multi-electrode IMT model

A 3-electrode device was custom designed and fabricated for preclinical evaluation of expanded IMT parameters, including phase-shifted waveforms, in 3D glioma models. The hardware was adapted for 7 mm culture wells with embedded tumor spheroids and organoids, as described above, and consisted of three biocompatible, uninsulated,

platinum electrodes (6 mm length, 0.25 mm diameter, 2 mm inter-electrode distance) mounted to a common pedestal made of polyether ether ketone. A thread and groove system on the pedestal allowed fixation to a modified culture lid and secure cable connection to the waveform generator (Rigol DG1022; Electro-Meters Ltd). The device was positioned within the Matrigel 24 hours following spheroid or organoid implantation to create sham control (i.e., implanted hardware but no stimulation) or IMT conditions for a 72-hour period using electrode configurations guided by the simulation analysis. A third tumor specimen provided a no-hardware control scenario for each run.

4.2.2 Computer simulation of IMT electric fields

The computer simulations used physical geometries of the culture models so that *in silico* treatment parameters could be subsequently evaluated in HGG spheroids and organoids. Simulated electric field maps generated using the following electrode configurations were evaluated: 1) a single stimulating electrode with a paired ground electrode, 2) 2 stimulating electrodes using in-phase waveforms with 1 ground electrode and 3) 3 electrodes each with an equal 120 degree phase-shift between output waveforms [Iredale, 2020]. The electrical output of all configurations included a sinusoidal waveform of 4V peak-to-peak amplitude ($\pm 2V$, max/min) and 200 kHz frequency which have previously been effective in HGG cell culture and *in vivo* models [DiSebastiano, 2018; Deweyert, 2019]. IMT models were constructed using the AC/DC module, electric currents user interface in COMSOL Multiphysics (v 5.4) with biocompatible, platinum stimulating and ground electrodes. The 3-electrode model permitted a choice of waveform for each electrode, including selection of relative phase-shifts. Material electrical properties of conductivity and relative permittivity were assigned to the components of the treatment models, with respective values of 1.5 S/m and 81 for Matrigel and 9.43×10^6 S/m and 1 for the platinum electrodes [Taghian, 2015; Arnold, 1994; Chen, 2009]. Terminal boundary conditions were applied to each electrode and electrical insulation was assumed on all outer boundaries of the model [Iredale, 2020]. A tetrahedral mesh was used and the electric field computed over a waveform period for each scenario. The average electric field delivered to each voxel over time was analyzed in MATLAB R2020b using the COMSOL MATLAB Livelink to generate average electric field maps and electric field

volume histograms (EVH) outlining the percentage of Matrigel tumor bed volume covered by the corresponding time average electric field.

4.2.3 Tumor viability assays

Spheroid viability was measured using BLI emission intensity captured with a cooled CCD camera mounted in a light-tight specimen box (IVIS hybrid optical/Xray scanner, IVIS Lumina XRMS, PerkinElmer) [Parkins, 2020]. The luciferase substrate, D-luciferin (300 $\mu\text{g}/\text{mL}$), was added to the culture media following the treatment period and imaging performed at 60 second intervals until peak signal was obtained and the mean photon flux (photons/second/ mm^2) measured (Living Image, Xenogen). A second measure of spheroid viability was obtained using the 3-(4,5-dimethylthiazol-2-yl)-2,5-diphenyltetrazolium (MTT) assay (Sigma Aldrich). This spectrophotometric test measures the reduction of yellow MTT by mitochondrial succinate dehydrogenase to an insoluble, dark purple Formosan product. Following treatment, MTT (20 μl at 5 mg/ml) was added to the culture media and spheroids incubated for 3 hours at 37 $^{\circ}\text{C}$ in a humidified 5% CO_2 atmosphere. Spheroids were then lysed to release the purple Formosan product by the addition of 80 μl dimethyl sulfoxide (DMSO) for 15 minutes at room temperature. Absorbance was measured using a microplate spectrophotometer (Epoch) and viability estimated using optical density values at 570 nm with references at 655 nm [Taghian, 2015; Chen, 1994].

Glioma and control organoids were similarly assessed using the MTT assay. However, these solid tumor specimens did not readily lyse with DMSO for measuring absorbance so viability was quantified using densitometry analysis (ImageJ, version:2.0.0-rc-69/1.52p). Tissue density readings were obtained by isolating the organoid image using the automated thresholding tool. The optical density was then measured using the analysis tool to produce a densitometry plot. The area under the plot was quantified and normalized to the cross-sectional area of the corresponding organoid to account for variations in organoid size. All BLI, MTT and densitometry values obtained following sham or IMT conditions in spheroid and organoid models were normalized to the respective no hardware control measures.

4.2.4 *In vivo* IMT control studies

The same 3-electrode device and phase-shift IMT parameters described above were evaluated in normal rodent brain to assess for neurological and lesional adverse effects. IMT devices were stereotactically implanted under isoflurane anesthesia bilaterally into the striatum in 3 male Fischer rats (coordinates from bregma: anteroposterior 1 mm, lateral \pm 3 mm, dorsoventral -6 mm). On postoperative day 4, IMT was randomized to the right or left side and the respective device connected to a waveform generator (Rigol DG1022; Electro-Meters Ltd) via an extension cable and a commutator that permitted the animal to move freely throughout the home cage [Di Sebastiano, 2018]. The contralateral hemisphere served as an internal sham control (i.e., identical hardware implants but without stimulation). Continuous multi-electrode, phase-shift IMT was delivered between postoperative days 4–11 with the same parameters used to treat the HGG spheroids and organoids. All animals were given free access to food and water, perioperative antibiotics and analgesics, and monitored daily for medical or neurological complications. On postoperative day 11, animals were deeply anesthetized with sodium pentobarbital and transcardially perfused with 4% paraformaldehyde. Brains were cut on a cryotome into 25 μ m thick sections through electrode implantation sites, mounted onto microscope slides and stained with thionine. Processed sections were digitally imaged with a Nikon Eclipse Ni-E microscope.

4.2.5 Statistical Analysis

Datasets were compared using a Student's t-test with significance considered at p-values < 0.05 (Graphpad Prism8, CA, USA). Values are presented as mean \pm standard deviation (SD).

4.3 Results

4.3.1 Phase-shifting markedly enhances IMT electric field distribution

The computer simulation modeled various electrode configurations and treatment parameters that could be evaluated using the newly fabricated IMT device for patient HGG spheroids and organoids (Fig. 4.1). Specifically, these studies compared the electric field distribution and amplitude resulting from a single stimulating electrode versus a multi-electrode strategy that more accurately reflects the clinical vision of IMT. The 3-electrode construct used here provides the simplest form of multi-electrode IMT that can accommodate a phase-shift approach and create a dynamically rotating electric field about the central axis of the construct. The geometry of the hardware was replicated in COMSOL with 2 or 3 biocompatible platinum stimulating or ground electrodes. The electric field threshold of 1 V/cm is recognized as effective in GBM and was used as an exemplary measure of IMT coverage for each electrode configuration [Latikka, 2019; Palti, 1966; Ghiaseddin, 2020]. Based on the EVH analysis, this amplitude was achieved across 99% of the target treatment volume (i.e., culture well) using the phase-shift, multi-electrode configuration, compared to 55% and 63% coverage using 2-electrode and 3-electrode stimulation without phase-shift, respectively. Similarly, the volume percentage covered by 2 V/cm for the 2-electrode, 3-electrode without and with phase-shift was 23%, 30%, and 68% respectively. Of the 3 configurations, only the phase-shift, multi-electrode stimulation produced symmetric, dynamically rotating electric fields (Fig. 4.1).

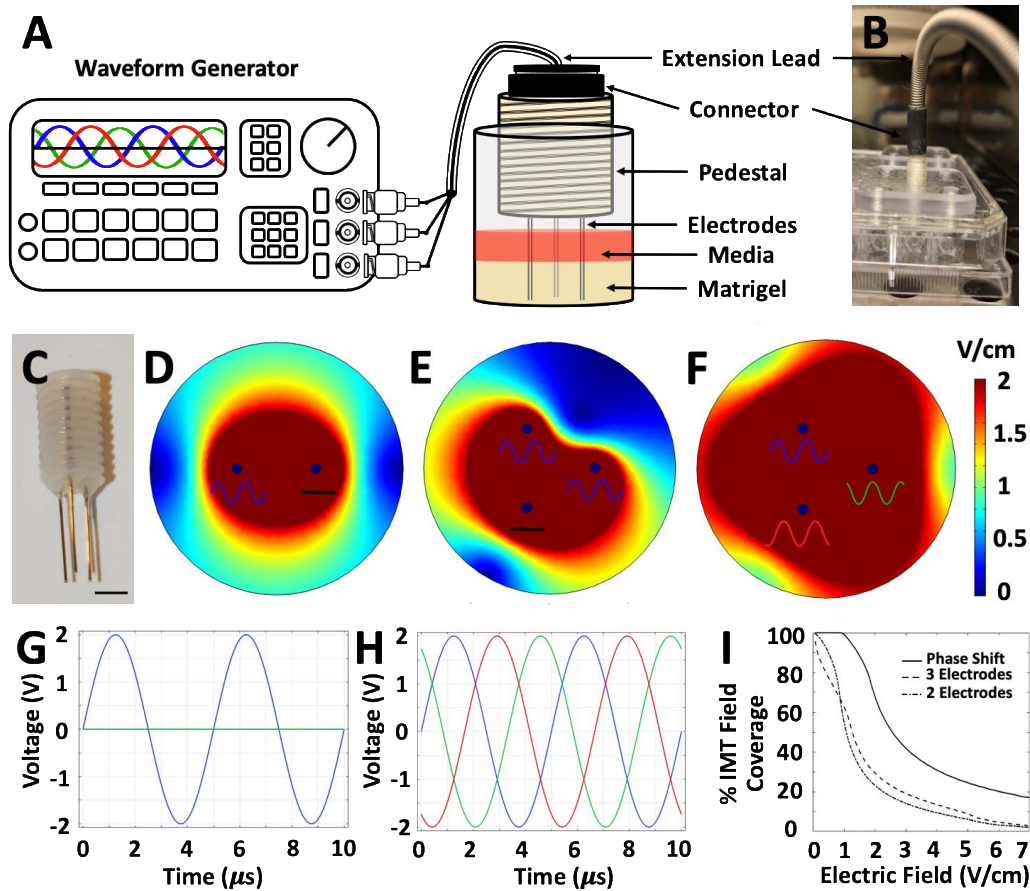


Figure 4-1. Transition from single to multiple stimulating electrodes with phase-shift output enhances electric field coverage.

A) A 3D IMT model was created in which broad variations in stimulation parameters could be evaluated in patient-derived HGG spheroids and GBM organoids. B) Photo showing the modified culture plate that accommodates fixed implantation of the IMT electrode device into the tumor bed and connection of the device to a waveform generator. C) Custom fabricated preclinical IMT multi-electrode device used both in the 3D HGG models and *in vivo* control rat brains⁵. D)-F) Cross sectional area of the 3D culture well is shown with computer simulation of the IMT model using COMSOL geometry to produce time average electric field maps for D) 2 electrodes (1 stimulating + 1 ground), E) 3 electrodes (2 in-phase stimulating + 1 ground), and F) 3 stimulating electrodes equally phase-shifted. The transition to a multi-electrode, phase-shifted output created marked improvement in field distribution, with less cold spots due to field cancellation effect (Also see Supplementary video Fig S1). G) Graphical depiction of the waveform output for 1 stimulating + 1 ground or 2 in-phase stimulating + 1 ground scenarios. The single or overlapping (in-phase) waveforms result in limited electric field distribution. H) In contrast, the phase-shift IMT scenario, with a 120-degree offset between waveforms, produces a broad, dynamically-oriented electric field. I) Electric volume histograms of IMT field coverage with each of the stimulation scenarios. Only

the phase-shift 3-electrode configuration reached a 1 V/cm threshold known to impact HGG viability across nearly 100% of the culturing well [Iredale, 2020].

4.3.2 Patient demographics and HGG specimens

Ten patients provided HGG specimens for this study (3 male: 7 female, age 29-75 years). All tumors were supratentorial in location. Of the 9 HGG tumors diagnosed as GBM, 8 were de novo and 1 transformed from an anaplastic astrocytoma which had been treated with surgery and chemoradiation 2 years prior. The remaining tumor sample was obtained from a stereotactic biopsy in the youngest patient, who had no tumor history, and diagnosed as anaplastic astrocytoma (Table 4.1).

Table 4-1. Patient and tumor characteristics.

| Patient # | Age (years) | Sex | Tumor location | Tumor model | Diagnosis (WHO grade) | IDH1(R132H) mutation | Nuclear ATRX retained | EGFR amplified (Polysomy 7) |
|-----------|-------------|--------|--------------------------|-------------|---|----------------------|-----------------------|-----------------------------|
| 1 (49) | 29 | Female | Splenium (left) | Spheroid | AA (III) | No | No | No (yes) |
| 2 (23) | 65 | Female | Parietal (right) | Spheroid | GBM (IV) | No | N/A | N/A |
| 3 (41) | 66 | Female | Parietal (right) | Spheroid | GBM (IV) | No | Yes | No (yes) |
| 4 (46) | 67 | Female | Temporo-parietal (right) | Spheroid | GBM (IV) | No | Yes | Yes (yes) |
| 5 (20) | 39 | Male | Fronto-temporal (right) | Spheroid | GBM (IV) *was AA two years prior with surgery and chemoradiation | Yes | N/A | No (yes) |
| 6 (58) | 56 | Female | Hypothalamic (right) | Organoid | GBM (IV) | No | Yes | No (yes) |
| 7 (60) | 49 | Female | Temporal (left) | Organoid | GBM (IV) | Yes | No | No (yes) |
| 8 (61) | 65 | Male | Parietal (right) | Organoid | GBM (IV) | No | Yes | No (yes) |
| 9 (62) | 54 | Female | Frontal (right) | Organoid | GBM (IV) | No | Yes | Yes (yes) |
| 10 (63) | 58 | Male | Parietal (left) | Organoid | GBM (IV) | No | Yes | No (no) |

4.3.3 Evidence of HGG spheroid response to IMT

The HGG spheroid model enabled the first multi-modality assessment of IMT impact within a 3D tumor environment. Spheroids were created in triplicate for parallel 3-day

exposure to 1. no hardware control, 2. sham and 3. IMT conditions. Based on superior field coverage revealed by the computer simulation data, the 3-electrode construct was applied using phase-shifted sinusoidal output of 4V peak-to-peak at a frequency of 200 kHz. Five biological replicates were assessed using MTT and BLI with sham and IMT values normalized to the corresponding no hardware control measures. The MTT assay revealed marked viability loss following IMT compared to sham ($52.2 \pm 6.4\%$: $100.4 \pm 6.5\%$ of no hardware control values, respectively; $n = 5$; $p < 0.001$; Fig. 4.2). The BLI intensity measured in an independent series revealed consistently dramatic loss of viability following IMT compared to sham treatment ($18.9 \pm 16.6\%$: $105 \pm 32\%$ of control values, respectively; $n = 5$; $p > 0.001$). No overtly recalcitrant tumors were identified, including the anaplastic astrocytoma in patient 1 and recurrent GBM in patient 5 which were both exquisitely sensitive to IMT (Fig. 4.3).

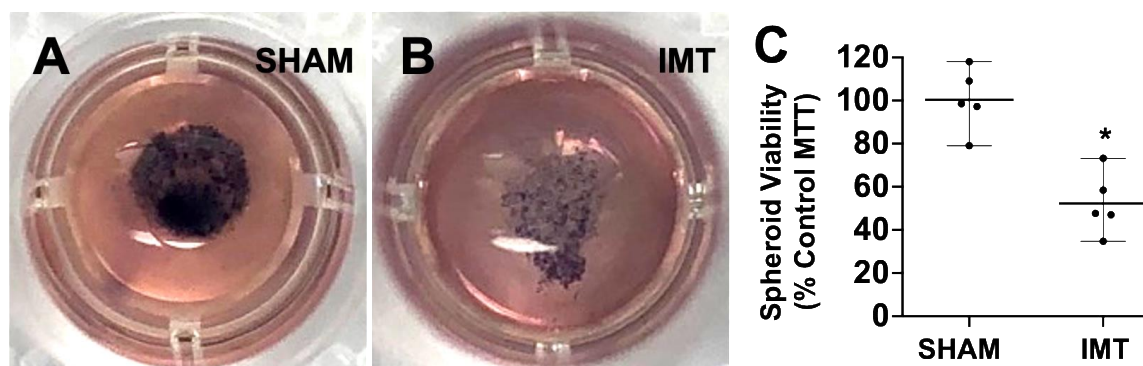


Figure 4-2. Phase-shift IMT reduces patient HGG spheroid viability.

A, B) Representative photographs showing the MTT assay in 3D HGG spheroids following 3-day exposure to sham or IMT conditions, as indicated. Note the dramatic reduction of the dark Formosan MTT product, consistent with viability loss, following IMT C) MTT measures were normalized to the respective no-hardware control values and revealed ~50% reduction in HGG spheroid viability with IMT compared to sham ($n = 5$, $*p < 0.001$). Individual values are shown together with the cohort mean (horizontal line) \pm SD.

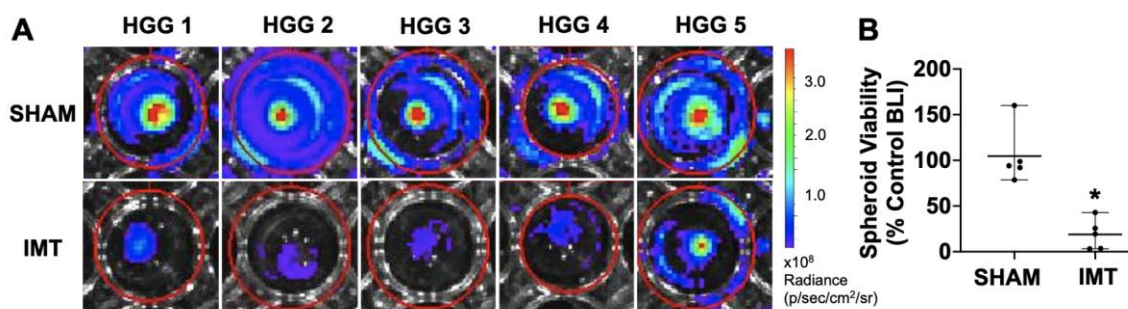


Figure 4-3. BLI reveals the robust impact of IMT in patient-derived HGG spheroids.

A) Peak BLI signal from patient-derived HGG spheroids following 3-day exposure to sham or IMT conditions. There was a dramatic loss of signal intensity following dynamic field IMT compared to sham treatment in all specimens. B) BLI measures were normalized to the respective no-hardware control values and revealed >80% reduction in HGG spheroid viability with IMT compared to sham ($n = 5$, $*p > 0.001$). Individual values are shown together with the cohort mean (horizontal line) \pm SD.

4.3.4 Solid GBM organoids are highly sensitive to phase-shift IMT that does not injure normal brain parenchyma

A 3-day parallel period of no hardware control, sham or IMT conditions was implemented with 5 biologically distinct HGG and control organoids, all organoids in this series, followed by evaluation with MTT densitometry to estimate tissue viability. Consistent with the spheroid data, naïve GBM organoids exhibited marked sensitivity to multi-electrode, phase-shift IMT. The post-treatment MTT density was visibly reduced following IMT. The impact did not appear ablative and margins of the tumor fragments remained delineated. Organoid viability measures decreased to $58.1 \pm 14.7\%$ compared to $101.4 \pm 11.7\%$ of control values following IMT or sham conditions, respectively ($n = 5$; $p = 0.003$; Fig. 4.4). In contrast to the impact on GBM organoids, IMT did not produce overt alterations in morphology or viability of non-neoplastic brain organoids taken from epilepsy and benign axial tumor patients (relative MTT values: sham = $96.92 \pm 6.10\%$; IMT = $104.80 \pm 11.13\%$; $p = 0.1605$; Figure 4.5). A control cohort of Fischer rats ($n=3$) was then used to determine if the new multi-electrode, phase-shift IMT parameters would

produce overt functional deficits or parenchymal injury in normal (i.e., non-tumor-bearing) living brain. During a 1-week trial of dynamic field IMT, the animals exhibited no changes in feeding, grooming, sleeping, nor any overt seizures or motor weakness. The postmortem histology revealed expected parenchymal disruption along the electrode tracts with no signs of electrolysis or substantial hemorrhage in either sham or IMT-treated hemispheres (Fig. 4.6).

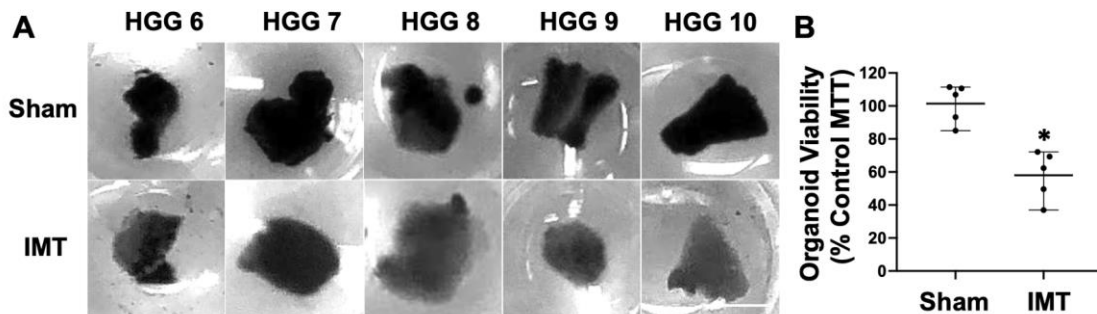


Figure 4-4. Patient GBM organoids are highly sensitive to dynamically-oriented electric fields.

HGG organoids, all diagnosed as GBM, were created from patient tumor specimens immediately following surgical resection. A) Representative photographs depicting 5 GBM organoid cultures exposed to MTT following sham or dynamic field IMT conditions. B) Quantification of GBM organoid viability with densitometry analysis. MTT measures were normalized to the respective no-hardware control values and revealed >40% reduction in organoid viability with IMT compared to sham (n = 5, *p = 0.003). Individual values are shown together with the cohort mean (horizontal line) \pm SD.

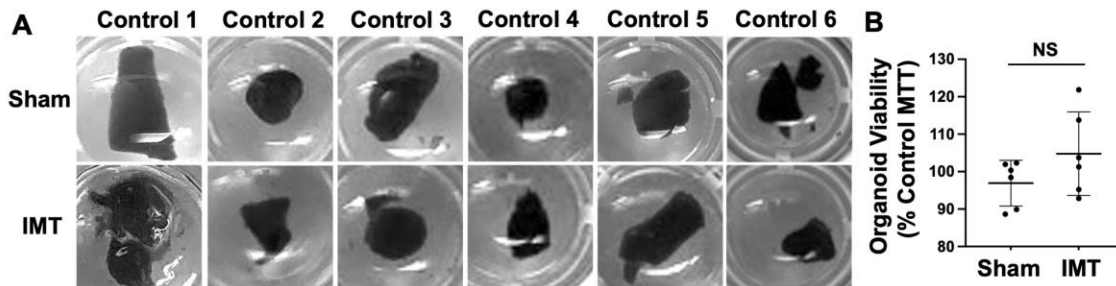


Figure 4-5. Multi-electrode phase-shift IMT does not produce overt injury non-neoplastic brain organoids.

Normal brain organoids, were created from patient specimens immediately following surgical resection from epilepsy patients. A) Representative photographs depicting 5 brain organoid cultures exposed to MTT following sham or dynamic field IMT conditions. B) Quantification of brain organoid viability with densitometry analysis. MTT measures were normalized to the respective no-hardware control values and revealed a non-significant difference in brain organoid viability with IMT compared to sham ($n = 6$, $p = 0.1605$). Individual values are shown together with the cohort mean (horizontal line) \pm SD.

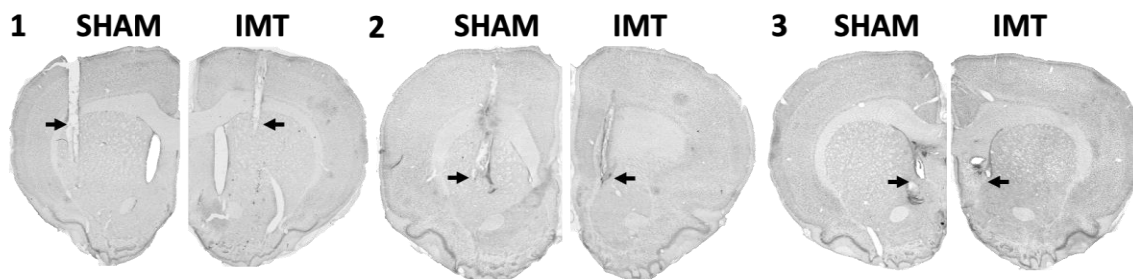


Figure 4-6. Multi-electrode phase-shift IMT does not produce overt injury in the normal living brain.

The multi-electrode devices used in the HGG spheroid and organoid models were implanted bilaterally in the brain of living rats with one hemisphere randomized to 1 week of sham conditions (*i.e.*, hardware but no stimulation) and the other to phase-shift IMT [5,9]. Representative sections are shown from each brain, numbered 1-3, and stained with thionine. Symmetric defects from the electrode passages were evident bilaterally (arrows) without overt parenchymal injury related to the stimulation.

4.4 Discussion

This study provided the first simulation and validation platform for multi-electrode IMT in 3D patient-derived HGG models. These efforts demonstrated the dramatic field distribution advantage of multiple versus single electrodes, and of phase-shift versus in-phase output waveforms. The computer simulation allowed comparison of treatment strategies in these proof-of-concept preclinical models that sets groundwork for advances in electrotherapy planning systems for CNS cancer. The demonstration that multiple electrodes provide greater tumor coverage than a single electrode is perhaps intuitive; however, the delivery of such complex electric fields requires careful programming to avoid untoward cumulative or cancellation effects [Iredale, 2020]. These challenges may

be mitigated by phase-shifting, or temporally offsetting, output waveforms to create dynamically-oriented electric fields that produce broader coverage than with in-phase delivery. The current stimulation parameters did not produce overt injury to human non-neoplastic organoids and normal living brain but yielded powerful control of HGG spheroids and naive human GBM organoids, providing resounding evidence of therapeutic potential.

The new concept of IMT is distinct from existing electrotherapeutics in the application of an indwelling source of personalized electric fields to yield perpetual CNS cancer control. The stimulation parameters ideally would not produce neural entrainment or interference to permit overlap between tumor and normal tissue without inciting adverse effects. The kHz waveform frequency applied here is above neural entrainment range however its safety and efficacy have not been established by long-term clinical experience using implantable CNS electrodes [Latikka, 2019; Palti, 1966; Ghiaseddin, 2020]. Deep brain stimulation (DBS) is a common neuromodulation technique to quell the symptoms of various non-oncological conditions, such as Parkinson's Disease (PD), and presently the only clinical indication for chronic intracerebral electrodes [Kogan, 2019]. DBS is typically delivered at low voltage (< 5V) and frequency (90-180 Hz) to create highly focused electric fields at precise anatomic targets. The low frequency incites neural entrainment to subvert pathological firing patterns but adds risk of off-target stimulation effects (*e.g.*, paresthesia, motor contractions) [Jakobs, 2019]. A recent DBS trial in PD patients evaluated an initial experience using kHz stimulation, intending to maintain therapeutic efficacy with reduced side effects. The team reported similar symptom control in patients receiving low (*i.e.*, Hz) and kHz-range frequencies. The novel kHz-DBS was associated with less adverse impact and no patient safety concerns [Harmsen, 2019]. The question remains however whether these parameters could interfere with normal neural activity through alternate mechanisms when the electric fields are more broadly distributed across CNS regions, as intended with IMT-based strategies. This concern requires further attention but may be eased by the clinical experience with an approved externally-applied electrotherapeutic for GBM. Compared to the indwelling IMT delivery system, the external device is mounted on the scalp to create low amplitude, kHz-range transcranial electric fields without significant

neurological adversity [Stupp, 2017]. These experiences safely treating PD and GBM with kHz stimulation align with the absence of neurological deficits or tissue injury in the present study using implanted electrodes to create 200 kHz dynamic electric fields in the living rat brain.

The cumulative data support preclinical IMT efficacy in various HGGs (*i.e.*, anaplastic astrocytoma, *de novo* and recurrent GBM, diffuse intrinsic pontine glioma) grown in monolayer and 3D cell culture, patient-derived organoids and *in vivo* allografts [Xu, 2016; DiSebastiano, 2018; Deweyert, 2019]. Emerging image- and simulation-guided algorithms may help define electrode number and placement, as well as treatment parameters that yield optimal coverage [Iredale, 2020]. The therapeutic promise of IMT must be weighed not only against potential adverse sequelae of the electric fields but also the physical risk of electrode implantation in and around CNS tumors. One of the most feared surgical complications of brain surgery is intracerebral hemorrhage (ICH) and data reported from common neurosurgical procedures may help estimate the ICH risk of IMT. For example, stereotactic brain biopsies are performed to obtain tissue diagnosis and may involve collection of several core tumor samples. Biopsy studies from the last three decades have cited reasonably low incidence of clinically-relevant ICH, including 1.4% ICH-related major deficits or death after image-guided brain biopsies in 300 patients [Bernstein, 1994], 1.2% hemorrhage-related neurological deficits in 500 consecutive biopsies [Field, 2001], 4% incidence of symptomatic ICH in 270 patients [27], and 2.6% transient ICH-related symptoms in an 80-patient cohort [Mizobuchi, 2019]. Similarly low ICH risk has been associated with laser interstitial thermal therapy (LITT), a minimally invasive cancer procedure using stereotactic placement of a laser probe to ablate a target brain tumor [Holste, 2019]. A series of 100 LITT cases with various neuro-oncological pathologies reported a 4% complication rate, none of which were hemorrhagic in nature [Shah, 2020]. Another study of 58 LITT outcomes in *de novo* and recurrent GBM found a 15.5% overall complication rate mostly related to edema and seizures, with 1 mortality from hemorrhage in a large tumor [Kamath, 2019]. Consistently, a recent review of 17 reports and 203 patients with recurrent GBM receiving LITT found a 0.5% incidence of hemorrhage [Montemurro, 2020]. Other neurosurgical procedures involving implantation of multiple brain electrodes, such as DBS and stereo electroencephalography (sEEG),

also have acceptable complication profiles. Most bleeding events associated with these surgeries are small and have no overt clinical sequelae [Tonge, 2015]. DBS often entails placement of one or two permanent electrode leads and, over the past two decades, has a reported ICH incidence 1.0% to 3.4% per lead [Liu , 2015; Binder , 2005; Ben-Haim , 2009; Falowski , 2015]. sEEG used for seizure monitoring can be associated with numerous implanted brain electrodes [Cardinale, 2016]. In 30 reports describing outcomes of 2624 sEEG patients, the pooled incidence of ICH was 0.7% [Mullin, 2016]. Two additional series described 549 consecutive sEEG implantations (total 7029 electrodes) with 1.5% symptomatic ICH [40] and 742 patients with 0.03% of clinically-relevant ICH [Cardinale, 2016; McGovern, 2019]. The overall low complication risk, including that of ICH, associated with these neurosurgical procedures supports the safe feasibility of a multi-electrode IMT approach for CNS cancer.

This study sheds new light on the potential of electric field treatment for brain cancer and introduces the utility of phase-shifted waveforms to produce broad, consistent tumor coverage. It offers a novel demonstration of computer simulation, programming and efficacy of dynamic field IMT in patient-derived HGG. Within the limits of the treatment models, the current multi-modality analysis provides compelling evidence of IMT susceptibility in patient glioma specimens without harmful effects in normal living brain. The essential next steps in the translational pipeline will be definition of key technical elements and impact of dynamic field therapy *in vivo* and in combination with chemotherapy and radiation. The present data support the intriguing prospect of IMT-based strategies in neuro-oncology.

4.5 References

1. Nam JY, Groot JFD. Treatment of glioblastoma. *J. Oncol. Pract.* 2017; 13: 629–638.
2. Mun EJ, Babiker HM, Weinberg U, et al. Tumor-treating fields: a fourth modality in cancer treatment. *Clin Cancer Res.* 2018; 15;24(2): 266-275.
3. Hu X, Bihari F, Whitehead S, et al. In vitro validation of intratumoral modulation therapy for glioblastoma. *Anticancer Res.* 2016; 36: 71–80.
4. Kirson ED, Gurvich Z, Schneiderman R, et al. Disruption of cell replication by electric fields. *Cancer Res.* 2004; 64(9): 3288-3295.
5. Di Sebastiano AR, Deweyert A, Benoit S, et al. Preclinical outcomes of intratumoral modulation therapy for glioblastoma. *Sci. Rep.* 2018; 8(1):7301.
6. Ghiaseddin AP, Shin D, Melnick K, et al. Tumor treating fields in the management of patients with high grade gliomas. *Curr. Treat. Options in Oncol.* 2020; 21: 76.
7. Chang E, Patel CB, Pohling C, et al. Tumor treating fields increases membrane permeability in glioblastoma cells. *Cell Death Discov.* 2018; 4: 113.
8. Karanam NK, Ding L, Aroumougame A, et al. Tumor treating fields cause replication stress and interfere with DNA replication fork maintenance: Implications for cancer therapy. *Transl. Res.* 2020; 217: 33-46.
9. Robins HI, Nguyen HN, Field A, et al. Molecular Evolution of a Glioblastoma Controlled With Tumor Treating Fields and Concomitant Temozolomide. *Front. Oncol.* 2018; 8: 451.
10. Deweyert A, Iredale E, Xu Hu, et al. Diffuse intrinsic pontine glioma cells are vulnerable to low intensity electric fields delivered by intratumoral modulation therapy. *J Neurooncol.* 2019; 143: 49–56.

11. Iredale E, Deweyert A, Hoover DA, et al. Optimization of multi-electrode implant configurations and programming for the delivery of non-ablative electric fields in intratumoral modulation therapy. *Med Phys*. 2020; 47(11): 5441-5454
12. Parkins KM, Dubois VP, Kelly JJ, et al. Engineering circulating tumor cells as novel cancer theranostics. *Theranostics*. 2020; 10(17): 7925-7937.
13. Hamilton A, Foster PJ, Ronald JA. Evaluating non-integrating lentiviruses as safe vectors for noninvasive reporter-based molecular imaging of multipotent mesenchymal stem cells. *Hum Gene Ther*. 2018; 9(10): 1213-1225.
14. Taghian T. 2015. Interaction of an electric field with vascular cells. Available at <https://etd.ohiolink.edu/>. Accessed December 27, 2020.
15. Arnold WM, Fuhr G. Increasing the permittivity and conductivity of cellular electromanipulation media [abstract]. *Proceedings of 1994 IEEE Industry Applications Society Annual Meeting*. 1994; 2:1470-1476.
16. Chen MT, Jiang C, Vernier PT, et al. Two-dimensional nanosecond electric field mapping based on cell electroporation. *PMC Biophys*. 2009; 2(1): 9.
17. Kupcsik L. Estimation of cell number based on metabolic activity: the MTT reduction assay. In: Stoddart M, eds. *Methods in Molecular Biology*. Vol 740. Humana Press. Available at doi-org.proxy1.lib.uwo.ca/10.1007/978-1-61779-108-6_3.
18. Latikka J, Eskola H. The resistivity of human brain tumours in vivo. *Ann Biomed Eng*. 2019; 47(3): 706-713.
19. Palti Y. Stimulation of internal organs by means of external applied electrodes. *J. Appl. Physiol*. 1966; 21: 1619–1623.
20. Ghiaseddin AP, Shin D, Melnick K, et al. Tumor treating fields in the management of patients with high grade gliomas. *Curr. Treat. Options in Oncol*. 2020; 21:76.

21. Kogan M, McGuire M, Riley. Deep Brain Stimulation for Parkinson Disease. *J.Neurosurg Clin N Am.* 2019; 30(2): 137-146.
22. Jakobs M, Fomenko A, Lozano AM, et al. Cellular, molecular, and clinical mechanisms of action of deep brain stimulation-a systematic review on established indications and outlook on future developments. *EMBO Mol Med.* 2019; 11(4): e9575.
23. Harmsen IE, Lee DJ, Dallapiazza RF, et al. Ultrahigh frequency deep brain stimulation at 10 000 Hz improves motor function. *Neurosurgery.* 2019; 66(Suppl):1
24. Stupp R, Taillibert S, Kanner A, et al. Effect of Tumor-Treating Fields Plus Maintenance Temozolomide vs Maintenance Temozolomide Alone on Survival in Patients with Glioblastoma A Randomized Clinical Trial. *JAMA.* 2017; 318(23): 2306-2316.
25. Bernstein M, Parrent AG. Complications of CT-guided stereotactic biopsy of intra-axial brain lesions. *J. Neurosurg.* 1994; 81(2): 165-168.
26. Field M, Witham TF, Flickinger JC, et al. Comprehensive assessment of hemorrhage risks and outcomes after stereotactic brain biopsy. *J. Neurosurg.* 2001; 94(4): 545-551.
27. McGirt MJ, Woodworth GF, Coon AL, et al. Independent predictors of morbidity after image-guided stereotactic brain biopsy: a risk assessment of 270 cases. *J. Neurosurg.* 2005; 102(5): 897-901.
28. Mizobuchi Y, Nakajima K, Fujihara T, et al. The risk of hemorrhage in stereotactic biopsy for brain tumors. *J. Med. Invest.* 2019; 66(3): 314-318.
29. Holste KG, Orringer DA. Laser interstitial thermal therapy. *NOA.* 2019; 2(1).
30. Shah AH, Semonche A, Eichberg DG, et al. The Role of laser interstitial thermal therapy in surgical. *Neuro-Oncology:* 2020; 87(2): 266–275.

31. Kamath AA, Friedman DD, Hassan S, et al. Glioblastoma treated with magnetic resonance imaging-guided laser interstitial thermal therapy: safety, efficacy, and outcomes. *Neurosurgery*. 2019; 84(4) 836–843.
32. Montemurro N, Anania Y, Cagnazzo F, et al. Survival outcomes in patients with recurrent glioblastoma treated with Laser Interstitial Thermal Therapy (LITT): A systematic review. *Clin. Neurol. Neurosurg*. 2020; 195: 105942.
33. Tonge M, Ackermansa L, Kocabicakbe E, et al. A detailed analysis of intracerebral hemorrhages in DBS surgeries. *Clin. Neurol. Neurosurg*. 2015; 139: 183-187.
34. Liu JK, Soliman H, Machado A, et al. Intracranial hemorrhage after removal of deep brain stimulation electrodes. *J. Neurosurg*. 2012; 116(3): 525-528.
35. Binder DK, Rau GM, Starr PA, et al. Risk factors for hemorrhage during microelectrode-guided deep brain stimulator implantation for movement disorders. *Neurosurgery*. 2005; 56(4): 722–732.
36. Ben-Haim S, Asaad WF, Gale JT, et al. Risk factors for hemorrhage during microelectrode-guided deep brain stimulation and the introduction of an improved microelectrode design. *Neurosurgery*. 2009; 64(4):754–763.
37. Falowski SM, Ooi YC, Bakay RA. Hardware-related complications with deep brain stimulation. *Neuromodulation*. 2015; 18: 670-677.
38. Cardinale F, Casacel G, Raneri f, et al. Implantation of stereoelectroencephalography electrodes: a systematic review. *J. Clin. Neurophysiol*. 2016; 33(6): 490-502.
39. Mullin JP, Shriver M, Alomar S, et al. IsSEEG safe? A systematic review and meta-analysis of stereo-electroencephalography-related complications. *Epilepsia*. 2016; 57: 386–401.
40. McGovern RA, Knight EP, Gupta A, et al. Robot-assisted stereoelectroencephalography in children. *J. Neurosurg*. 2019; 23(3): 288-296.

Chapter 5

5 Discussion

5.1 Summary of Major Results

My thesis was designed to address three major research goals. First, we aimed to develop and test a unique set of IMT stimulation parameters outside the range of neural entrainment and establish both *in vitro* and *in vivo* models of GBM. Using these and other methods, we next aimed to define the efficacy of IMT treatment for the highly fatal pediatric brain tumor DIPG. Finally, we aimed to apply these concepts to improve IMT hardware and test treatment effect in completely novel, 3D patient-derived HGG models. The work presented in this thesis yielded key information that allowed expansion of the IMT treatment paradigm to other CNS neoplasms, led to improved IMT delivery and, for the first time, directly demonstrated the preferential impact of IMT against HGG compared to non-neoplastic normal human brain.

The research presented in Chapter 2 aimed to address the need for intermediate frequency (200 kHz) stimulation IMT electric fields that is beyond the range of neural entrainment. Additionally, we aimed to translate these novel stimulation parameters into cultures with primary patient GBM cells and in an F98 Fischer rat syngeneic glioma model. We hypothesized that intermediate-frequency IMT electric fields will provide a novel, effective means of primary tumor control both *in vitro* and *in vivo*. IMT produced tumor-selective cell death of primary patient-derived GBM cells *in vitro*. IMT-treated cells demonstrated reduced cell density and a pyknotic morphology compared to the sham cells. Analysis of viability revealed a significant reduction in cellular metabolic viability in the IMT treatment group. In contrast, when rat cortical neurons were treated with either sham or IMT, no difference in cellular viability was detected, suggesting that our 200 kHz treatment parameters are selective for neoplastic, highly-proliferative cells and will not harm the normal brain parenchyma [DiSebastiano, 2018]. Preliminary studies into the mechanisms of IMT *in vitro* demonstrated robust activation of apoptotic markers and programmed cell death; however, the initiation factors of the apoptotic pathways are yet to be elucidated. These findings prompted the translation of IMT into an F98 Fischer

rat glioma model. Bilateral orthotopic tumors were established by implanting F98 cells into the caudate putamen of syngeneic adult Fischer rats, following a protocol established by Mathieu et al. [DiSebastiano, 2018; Desmarais, 2012; Mathieu, 2007; Mathieu, 2005; Lenting, 2017; Barth, 1998]. Utilizing this model, we were able to assess F98 tumor growth, treatment effect of IMT, and the effects of IMT on the normal brain parenchyma. We observed a significant ~20% reduction in tumor volumes in tumors treated with a 7-day course of first-generation IMT compared to their respective internal sham controls. These results, though exciting, raised the question of why we observed a limited treatment effect of IMT *in vivo* compared to *in vitro* studies. Utilizing a computational workflow, our team determined that the rudimentary single electrode hardware only delivered electric fields of 1 V/cm across 24% of the tumor volume and was insufficient for generating the electric fields necessary to encompass the robust tumors grown in the F98 model. These observations prompted the development of multi-electrode hardware to extend electric field coverage across these tumors and to surrounding tumor-affected brain regions.

The development of the methods outlined in Chapter 2 allowed for the investigation and application of IMT for DIPG, another HGG, which was explored in Chapter 3. We aimed to determine the responsiveness of DIPG to IMT in combination with chemoradiotherapy *in vitro*. Based on the findings from Chapter 2, we hypothesized that IMT in combination with chemoradiotherapy would provide an effective means to increase drug sensitivity and reduce viability of patient-derived DIPG cells. We demonstrated the *in vitro* efficacy of intermediate-frequency IMT on primary DIPG patient tumors. IMT as a monotherapy profoundly reduced the viability of patient derived DIPG cells (~50%) and was determined to be apoptosis mediated. The addition of IMT to the combined TMZ-RT paradigm dramatically reduced DIPG cell viability from ~ 60% to 20% [Deweyert, 2019]. To date, the effects of the combination therapies appear to be additive in DIPG cells. To our knowledge, this research is the first to demonstrate the innate sensitivity of DIPG cells to perturbations in their local electrical environment. The results presented in this chapter highlight that all patient derived DIPG cell cultures tested were sensitive to IMT monotherapy, and that IMT increased the efficacy of the current standard of care *in vitro*. We also observed DIPG cells treated with IMT to have an increased sensitivity to

chemotherapeutics. These findings are exciting as DIPG remains recalcitrant to current pharmacological interventions, and IMT may offer a method of drug delivery and sensitization. These proof-of-concept findings demonstrate the potential of IMT as a novel electrotherapeutic strategy for the treatment of DIPG and support further investigation of IMT for other primary CNS neoplasms and metastases.

The research presented in Chapter 4 builds upon that of previous chapters. Guided by these studies, we aimed to improve the delivery of IMT electric fields through the development of multi-electrode hardware and novel phase-shifted stimulation parameters [DiSebastiano, 2018; Iredale, 2020]. To test the efficacy of newly designed IMT delivery systems, we developed a high throughput 3D model of GBM that emulates the growth and invasive properties of HGGs. Therefore, we hypothesized that multiple IMT therapeutic electrodes will produce electric fields that cover the extent of HGGs, increasing the therapeutic effect of IMT, without negatively impacting the surrounding brain parenchyma. Chapter 4 provided novel evidence of GBM cell vulnerability to phase-shifted, low-intensity electric fields delivered using a high throughput, preclinical IMT protocol. Phase-shifted IMT reduced the viability of tumor cells and prevented tumor invasion of the peritumoral matrix using stimulation parameters previously demonstrated to be non-injurious to normal neural cells [DiSebastiano, 2018; Deweyert, 2019, Hu, 2016; Rominiyi, 2021; Kirson, 2009; Pless, 2011; Mittal, 2017]. IMT monotherapy reduced GBM cell viability by ~50% in spheroid cultures; this effect was amplified on the exquisitely sensitive BLI studies that showed ~90% reduction in signal. Cultures exposed to IMT treatment displayed limited growth, and in some cases, a reduction in tumor mass. Tumor cell invasion was also limited by IMT therapy, suggesting that IMT may not only eliminate the bulk of the tumor mass, but also effectively treat the invasive GBM cells responsible for disease recurrence. Studies with naive GBM organoids recapitulated the spheroid results and represent first time evidence of human disease sensitivity to IMT. Future studies are needed to investigate the combinatory effect of IMT with chemoradiation in 3D models to determine if IMT exerts synergistic treatment effects. Control studies were performed to assess the safety of multi-electrode phase shift IMT on both non-neoplastic brain organoids and normal brain parenchyma. In these studies, IMT was delivered *in vitro* to non-tumor brain tissue and to

rat brains. Results showed that the hardware and treatment parameters did not reduce the viability of the non-neoplastic brain organoids and was well tolerated with no observable behavioral or histological changes due to treatment in the animals. These studies help provide evidence that IMT and phase shift are safe and well tolerated in a living system. Though the effects of multi-electrode, phase shift IMT have not been tested *in vivo*, we hypothesize that the field planning methods and delivery system outlined in these preclinical models will translate well to *in vivo* applications. We envision IMT as a source of chronic, highly selective, therapeutic fields that combat the infiltrative nature of HGGs and highly fatal brain cancers.

5.2 Experimental Limitations

While we have made marked progress in the development of IMT towards human use, we still have not shown the efficacy of IMT in human HGG using *in vivo* models. To do this, we would require translation to a human patient-derived xenograft (PDX) model and hopefully human trials will follow. To date, we have shown significant but limited efficacy of single electrode IMT in a Fischer rat F98 animal and have yet to translate the newly developed multi-electrode design, which is expected to improve tumor coverage and response. We used a single 3-electrode construct for convenience in the preclinical models here, however we would envision various, personalized multiple electrode strategies, such as multiple implantable electrode leads and or arrays, in human application. While the Fischer rat F98 model has been a useful, highly reproducible tool to explore these novel treatment paradigms, it has a few limitations that have likely led to the underestimation of treatment effect. For example, the highly rapid tumor growth rate in the F98 model is far beyond that observed in human tumors and PDX models. The tumors rapidly progress from 40,000 cells on the day of implant to encompassing the entire hemisphere by day 11. The treatment fields tested to date have not been designed to encompass a rapidly expanding tumor and is likely that the tumor growth is beyond the borders of the electric fields before the initiation of treatment. Thus, these tumors can grow uninhibited in these regions, limiting observed treatment effect. Additionally, this model lacks some key features of human HGG that are integral to understanding disease recurrence and progression, such as the molecular drivers of disease and the hallmark

migration and invasion into the surrounding brain parenchyma. It is likely that studies utilizing the Fischer F98 model will be effective for determining the efficacy of IMT against the bulk tumors mass. To understand the role IMT against diffuse infiltrative disease, additional humanized models will need to be developed.

The treatment effect of IMT *in vivo* may be limited by the analysis methods. Quantification by stereology was unable to distinguish necrotic centers of the large F98 tumors from areas of IMT induced cell death. For this reason, treated tumors likely have an overestimation of viable tumor volume, and conservative estimates of treatment effect *in vivo*. While these conservative findings show great promise for the further development of IMT, it will be important to overcome this limitation to fully understand the degree of treatment efficacy. The addition of highly sensitive tumor monitoring and imaging techniques such as BLI and MRI in conjunction with stereology is expected to improve our understanding of treatment effect.

Another limitation of the current IMT models is the relatively short duration of treatment. Our current models do not allow for longer than one week delivery of IMT fields, due to the need for media changes *in vitro* and the aggressive nature of the F98 cells *in vivo*, causing animals to quickly reach humane end points. Short treatment duration has likely led to underestimation of the ability of IMT to control disease. A potential future study will be the implementation of longitudinal IMT. The study will require the development of appropriate rat and large animal PDX models that demonstrate a reduced rate of disease progression more akin to human disease. Longitudinal IMT experiments will be able to assess treatment effects over an undefined period, and the animals can be followed with medical imaging such as MRI and BLI to monitor disease progression.

5.3 Future Directions

My work, in conjunction with concurrent team collaborations, has substantially advanced our knowledge of IMT efficacy and improved delivery strategies for treatment of devastating HGGs. This thesis demonstrated that IMT attenuates HGG growth in novel *in*

vitro models and in a syngeneic rat glioma model. With our collaborative research team, we established a phase shifted treatment parameters, and implement both a multi-electrode IMT hardware and new optimized stimulation parameters. The next critical step will be to translate the *in vitro* findings presented in this thesis to *in vivo* models. IMT will be tested in the syngeneic F98 Fischer rat model; however, due to limitations of this model, it is also critical to develop a host of PDX models using patient derived cells to better recapitulate human disease. These models may include PDX models in immunodeficient rats (in-house model is in development), which will provide long-term GBM engraftment and growth [Noto, 2020]. The human HGGs transplanted into these models behave more like patient tumors and better recapitulate the genetics and tumor behavior that the current F98 model lacks. Specifically, the rate of xenograft growth emulates growth seen in patients, with tumors growing over many weeks. Perhaps most importantly, these models demonstrate parenchymal infiltration and a genetic profile that mimics human patients [Stringer, 2019]. These newly developed PDX models will allow for the implementation of longitudinal IMT studies and will be able to assess treatment effects over an undefined period. Additionally, animals may be followed with medical imaging such as MRI and BLI to monitor disease progression [Parkins, 2016]. Demonstrating a quantifiable and measurable increase in lifespan with IMT is a necessary step towards the goal of clinical translation.

To date, we have primarily explored IMT as a monotherapy of HGGs, with some evidence of the efficacy of combination therapies with the standards of care for GBM *in vitro* [DiSebastiano, 2018; Deweyert, 2019; Hu, 2016]. Though we predict to see a positive treatment effect of combining multi-electrode IMT with chemoradiotherapy *in vitro*, it remains largely unknown if these benefits will translate *in vivo*. Utilizing our established animal model, we can begin to explore these combination therapies in living systems.

It is evident from our studies that IMT initiates apoptotic pathways leading to cell death; however, how these pathways are initiated and why they are selective to neoplastic cells compared to the normal brain parenchyma is poorly understood. The underlying mechanisms may involve interference with cytokinesis and/or more complex mechanism

involving membrane channels and cell permeability [Chang, 2018; Karanam, 2020; Serpersu, 1985; Wei, 2015; Penuela, 2012]. Overall, further investigation is required to better understand the underlying mechanisms of how IMT exerts anti-neoplastic effects and attenuates tumor growth. Understanding these mechanisms may allow for further guidance in the optimizing stimulation parameters and could potentially improve IMT treatment efficacy as a monotherapy and in combination with standard and other burgeoning therapies.

5.4 Significance and Overall Conclusions

There is a dire need for new treatments for rapidly fatal HGGs. The work in this thesis clearly demonstrated the efficacy of a novel treatment modality, IMT. IMT selectively kills HGG cells over normal neural cells and takes advantage of the innate electrosensitivity of neoplastic cells while remaining inert to normal brain parenchyma. We have conclusively demonstrated that GBM and DIPG cells are susceptible to low-intensity electric fields delivered using an implantable/indwelling system, which are a powerful and titratable force that matches the diffuse infiltrative nature of these diseases. We have discovered that IMT provides highly effective primary anti-neoplastic control *in vitro* and displays proof-of-concept efficacy in animal models. Importantly, IMT also markedly increases tumor sensitivity to concurrent chemoradiation. The newly-developed IMT technology is readily translatable, and we think may offer safe and feasible human application. The collaborative interdisciplinary data presented within this contributes to the fundamental framework which establishes IMT as a putative new and effective therapeutic modality for highly-fatal brain cancers.

5.5 References

1. DiSebastiano, A., Deweyert, A., Benoit, S., et al. (2018) Preclinical Outcomes of Intratumoral Modulation Therapy for Glioblastoma. *Sci Rep* 8;8(1):7301. doi: 10.1038/s41598-018-25639-7.
2. Desmarais, G., Fortin, D., Bujold, R., et al. (2012) Infiltration of Glioma Cells in Brain Parenchyma Stimulated by Radiation in The F98/Fischer Rat Model. *International Journal of Radiation Biology*. 88:8, 565-574. DOI: 10.3109/09553002.2012.692495
3. Mathieu, D., Lecomte, R., Tsanaclis, et al. (2007) Standardization and Detailed Characterization of the Syngeneic Fischer/F98 Glioma Model. *Can. J. Neurol. Sci.* 34:296–306.
4. Mathieu, D., Lamarche, J. & Fortin, D (2005) The Importance of a Syngeneic Glioma Implantation Model: Comparison of the F98 Cell Line in Fischer and Long-Evans Rats. *J Appl Res* 5:17–25.
5. Lenting, K., Verhaak, R., Laan, M., et al. (2017) Glioma: Experimental Models and Reality. *Acta Neuropathol.* 133:263–282.
6. Barth, R. (1998) Rat Brain Tumor Models in Experimental Neuro-Oncology: The 9L, C6, T9, F98, RG2 (D74), RT-2 And CNS-1 Gliomas. *J Neurooncol.* 36, 91–102. doi.org/10.1023/A:1005805203044
7. Deweyert, A., Iredale, E., Xu, H., et al. Diffuse Intrinsic Pontine Glioma Cells are Vulnerable to Low Intensity Electric Fields Delivered by Intratumoral Modulation Therapy. *J Neurooncol.* 2019; 143: 49–56
8. Iredale, E., Deweyert, A., Hoover, D., et al. (2020) Optimization of Multi-electrode Implant Configurations and Programming for the Delivery of Non-ablative Electric Fields in Intratumoral Modulation Therapy. *Med Phys.* 47(11): 5441-5454

9. Hu, X., Bihar, F., Whitehead, S., et al. (2016). In Vitro Validation of Intratumoral Modulation Therapy for Glioblastoma. *Anticancer Res.* 36(1):71-80.
10. Rominiyi, O., Vanderlinden, A., Clenton, S.J. et al. (2021) Tumour Treating Fields Therapy for Glioblastoma: Current Advances and Future Directions. *Br J Cancer.* 124:697–709. doi.org/10.1038/s41416-020-01136-5
11. Kirson, E., Schneiderman, R., Dbalý, V., et al. (2009) Chemotherapeutic Treatment Efficacy and Sensitivity are Increased by Adjuvant Alternating Electric Fields (Ttfields). *BMC Med Phys.* 8(9):1. <https://doi.org/10.1186/1756-6649-9-1>
12. Pless, M., Weinberg, U. (2011) Tumor Treating Fields: Concept, Evidence and Future. *Expert Opinion on Investigational Drugs.* 20:8:1099-1106. DOI:10.1517/13543784.2011.583236
13. Mittal, S., Klinger, N., Michelhaugh, S., et al. (2017) Alternating Electric Tumor Treating Fields for The treatment Of Glioblastoma, Rationale, Preclinical, and Clinical Studies. *J Neurosurg.* 24:1-8.
14. Noto, F., Sangodkar, J., Adedeji, B., et al. (2020) The SRG Rat, A Sprague-Dawley Rag2/Il2rg Double-Knockout Validated for Human Tumor Oncology Studies. *PLoS One.* 7;15(10):e0240169
15. Stringer, B.W., Day, B.W., D'Souza, R.C.J. et al. (2019) A Reference Collection of Patient-Derived Cell Line And Xenograft Models of Proneural, Classical and Mesenchymal Glioblastoma. *Sci Rep.* 9:4902. doi.org/10.1038/s41598-019-41277-z
16. Parkins, K., Hamilton, A., Makela, A., et al. (2016) A Multimodality Imaging Model to Track Viable Breast Cancer Cells from Single Arrest to Metastasis in the Mouse Brain. *Sci Rep.* 21;6:35889.
17. Chang, E., Patel, C., Pohling, C., et al. (2018) Tumor Treating Fields Increases Membrane Permeability in Glioblastoma Cells. *Cell Death Discov.* 4:113.

18. Karanam, N., Ding, L., Aroumougame, A., et al. (2020) Tumor Treating Fields Cause Replication Stress and Interfere With DNA Replication Fork Maintenance: Implications for Cancer Therapy. *Transl. Res.* 217:33-46.
19. Serpersu, H., Kinosita, K., Tsong, Y. (1985) Reversible and Irreversible Modification of Erythrocyte Membrane Permeability by Electric Field. *Biomembranes.* 81(3):779-785.
20. Wei, L., Yang, X., Shi, X., et al. (2015). Pannexin1 Silencing Inhibits the Proliferation of U87MG cells. *Mol Med Rep.* 11:3487-3492.
21. Penuela, S., Gyenis, L., Ablack, A., et al. (2012) Loss of Pannexin 1 Attenuates Melanoma Progression by Reversion to a Melanocytic Phenotype. *J Biol Chem.* 287:29184-29193.

Curriculum Vitae

Name: Andrew Deweyert

Post-secondary Education and Degrees: University of Western Ontario
London, Ontario, Canada
2010-2016 BMSc, Honors Specialization in Medical Cell Biology

The University of Western Ontario
London, Ontario, Canada
2016-present Ph.D. Candidate

Summary of Student Activities

Coursework:

- Anatcell 9555 Advanced Topics in Cell Biology – Completed – 94%
- Anatcell 9520 Cell and Neurobiology Seminar – Completed – 93%
- Anatcell 9605Y Comprehensive in Cell Biology – Completed – Passed
- Anatcell Seminar Lecture – Completed

Scholarships:

2020-23 Frederick Banting and Charles Best Canada Graduate Scholarship Doctoral Awards - \$105,000

2020-21 Ontario Graduate Scholarship (OGS) \$15,000 – Declined

2019-20 Herold Brett Memorial Fellowship \$1,200

2019-20 Western Graduate Research Scholarship \$7,000/year

2018-19 Ontario Graduate Scholarship (OGS) \$15,000

2017-18 Canadian Graduate Scholarship (CGSM) \$17,500

2017-18 Ontario Graduate Scholarship (OGS) \$15,000 – Declined

2016-17 Ontario Graduate Scholarship (OGS) \$15,000

Teaching Assistantships:

2017-21 **Human Gross Anatomy Teaching Assistant**

2020-21 **Human Gross Anatomy Virtual Labs Facilitator / Content Development**

2016-21 **Mammalian Histology Teaching Assistant**

2020-21 **Neuroanatomy (Online) Lecturer**

2021 **Translational Models of Cancer Guest Lecture**

2018-20 **Functional Human Anatomy Instructor**

2020 **Selected Topics in Medical Sciences Guest Lecture**

2016-18 **Integrative Neuroscience Teaching Assistant**

2018 **Biology for the Sciences II Teaching Assistant**

Publications:

2021 **Submitting: Deweyert, A.**, Iredale, E., Xu, H., Hamilton, A., Ronald, J., Peters, T., Wong, E., Schmid, S., Hebb, M. Simulation and treatment of high-grade glioma with dynamically oriented electric fields. Anti-cancer.

2020 Iredale, E., **Deweyert, A.**, Hoover, A., Chen, J., Schmid, S., Hebb, M., Peters, T., Wong, E. Optimization of implanted multi-electrode configurations and programming for

non-ablative electric fields delivered using intratumoral modulation therapy. *Med Phys*, 47: 5441-5454. <https://doi.org/10.1002/mp.14496>

2019 **Deweyert, A.**, Iredale, E., Wong, E., Schmid, S., Hebb, M. Diffuse intrinsic pontine glioma cells are vulnerable to low intensity electric fields delivered by intratumoral therapy. *Journal of Neuro-Oncology*. 43(1): 49-56

2018 **Deweyert, A.**, DiSebastiano, A., Benoit, S., Iredale, E. Xu, H., De Oliveira, C., Wong, E., Schmid, S., Hebb, M. Preclinical outcomes of intratumoral modulation therapy for glioblastoma. *Scientific Reports*. 8(1):7301.

Conference Abstracts/Talks:

2021 **ABSTRACT – Deweyert, A.**, Iredale, E., Xu, H., Wong, E., Schmid, S., Hebb, M. Patient-derived malignant glioma response to 3D dynamically-oriented electric fields. London Health Research Day. London, ON, Canada. *Platform Presentation*. May 2021.

2020 **ABSTRACT – Deweyert, A.**, Iredale, E., Xu, H., Wong, E., Schmid, S., Hebb, M. Custom 3D Brain Cancer Model to Test a Novel Anti-Cancer Electrotherapy. AAA at AAA at FASEB. San Diego, CA, USA. *Platform Presentation*. April 2020.

* Award Finalist for AAA

2019 **ABSTRACT – Deweyert, A.**, Iredale, E., Xu, H., Wong, E., Schmid, S., Hebb, M. Intratumoral Modulation Therapy Enhances Multi-Modality Treatment Platforms for Pediatric and Adult High-Grade Gliomas. Society for Neuroscience, Chicago IL, USA. *Poster Presentation*. October 2019.

2019 **ABSTRACT – Deweyert, A.**, Iredale, E., Xu, H., Wong, E., Schmid, S., Hebb, M. Intratumoral Modulation Therapy Enhances Multi-Modality Treatment Platforms for Diffuse Intrinsic Pontine Glioma. Canadian Association for Neuroscience, Toronto, ON, Canada. *Poster Presentation*. May 2019.

2019 **ABSTRACT – Deweyert, A.**, Iredale, E., Xu, H., Wong, E., Schmid, S., Hebb, M. Intratumoral Modulation Therapy in Combination with Chemoradiation for the Control of Pediatric Diffuse Intrinsic Pontine Glioma. The Canadian Student Health Research Forum, Winnipeg, MA, Canada. *Poster Presentation*. June 2019. *Award CIHR Gold Medal

2019 **ABSTRACT – Deweyert, A.**, Iredale, E., Xu, H., Wong, E., Schmid, S., Hebb, M. Intratumoral Modulation Therapy Enhances Multi-Modality Treatment Platforms for Diffuse Intrinsic Pontine Glioma. Clinical Neurological Sciences Research Day. London, ON, Canada. *Platform Presentation*. April 2019. *Awarded Top Platform Presentation

2018 **ABSTRACT – Deweyert, A.**, Iredale, E., Xu, H., Wong, E., Schmid, S., Hebb, M. Intratumoral Modulation Therapy: A Novel Electrotherapeutic Strategy for Patient-Derived DIPG Cells. International Symposium for Pediatric Neuro-Oncology. Denver, CO, USA. *Poster Presentation*. July 2018.

2018 **ABSTRACT – Deweyert, A.**, Iredale, E., Xu, H., Wong, E., Schmid, S., Hebb, M. Developing Novel Electrotherapeutic Interventions for Glioblastoma and Pediatric Diffuse Intrinsic Pontine Glioma. Clinical Neurological Sciences Research Day. London, ON, Canada. *Platform Presentation*. April 2018. *Awarded Top Platform Presentation

2018 **ABSTRACT – Deweyert, A.**, Iredale, E., Xu, H., Wong, E., Schmid, S., Hebb, M. Patient-Derived Glioblastoma Cells are Susceptible to Intratumoral Modulation Therapy Both in 2D and Neurosphere Culture. Society for Neuroscience, Washington DC, USA. *Poster Presentation*. November 2017.

2017 **ABSTRACT – Deweyert, A.**, Iredale, E., Xu, H., Wong, E., Schmid, S., Hebb, M. Optimizing Stimulation Parameters and Treatment Fields for Intratumoral Modulation Therapy. Canadian Association for Neuroscience. *Poster Presentation*. May 2017.

2017 **ABSTRACT – Deweyert, A.**, Iredale, E., Xu, H., Wong, E., Schmid, S., Hebb, M. Optimizing Stimulation Parameters and Treatment Fields for Intratumoral Modulation Therapy. London Health Research Day, London, ON, Canada. *Poster Presentation*. May 2017.

2017 **ABSTRACT – Deweyert, A.**, Iredale, E., Xu, H., Wong, E., Schmid, S., Hebb, M. Intratumoral Modulation Therapy for Glioblastoma: Determination of Electric Field Intensity Thresholds for the Induction of Apoptosis in Low Passage Patient- Derived Cells. Oncology Research and Education Day, London, ON, Canada. *Platform Presentation*. July 2017.

2016 **ABSTRACT – Deweyert, A.**, Iredale, E., Xu, H., Wong, E., Schmid, S., Hebb, M. Intermediate Frequency Intratumoral Modulation Therapy. Anatomy and Cell Biology Research Day, London ON, Canada. *Poster Presentation*. October 2016. *Top Poster Presentation Award

Other Contributions:

Department of Anatomy and Cell Biology, Western University

2019-21 National Scholarship Ranking Volunteer

2018-20 Research Committee Student Representative

2019-20 Student Volunteer, Donor Body Memorial Service

2017-20 Student Chair of the Professional Development Committee

2017-19 Anatomy and Radiology Contouring Bootcamp Gross Anatomy Demonstrator

2017-18 Secretary and Communications Officer for Anatomy and Cell Biology Graduate Student Council

2017-20 Department of Anatomy and Cell Biology Recruitment Weekend Volunteer

2016–17 Social Committee Chair of Anatomy and Cell Biology Graduate Student Council

COMMUNITY SERVICE & OUTREACH

2018-21 Thames Valley District School Board Science Fair Judge

2018-19 Anatomy and Cell Biology Booth Volunteer at South Western Ontario's Science Rendezvous Event.

PROFESSIONAL DEVELOPMENT

NATIONAL

AAA Annual Meeting at Experimental Biology, San Diego, CA, USA. April 2020.

Society for Neuroscience, Chicago, IL, USA. October 2019.

Canadian Student Health Research Form, Winnipeg, MA, Canada. June 2019.

Canadian Association of Neuroscience, Toronto, ON, Canada. May 2019.